Improved Colorimetry Through Fundamental Appearance Scales

by

Saeedeh Abasi

A dissertation proposal submitted in partial fulfillment of the
requirements for the degree of Doctor of Philosophy
in the Munsell Color Science Laboratory for Color Science
College of Science
Rochester Institute of Technology

April 2026

MUNSELL COLOR SCIENCE LABORATORY
COLLEGE OF SCIENCE
ROCHESTER INSTITUTE OF TECHNOLOGY
ROCHESTER, NEW YORK

CERTIFICATE OF APPROVAL

Ph.D. DEGREE PROPOSAL

The Ph.D. Degree Proposal of Saeedeh Abasi
has been examined and approved by the
dissertation committee as satisfactory for the
dissertation required for the
Ph.D. degree in Color Science

04/27/2026

Dr. Mark D. Fairchild , Dissertation Advisor Date

4/28/2026

Coordinator Ph.D. Degree Program Date

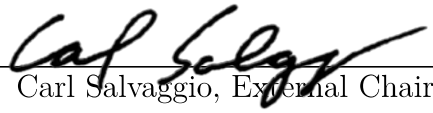

04/27/2026

Dr. Carl Salvaggio, External Chair

04/27/2026

Dr. Michael J. Murdoch

4/28/2026

Dr. Susan Farnand

Improved Colorimetry Through Fundamental Appearance Scales

by

Saeedeh Abasi

Submitted to the
Munsell Color Science Laboratory
in partial fulfillment of the requirements
for the Doctor of Philosophy Degree
at the Rochester Institute of Technology

Abstract

This dissertation introduces a new framework for color appearance modeling, referred to as the Fundamental Color Appearance Model (FCAM). The primary objective of this work is to develop perceptually meaningful color appearance scales that are directly derived from cone fundamentals and formulated as independent one-dimensional scales. Unlike conventional color appearance models that rely on complex three-dimensional color spaces and extensive nonlinear processing, FCAM describes color appearance attributes individually through mathematically simple and physiologically grounded formulations.

FCAM consists of four independent one-dimensional scales: the Fundamental Hue Scale (FHS), Fundamental Lightness Scale (FLS), Fundamental Brightness Scale (FBS), and Fundamental Saturation Scale (FSS). Each scale is derived directly from LMS cone responses and can incorporate chromatic adaptation in a straightforward manner. This structure reflects the perceptual independence of color appearance attributes and avoids assumptions about an underlying multidimensional geometry.

The proposed scales were evaluated using a wide range of existing psychophysical data sets as well as newly collected experimental data. Results demonstrate that the fundamental one-dimensional scales achieve performance that is comparable to, and

in some cases exceeds, that of established and more complex color appearance models. Despite their simplicity, the proposed scales successfully predict key perceptual properties such as hue linearity and spacing, lightness and brightness behavior under varying viewing conditions, and saturation constancy across hue and luminance changes.

An important achievement of this research is the flexibility of the proposed one-dimensional framework. Each scale can be optimized independently using new or application-specific data sets without affecting the remaining attributes. This modular structure allows FCAM to be adapted to different observers, viewing conditions, and emerging display technologies while maintaining computational efficiency and conceptual clarity.

Overall, this dissertation demonstrates that accurate color appearance prediction does not require highly complex mathematical models. Instead, perceptually effective and physiologically meaningful color appearance modeling can be achieved through simple, independent, and adaptable one-dimensional scales derived directly from cone fundamentals.

Contents

List of Figures

List of Tables

Chapter 1

Introduction

Color is a perceptual attribute of visual sensation, and colorimetry refers to the measurement of color. Traditional colorimetry is concerned with determining whether two stimuli with different spectral power distributions will match in color for certain given conditions of observation. Color appearance models include methods for assessing the appearance of color stimuli presented to the observer in complicated surroundings, not only a certain viewing condition. The ultimate goal of colorimetry is to provide color appearance models for different viewing conditions [1].

The encoding of color signals (e.g., LMS or XYZ) and the specification of perceptual color attributes (e.g., lightness, saturation, hue) represent distinct domains. The focus of this research lies in the latter which is developing perceptually meaningful, physiologically grounded descriptions of color appearance rather than color-match specification [2].

Considering the conceptual and practical differences between colorimetry and color appearance models, the central aim of this dissertation is to develop a physiologically based model that is called FCAM, for **F**undamental **C**olor **A**ppearance **M**odel. FCAM proposes a set of one-dimensional, independent perceptual scales that are each derived directly from cone fundamentals to describe color appearance attributes more flexibly than traditional three-dimensional models. These scales are built directly from the cone fundamentals as this is the best way to account for individual variations of visual perception. Also, it is a straightforward way to incorporate chromatic adaptation models into color appearance scales when those scales are formulated based on cone fundamentals.

1.1 A New Colorimetric System

Current color appearance models are based on the CIE XYZ trichromatic system that was the best choice at the time that it was developed. This XYZ-based system has some disadvantages. For example, the $\bar{x}(\lambda)$ function has a bimodal form that has no direct physiological analogue. Also, the $\bar{x}(\lambda)$, $\bar{y}(\lambda)$, $\bar{z}(\lambda)$ functions are defined based on experiments conducted for a group of observers in limited geographical regions. Based on a technical report recently published by CIE [3], it is now required to develop a new colorimetric system that can account for the underlying physiology of the human visual system and also account for the normal variations in human visual perception. A new colorimetric system that is based on the cone fundamentals can fulfill these requirements [3].

"Cone fundamentals" are defined in CIE publications as "the spectral sensitivity functions of the long- (L-), medium- (M-), and short-wave sensitive (S-) cones, measured in the corneal plane" [3]. Individual differences in macular and lens optical densities, photopigment optical densities and spectral shifts in the underlying cone photopigment spectra result in considerable variations in human color vision. Additionally, the spectral sensitivities of the L-, M-, and S-cones vary across the normal population [4]. Developing a new colorimetric system that incorporates these physiological differences is essential for improving color prediction accuracy and for addressing the growing needs for observer-specific rendering in modern imaging technologies. It is time to transfer from the XYZ-based colorimetric systems into LMS-based colorimetric systems.

The transition from the XYZ-based system toward the LMS-based system can involve two different approaches. The first method is to replace the XYZ tristimulus values in a XYZ-based colorimetric formula with equivalent LMS-based tristimulus values. The second approach is to develop new colorimetric scales directly based on cone fundamentals. The second approach is more direct, and better accounts for the individual variations of cone fundamentals [3].

The second approach was taken in this dissertation to introduce a color appearance model. The resulting model, the **F**undamental **C**olor **A**ppearance **M**odel (FCAM), introduces four independent one-dimensional scales:

- **F**undamental **H**ue **S**cale (**FHS**)
- **F**undamental **L**ightness **S**cale (**FLS**)
- **F**undamental **B**rightness **S**cale (**FBS**)
- **F**undamental **S**aturation **S**cale (**FSS**)

These names were chosen for the proposed scales to clearly distinguish them from the XYZ-based scales (as was requested in a recent CIE technical report [3]), as well as to show that they are based on the fundamental CMFs.

FCAM as an LMS-based model is considered to have broad applicability in newly developed displays and projectors that use spectrally narrow-band lights to produce a wider color gamut. Recent technologies have made the problems with observer metamerism far worse and worth revisiting. Personalizing color reproduction through physiologically grounded models can be a potential solution for these emerging problems. It was shown that the use of fundamental CMFs can enhance the accuracy of color reproduction [4].

The following sections discuss the rationale for developing one-dimensional independent scales and for constructing these scales directly from cone fundamentals.

1.2 Proposing One-Dimensional Independent Scales

Color has traditionally been represented within three-dimensional color spaces. The concept of using three-dimensional color spaces to describe the appearance of the color is sometimes misleading. In reality, perceptual color dimensions such as hue, brightness, lightness, saturation, and chroma are often experienced as qualitatively independent attributes. Research suggested representing the color appearance using six one-dimensional color scales instead of one or two three-dimensional color spaces [5].

Three-dimensional color spaces were used as a representation of color stimuli, or color appearance, and to express/calculate perceived color differences using a Euclidean distances, despite an apparent lack of psychophysical evidence that such a space might exist [5]. It should be noted that the CIE does not consider tristimulus values, XYZ, or CIE xy chromaticity coordinates to be a color space. The CIE only uses the color space terminology for CIELAB and CIELUV [2].

Perhaps, the confusion in understanding the concept of color space is related to the definition of "space" outside of physical space–time. In reviewing the definition of "space" provided in dictionaries, it can be claimed that various specifications of color perception or color stimuli can be considered as a "set" or a "collection of measurements". So, arranging some of these collections in various higher-dimensional generalizations can be useful. These organizations of color dimensions are not actually a fundamental description of perceptual processes or helpful in understanding how color perceptions are formed, and the concept of color space does not represent any fundamental property of the human visual system [2].

Our perception of taste, smell, hearing, and touch are not commonly expressed in terms

of multi-dimensional spaces with Euclidean (or similar) difference metrics. These senses are described with independent one-dimensional scales. Similarly, color stimuli can also be described one dimension at a time, like the Munsell system with three independent perceptual dimensions, hue, value, and chroma, and the NCS system with hue, whiteness-blackness and chromaticness. Likewise, color appearance models such as CIECAM02 and CIECAM16 were developed with independent predictors of the six perceptual dimensions of brightness, lightness, colorfulness, saturation, chroma, and hue [5].

FCAM departs from this tradition by explicitly formulating each perceptual dimension as an independent one-dimensional scale, without assuming any underlying three-dimensional geometry. This conceptual independence carries both theoretical and practical advantages. It eliminates the need to enforce artificial uniformity through complex non-linear transforms and allows each scale to be modeled, calibrated, and validated separately using psychophysical data sets relevant to that attribute. From an applied perspective, this framework facilitates modular implementations as applications may use only those scales that are perceptually relevant, such as hue preservation in gamut mapping or brightness control in HDR display.

1.3 Proposing Fundamental Scales

Building the one-dimensional scales directly from cone fundamentals provides the most physiologically consistent representation of human color vision. The LMS cone responses are the primary signals upon which all higher-level perceptual processes depend. Basing appearance scales directly on these responses ensures that the model inherently accounts for individual differences in color vision.

Chromatic adaptation models are also expressed naturally in terms of cone responses. Thus, defining appearance scales as functions of cone fundamentals allows a straightforward integration of chromatic adaptation effects within each scale.

In this research, the one-dimensional independent scales are built directly from cone fundamentals to account for individual variations in color vision, also to incorporate chromatic adaptation models in a straightforward way.

Traditional CMFs, such as the CIE 1931 $\bar{x}(\lambda)$,$\bar{y}(\lambda)$,$\bar{z}(\lambda)$, represent an averaged observer and fail to capture this physiological variability [6]. By contrast, fundamental CMFs ($\bar{l}$,$\bar{m}$,$\bar{s}$) describe the spectral sensitivities of the L-, M-, and S-cones and can be adjusted for individual observers using models such as the Asano–Fairchild observer model [6, 7].

Adopting cone fundamentals also aligns with ongoing efforts in CIE to move toward LMS-

based colorimetry [3]. In addition, a vision model based on individualized CMFs can predict personalized color appearance, which is increasingly important in applications such as head-mounted displays, augmented and virtual reality imaging, and precision color reproduction in professional workflows.

1.4 Color Difference Formulas

Color differences are traditionally computed using the Euclidean distance between two stimuli in a color space such as CIELAB. As these metrics were not well correlated with color difference perception, weighted color difference equations such as CIEDE2000 were derived to provide a more perceptually uniform color difference metric, but they are complicated formulae. Alternatively, users can examine the individual components of the color difference (e.g. ΔL*, ΔC* and ΔH* in CIELAB) instead of "mononumerosis" provided by ΔE metrics. Since no geometrical relationship between the appearance scales has been claimed, the color difference can be calculated individually for one-dimensional appearance scales. This approach can also be extended to appearance dimensions that are not included in color differences such as gloss, texture, noise, flicker, etc [2].

The FCAM framework treats each perceptual attribute as a separate one-dimensional scale. Therefore, differences between two stimuli can be computed independently for each scale. For example, ΔHue, ΔLightness, ΔBrightness, and ΔSaturation without implying any underlying geometric interrelation. This approach mirrors perceptual experience more closely, allowing comparisons and tolerances to be defined per attribute rather than as a single aggregated "ΔE" value.

1.5 Research Objectives and Contributions

This research aims to design and validate a new framework for color appearance modeling that is physiologically grounded, perceptually meaningful, and adaptable to individual observers. Color appearance can be more accurately represented through a set of independent, one-dimensional scales derived from cone fundamentals rather than through traditional three-dimensional XYZ-based color spaces.

1.5.1 Research Objectives

- To develop a new colorimetry system named FCAM for Fundamental Color Appearance Model that defines independent one-dimensional scales of hue, lightness, brightness,

and saturation directly from cone fundamentals.

- To derive mathematical formulations for each fundamental scale (FHS, FLS, FBS, FSS), ensuring simplicity, physiological plausibility, and ease of implementation.
- To evaluate the proposed scales empirically using both historical and newly collected psychophysical data sets, assessing performance in terms of linearity, spacing, and agreement with perceived color appearance.
- To integrate the one-dimensional fundamental scales into a unified, observer-adaptive colorimetric system suitable for modern imaging and display applications.

1.5.2 Major Contributions

- A novel physiologically grounded color appearance model (FCAM) that departs from the traditional XYZ-based, three-dimensional paradigm.
- Definition of four independent fundamental scales (FHS, FLS, FBS, FSS) derived directly from LMS cone fundamentals, each representing a distinct perceptual attribute.
- Development and validation of the Fundamental Hue Scale (FHS) including separate predictors for hue discrimination and hue appearance.
- Formulation of the Fundamental Lightness and Brightness Scales (FLS and FBS) incorporating the surround effects, Helmholtz–Kohlrausch and Stevens effects.
- Formulation of the Fundamental Saturation Scale (FSS) and conceptual definition of colorfulness and chroma in terms of these fundamental attributes.
- Integration of chromatic adaptation models specifically vK20 and Weighted Geometric Mean (WGM) models, within the FCAM framework.

Collectively, these contributions advance the theoretical foundation of colorimetry by bridging the gap between physiological vision science and practical color appearance modeling.

1.6 Dissertation Organization and Publications

This dissertation introduces, develops, and validates the Fundamental Color Appearance Model (FCAM) through a sequence of chapters that progress from conceptual background to empirical evaluation and system integration.

- **Chapter 2** reviews background material on existing color appearance models and the evolution of colorimetry, emphasizing the role of cone fundamentals in modeling human vision.
- **Chapter 3** describes the overall structure of the FCAM framework, including the incorporation of chromatic adaptation models and the general computational workflow.
- **Chapter 4** focuses on the Fundamental Hue Scales (FHS), detailing their derivation, the dual-predictor formulation for hue discrimination and hue appearance, and evaluation using both traditional and newly acquired experimental data.
- **Chapter 5** presents the Fundamental Lightness and Brightness Scales (FLS and FBS), describing their formulation, and psychophysical validation for different viewing conditions.
- **Chapter 6** introduces the Fundamental Saturation Scale (FSS) and discusses how colorfulness and chroma can be defined based on other attributes.
- **Chapter 7** integrates all four scales into a complete LMS-based colorimetric system, providing a coherent framework for computing appearance differences one dimension at a time.
- **Chapter 8** concludes the dissertation, summarizing key findings and outlining potential directions for future research.

1.6.1 Associated Publications

Different sections of this dissertation have been published or submitted to peer-reviewed journals:

- Fundamental Scales of Hue Appearance and Discrimination, Saeedeh Abasi and Mark D. Fairchild, Color Research & Application, 48(6), pp. 673-688, 2023.
- Derivation and Evaluation of Fundamental Hue Scales, Saeedeh Abasi and Mark D. Fairchild, Color Research & Application, 50, pp. 522-541, 2025.
- Changes in Displayed Brightness/Lightness with Stimulus Size, Saeedeh Abasi, Luke Hellwig, Dale Stolitzka, and Mark D. Fairchild, Journal of Imaging Science & Technology, 69(2), pp. 1-11, 2025.

- Fundamental Lightness and Brightness Scales, Saeedeh Abasi and Mark D. Fairchild, Optics Express, 33(21), pp. 44405-44421, 2025.
- Fundamental Color Appearance Model (FCAM), Saeedeh Abasi and Mark D. Fairchild, Preparing to be submitted.

1.7 Summary

In summary, this chapter introduced the motivation, rationale, and objectives of developing a new colorimetric system based on cone fundamentals. The limitations of existing XYZ-based systems and three-dimensional color spaces were identified, leading to the proposal of one-dimensional independent scales that more closely align with the physiology of human vision. The Fundamental Color Appearance Model (FCAM) is presented as a comprehensive approach that unifies perceptual independence, physiological grounding, and observer adaptability within a single model. Subsequent chapters elaborate on the theoretical formulation, experimental validation, and integration of these fundamental scales into a new system of colorimetry.

Chapter 2

Background

This chapter provides the theoretical and historical background necessary to understand the development of the Fundamental Color Appearance Model (FCAM) introduced in Chapter 3. It reviews the evolution of colorimetry from early trichromatic theories to modern color appearance models, examines their limitations, and discusses the role of fundamental color matching functions (fundamental CMFs) in achieving physiologically grounded modeling.

2.1 Traditional Colorimetry

In traditional colorimetry, color is characterized by its match that is a mixture of three lights called "primary lights". Color matching of two stimuli, that are presented in the same context, is made at the level of the cones, and the excitations of the three cone types produced by these two stimuli should be identical [1, 7, 8].

While traditional colorimetry, such as the CIE 1931 system, provides a framework for quantifying colors based on standardized observer responses under strictly defined viewing conditions, it often falls short in accurately describing how colors appear to human observers in varied, real-world environments. So, more sophisticated models known as color appearance models have been developed to extend basic colorimetry to describe how a color stimulus appears to a human observer under diverse viewing conditions [1, 7, 8].

Color appearance models enhance traditional colorimetry to be able to predict the appearance of color stimuli in different viewing conditions rather than color matching evaluation of two stimuli [1].

2.2 Current Color Appearance Models

Color appearance models aim to predict "perceived color" as a characteristic of visual perception using unrelated attributes (such as hue, brightness, and colorfulness), and related attributes (such as lightness, saturation, and chroma), and by incorporating key phenomena such as chromatic adaptation, surround influences, viewing conditions, etc. [1, 9].

Current color appearance models start with the specification of the stimulus and viewing conditions in terms of CIE XYZ tristimulus values. Then, a linear transformation from XYZ tristimulus values to cone responses is usually applied. The data of viewing environment, the absolute luminance level, colorimetric data on the proximal field, background, and surround, and perhaps other spatial or temporal information can be used in different color appearance models. Given this data, a color appearance model generally starts with a chromatic adaptation transformation. The post-adaptation signals are then combined into higher level signals. These signals are then used to develop predictors of different color appearance attributes. This is a general framework for almost all color appearance models. However, each model has its specific features [1].

2.2.1 CIELAB and CIELUV

With the above-mentioned framework of a color appearance model, CIELAB and CIELUV can be defined as two initial color appearance models. CIELAB and CIELUV were introduced in 1976 as perceptually uniform color spaces to address non-uniformity of the chromaticity diagram. Both spaces improve perceptual uniformity over earlier models but they lack accurate chromatic adaptation transformation and they are still limited to describing color under a fixed set of viewing conditions [1, 8]. To overcome these limitations, different color appearance models were designed to account for color appearance phenomena and different viewing conditions.

2.2.2 Complex Models

Robert William Gainer Hunt developed the most extensive, complete, and complex color appearance model. This model is complicated as it was designed to predict a wide range of color appearance phenomena such as Bezold–Brücke hue shift, Helmholtz–Kohlrausch effect, Abney effect, Hunt effect, simultaneous contrast, Helson–Judd effect, Bartleson–Breneman effect, Stevens effect, color appearance changes due to light and chromatic adaptation, and cognitive discounting-the-illuminant. It was also designed to predict the appearance of stim-

uli in a variety of backgrounds and surrounds. It also includes the contributions of rod photoreceptors. Modeling all of these phenomena comes at the price of complexity [1, 10].

Another significant model was proposed by Nayatani et al., building on their own chromatic-adaptation research. This model, similar to the Hunt model, can predict many color appearance phenomena for different viewing conditions [1].

2.2.3 CIE Color Appearance Models

CIECAM97s was introduced as the first CIE color appearance model. CIECAM97s is structurally similar to Hunt's model and incorporates many color appearance phenomena and is applicable for a variety of viewing conditions. Later on, improved models were introduced by CIE such as CIECAM02 and CIECAM16. The CIECAM02 and CIECAM16 models were designed to predict perceptual attributes such as hue, lightness, brightness, chroma, saturation, and colorfulness, under varied viewing conditions. CIECAM16 was developed to address known issues of CIECAM02, specifically in terms of chromatic adaptation transformations, CATs [1, 11].

As CIE color appearance models have strong roots in Hunt's model, some of the disadvantages and ambiguities inherent in the Hunt's model have propagated into these later models. In particular, ambiguities related to the nonlinear relationship between brightness and lightness have remained in CIECAM02 and CAM16. Hellwig and Fairchild critically examined these issues and demonstrated that the nonlinear brightness formulation in CIECAM16 originates from assumptions inherited from the Hunt model. They proposed a revised formulation with a more physically and perceptually meaningful linear relationship between brightness and lightness, followed by updated equations for chroma, colorfulness, and saturation to maintain internal consistency within the model. In subsequent work, Hellwig et al. introduced a model to better account for the Helmholtz–Kohlrausch effect, improving the prediction of brightness changes with increasing chromatic purity. These studies significantly clarified the theoretical structure of CIECAM16 and highlighted the need for revisiting some long-standing assumptions in CIE color appearance modeling. Much research has been done so far to address these issues by introducing new approaches to model color appearance attributes or by modifying the current attributes [12–14]. In addition to these complicated models, simpler color appearance models that are adequate for different applications have been developed such as RLAB and LLAB models [1, 8].

2.2.4 Limitations of Current CAMs

Most current color appearance models for practical applications are built upon the CIE XYZ colorimetry system and inherit its limitations, including a lack of physiological grounding. Considering the lack of accurate CMFs based on cone fundamentals, the CIE XYZ system was the best choice at the time that color appearance models were developed. However, advances in vision science led to introducing CMFs based on cone fundamentals. This progress paves the way for developing new color appearance models based on cone fundamentals. The following section reviews the development of fundamental CMFs as an important achievement. Fundamental CMFs can address limitations of Current CAMs.

2.3 Fundamental Color Matching Functions (CMFs)

Human color vision starts with three uni-variant, color-blind cone types with different spectral sensitivities that are known as the LMS cone photoreceptors. When two lights excite the LMS cone responses identically, they are perceived to match regardless of their wavelength composition. This phenomenon, which is known as metamerism, helped to define the color matching functions, CMFs. The color matching functions, CMFs, were defined as the intensities of the three primary lights required to match test lights as a function of test wavelength. CMFs are often defined for matches that are made to test lights of equal energy [15].

The $\bar{r}(\lambda)$, $\bar{g}(\lambda)$, and $\bar{b}(\lambda)$ CMFs were defined based on this concept using three primary lights. Then, the $\bar{x}(\lambda)$, $\bar{y}(\lambda)$, and $\bar{z}(\lambda)$ CMFs were introduced using the imaginary primaries to avoid negative values in the $\bar{r}(\lambda)$, $\bar{g}(\lambda)$, and $\bar{b}(\lambda)$ CMFs and to provide a larger gamut [15].

The spectral sensitivities of the L-cones, M-cones and S-cones are known as the fundamental CMFs and are notated as $\bar{l}(\lambda)$, $\bar{m}(\lambda)$, and $\bar{s}(\lambda)$ in colorimetry. The fundamental CMFs cannot be stimulated by real primary lights, but they can be calculated by a linear transformation of any sets of CMFs [15]. The CIE preferred to sanction a set of fundamental CMFs, so a 3*3 matrix transformation should be defined to relate the $\bar{r}(\lambda)$, $\bar{g}(\lambda)$, and $\bar{b}(\lambda)$ to $\bar{l}(\lambda)$, $\bar{m}(\lambda)$, and $\bar{s}(\lambda)$ [3, 15].

To define such a transformation matrix, the three cone spectral sensitivities, $\bar{l}(\lambda)$, $\bar{m}(\lambda)$, and $\bar{s}(\lambda)$, should be measured directly. Considering the extensive overlaps in the three cone spectral sensitivities, these measurements become complicated. This issue can be addressed by measuring the cone sensitivities separately [15]. Stockman and Sharpe conducted measurements using color deficient observers who lack one or two of the normal cone types.

They chose the 10-deg CMFs of Stiles and Burch as the best and most comprehensive set of directly measured CMFs to build the new CIE standards. They defined the CIE 10-deg cone spectral sensitivities using Eq. 2.1 [15].

$$\begin{pmatrix} 2.846201 & 11.092490 & 1 \\ 0.168926 & 8.265895 & 1 \\ 0 & 0.010600 & 1 \end{pmatrix} \begin{pmatrix} \bar{r}_{10}(\lambda) \\ \bar{g}_{10}(\lambda) \\ \bar{b}_{10}(\lambda) \end{pmatrix} = \begin{pmatrix} \bar{l}_{10}(\lambda) \\ \bar{m}_{10}(\lambda) \\ \bar{s}_{10}(\lambda) \end{pmatrix}. \tag{2.1}$$

Then, they defined CIE 2-deg cone spectral sensitivities with the same method using macular and photopigment optical densities appropriate for a 2-deg target field. Currently, these are best estimates of the mean normal human cone spectral sensitivities, and they are tabulated as discrete values at 5- and 1-nm steps [15]. The cone spectral sensitivities introduced by Stockman and Sharpe became the basis of the CIE 2006 fundamental CMFs.

Stockman and Rider provided formulas for the above-mentioned discrete values of the three cone spectral sensitivities as continuous functions of wavelength from 360 to 850 nm. These formulae also allow computation of individual cone spectral sensitivities with different macular, lens and photopigment optical densities, and with spectrally shifted hybrid or polymorphic L- and M-cone photopigments that are appropriate for either normal or red-green color vision deficient observers [7].

The cone spectral sensitivities can vary in the population due to variations in the density of the pigment in the lens, in the density of macular pigment at the fovea, and in the axial optical density of the photopigment in the photoreceptor [1, 15]. Asano et al. proposed an observer model with ten physiological parameters to more accurately model individual CMFs [6]. Currently, the most advanced model for representing the parametric individual differences in cone fundamentals is the Asano model [3].

2.4 Modeling Color Appearance Attributes

2.4.1 Hue Modeling

Hue is one of the psychological/perceptual attributes used to describe color. According to the definition of hue, an area is described as similar to one of the perceptions such as the unique hues of red, yellow, green, and blue or their combination. It should be noted that this definition refers to a perceived combination of fundamental hue perceptions, not the physical system used to mix color stimuli [1, 8, 16].

Two types of hue specifications can be defined. The Munsell-type color models that aim to create scales of equal color discrimination, or color differences, and the NCS-type

opponent models that aim to specify colors according to their appearance. Two types of hue scales can be developed based on these two systems; a hue scale for color discrimination purposes which is consistent with Munsell system based on five, equally spaced, principal hues and a hue scale for color appearance consistent with NCS system based on four unique hues as cardinal axes [17]. Neither of these systems are more correct, nor more useful, than the other. They are simply two different approaches to describe human perception of hue. The Munsell-type hue scale is similar to a hue-angle metric such as those of CIELAB and CIECAM16. The NCS-type hue scale is similar to a hue-quadrature metric found as a secondary hue scale such as H in CIECAM16 [11]. It should be noted that these scales apply to the same hue perceptions, but using different approaches to assign numbers to those hues, just as the numbers themselves can be represented on different scales, for example, linear and logarithmic [17].

2.4.2 Brightness and Lightness Modeling

Brightness and lightness are key attributes in color appearance models. Brightness is defined as a perceptual attribute related to the amount of light that is emitting or reflecting from a surface or light source. Lightness is the brightness of an area judged relative to a white or highly transmitting area that is similarly illuminated. The main distinction is that brightness refers to the perception of absolute amounts of light, but lightness is a relative perception [1, 8].

During recent decades, there have been many studies to model these two attributes. Modeling brightness and lightness have some complexities, as these attributes are not a simple function of luminance [18, 19]. Two stimuli with equal luminance can be said to be equally bright under special circumstances, such as having identical spectral distributions or at least being judged to be equal in color and having identical surrounds [20]. The precise relationship between brightness/lightness and luminance has been studied using variety of visual experiments. Based on these studies, perceived brightness increases with the logarithm or with some power (less than 1.0) of stimulus luminance [21].

Brightness and lightness depend on other parameters as well. One of these parameters is the purity, or saturation, of the stimulus. Stimuli with greater purity appear brighter than stimuli with less purity if they are of the same luminance. This effect is known as the Helmholtz–Kohlrausch effect [19]. Another parameter is the background color which has been introduced in some research. For example, Moroney conducted experiments to define and model the relationship between the background color and perceived lightness [22]. Another parameter is the spatial arrangement, which was reported without effect in

some studies and with important effect in other studies. This effect is discussed by Gilchrist in [23]. The stimulus size is also an effective parameter on the perceived brightness, which was found to be important in standardization and quantification of brightness for displays, especially for HDR displays [24], [25]. The effect of stimulus size on perceived brightness was known in early studies and early models of brightness scales [26].

2.4.3 Saturation, Chroma, and Colorfulness Modeling

Colorfulness is defined as attribute of a visual sensation according to which the perceived color of an area appears to be more or less chromatic. Colorfulness of the related colors, with a given luminance factor and chromaticity, increases as the luminance is raised, except when the brightness is very high [1].

Chroma is defined as colorfulness of an area judged as a proportion of the brightness of a similarly illuminated area that appears white or highly transmitting [1].

Colorfulness and chroma are similar to brightness and lightness as chroma can be defined as relative colorfulness, in the same way, lightness can be defined as relative brightness. Also, similar to lightness, chroma stays relatively constant by changing the luminance level [1].

Saturation is defined as colorfulness of an area judged in proportion to its own brightness. Saturation can be thought of as a relative colorfulness, and it is similar to chroma in this case, but saturation is separate from chroma as a unique perceptual experience, because it is the colorfulness of a stimulus relative to its own brightness, while chroma is colorfulness relative to the brightness of a similarly illuminated area that appears white. Chroma can be defined when the stimulus is judged in relation to other colors, while a stimulus seen completely in isolation can have saturation [1].

Within CIECAM16, chroma is defined explicitly. Saturation simply serves as a perceptual correlate normalized by the brightness of the same stimulus. Colorfulness is computed as an absolute correlate proportional to the product of chroma and the adapted luminance factor of the viewing condition.

2.5 Summary

This chapter briefly reviewed the evolution of colorimetry and color appearance modeling, from early trichromatic frameworks to the development of color appearance models. Traditional colorimetry quantifies color matching, whereas color appearance models predict perceptual attributes under varied viewing conditions. While existing CAMs, such as

CIECAM16, successfully predict many phenomena, their reliance on the CIE XYZ colorimetry system limits physiological interpretability and observer adaptability.

Development of fundamental CMFs and observer-adaptive models such as the Asano model now makes it possible to develop color appearance models rooted directly in human visual physiology.

Chapter 3

Structure of Fundamental Color Appearance Model (FCAM)

The aim of this study is introducing a color appearance model with one-dimensional independent scales that are built directly from cone fundamentals. So, it is called FCAM, for **F**undamental **C**olor **A**ppearance **M**odel. These scales are built directly from the cone fundamentals as this is the best way to account for individual differences in the cone fundamentals. The structure of this new color appearance model is explained in the following section.

3.1 Structure of FCAM

The Fundamental Color Appearance Model (FCAM) is designed as a physiologically grounded framework that departs from conventional three-dimensional color spaces, such as CIELAB, by introducing four independent one-dimensional scales that are based on LMS cone responses: Fundamental Hue Scale (FHS), Fundamental Lightness Scale (FLS), Fundamental Brightness Scale (FBS), and Fundamental Saturation Scale (FSS). Scales of colorfulness and chroma can be derived directly from the brightness, lightness, and saturation scales. Unlike traditional models that embed these attributes within a uniform color space, FCAM emphasizes independent scaling, ensuring that each perceptual attribute can be modeled and optimized separately. This approach reflects the idea that hue, lightness, brightness, and saturation are perceptual dimensions rather than axes of a multi-dimensional space, and therefore FCAM does not aim to define a conventional color space.

The input to FCAM is the cone fundamental responses (LMS). These LMS responses can be computed directly using the CIE 2006 fundamental CMFs, or derived from individualized observer functions such as the Asano model, or obtained from the XYZ tristimulus values

through an appropriate transformation matrix. This flexibility allows FCAM to account for both standard observers and individual differences in color vision.

A chromatic adaptation step can be applied as the first stage of FCAM when it is necessary to model perception under different illumination conditions. In this respect, FCAM is compatible with recently proposed adaptation models, such as the vK20 or Weighted Geometric Mean (WGM) model [16, 17].

Once adapted LMS cone responses are calculated, the model proceeds to compute each of the one-dimensional color appearance scales. The overall structure of FCAM is presented in Figure 3.1 and can be described as below:

- Stimulus specification and LMS calculation as the input stage.
- Chromatic adaptation, when included, adjusts these values to the adapted visual state.
- Calculating independent one-dimensional scales of hue, lightness, brightness, and saturation.
- Color difference within FCAM is calculated for each attribute independently.

3.2 Chromatic Adaptation Model

The human visual system uses different mechanisms, including sensory and cognitive processes, to compensate for the color of the prevailing illumination, and to perceive object colors as relatively constant under different lighting. Sensory mechanisms such as retinal gain control are automatic responses to the stimuli. Cognitive mechanisms are based on observers' knowledge of scene content and objects' color. Fairchild showed that sensory adaptation is incomplete, spatially localized, and fast, and cognitive adaptation works better with real-world objects [1].

Several chromatic adaptation models have been introduced that are based on the von Kries model, to predict perceived colors across different media [1]. The von Kries model is reviewed in following section.

3.2.1 The von Kries model

The von Kries hypothesis suggests that adaptation in the three cone types is independent and inversely proportional with the response to a neutral adapting stimulus [27].

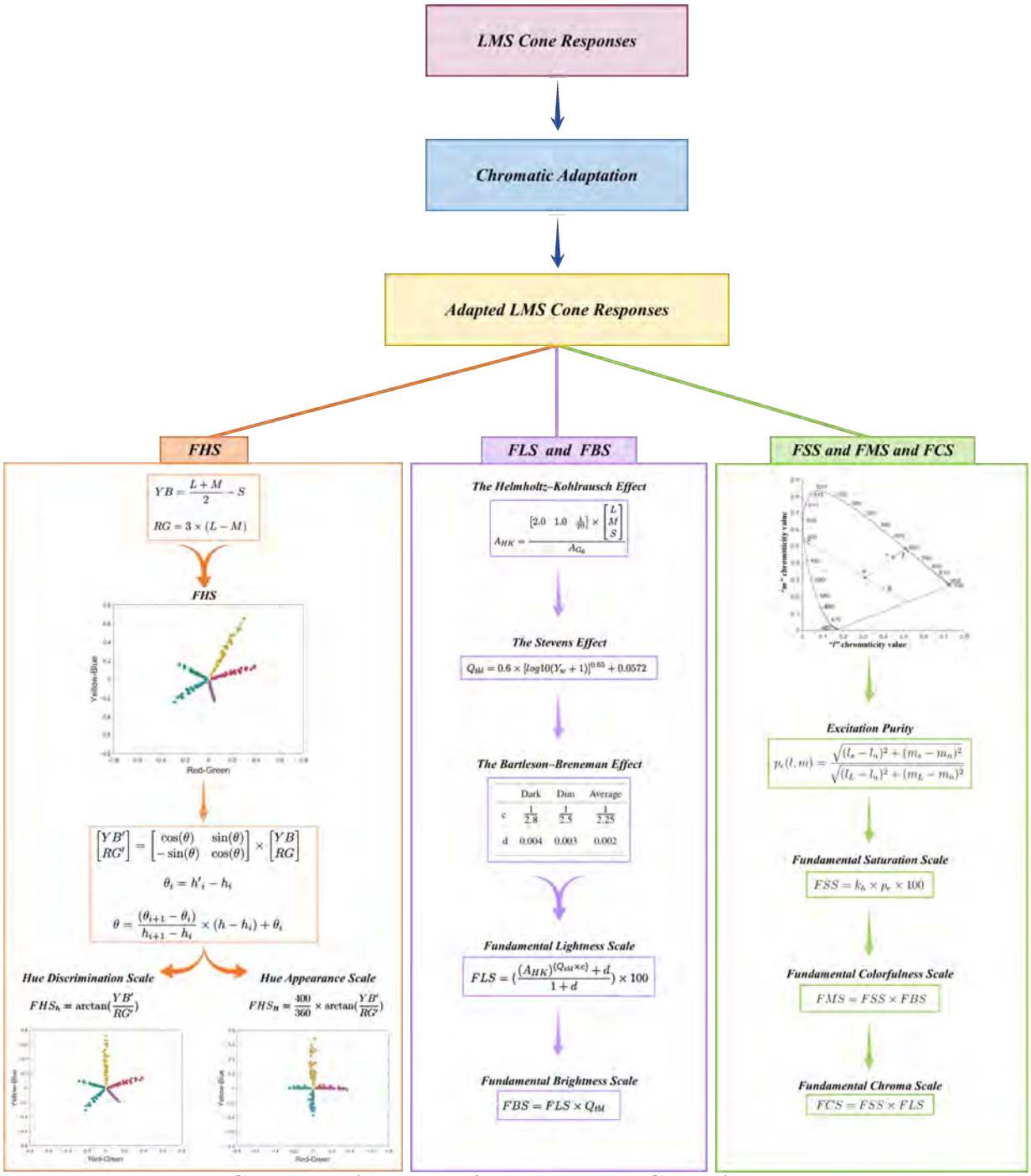

Figure 3.1: Graphical Abstract of Fundamental Color Appearance Model.

The von Kries hypothesis is a conceptual extension Grassmann's laws of additive color mixture to span changes in appearance across differences in illumination color [27].

The von Kries hypothesis was explicitly introduced as the von Kries chromatic adaptation transform that is summarized in Eq. 3.1, where L,M,S are the initial cone responses, L_n, M_n, S_n are the cone responses to the adapting stimulus (it is usually a similarly-illuminated diffuse white) and L_a, M_a, S_a are the post-adaptation cone signals [27].

$$\begin{bmatrix} L_a \\ M_a \\ S_a \end{bmatrix} = \begin{bmatrix} \frac{1}{L_n} & 0 & 0 \\ 0 & \frac{1}{M_n} & 0 \\ 0 & 0 & \frac{1}{S_n} \end{bmatrix} \begin{bmatrix} L \\ M \\ S \end{bmatrix} \tag{3.1}$$

Various chromatic adaptation transformation based on the von Kries model have been proposed. Even the chromatic adaptation transform incorporated in CIECAM02 and CIECAM16 is a simple von Kries model with slight modifications of the spectral definitions of the LMS fundamentals [27].

3.2.2 The vK20 Model

Recent studies suggest that adaptation is incomplete, varies among individuals, and depends not only on the current light source but also on the previous adapting conditions. Based on these findings, Fairchild [27] introduced a modification to the von Kries model, named vK20, which incorporates three adapting chromaticities instead of one. These three chromaticities are the current adapting stimulus, the immediately preceding adapting stimulus, and a newly proposed reference point at approximately 15000K (sky blue).

The structure of vK20 is given in Eq. 3.2, where L, M, S refer to the initial cone responses, L_a, M_a, S_a refer to the post-adaptation cone signals, L_n, M_n, S_n refer to the cone responses for the adapting illuminant, L_r, M_r, S_r refer to the responses for the reference illuminant (taken to be $u' = 0.185$, $v' = 0.425$, approximately 15000K, sky blue), and L_p, M_p, S_p refer to the responses for the previous adapting illuminant. D_n, D_r, and D_p refer to the degrees of adaptation to each of the three adapting chromaticities and must sum to 1.0 [27].

$$\begin{bmatrix} L_a \\ M_a \\ S_a \end{bmatrix} = \begin{bmatrix} \frac{1}{D_n L_n + D_r L_r + D_p L_p} & 0 & 0 \\ 0 & \frac{1}{D_n M_n + D_r M_r + D_p M_p} & 0 \\ 0 & 0 & \frac{1}{D_n S_n + D_r S_r + D_p S_p} \end{bmatrix} \begin{bmatrix} L \\ M \\ S \end{bmatrix} \tag{3.2}$$

Through re-analysis of past experiments and new supporting data, the vK20 model demonstrates improved accuracy in predicting incomplete and context-dependent adapta-

tion, offering a more physiologically plausible framework for understanding human color inconstancy and its application in color appearance modeling. This model can be improved by more accurate definition of 'D' factors that refer to the degrees of adaptation to each of the three adapting chromaticities [27].

3.2.3 The WGM Model

Shen and Fairchild introduced a chromatic adaptation model named Weighted Geometric Mean (WGM) model [28]. Unlike traditional models such as CAT02 and CAT16, WGM uses a geometric mean computation that predicts incomplete adaptation along realistic illumination paths like the Planckian or daylight locus. This approach is physiologically plausible and more accurate than current models, as was evaluated using several data sets. The weighted extension of the model also accounts for various cognitive adaptations, making WGM a simple and robust model [28].

The complete formulation of the WGM model is given in Eq. 3.3, where the weighting term D can be included to represent varying degrees of sensory and cognitive adaptation under different viewing conditions [28].

$$\begin{bmatrix} L_a \\ M_a \\ S_a \end{bmatrix} = \begin{bmatrix} L_n^D \cdot L_r^{1-D} & 0 & 0 \\ 0 & M_n^D \cdot M_r^{1-D} & 0 \\ 0 & 0 & S_n^D \cdot S_r^{1-D} \end{bmatrix} \begin{bmatrix} L \\ M \\ S \end{bmatrix} \tag{3.3}$$

3.2.4 Chromatic Adaptation Model within FCAM

In developing the FCAM model, which is based on cone fundamental responses and designed to account for individual differences in color vision, it is important to include a chromatic adaptation step. Among the available chromatic adaptation models, vK20 [27] and Weighted Geometric Mean (WGM) [28] models are particularly suitable. Together, these models provide both theoretical robustness and empirical accuracy, making them strong candidates to serve as the chromatic adaptation stage within FCAM.

3.3 One-Dimensional Color Scales within FCAM

Some color models describe color perception one dimension at a time rather than incorporating all color perceptions into one multidimensional space [5, 29]. The Munsell system was defined as a system of three independent perceptual dimensions, hue, value, and chroma. Also, the NCS system treats hue separately from whiteness-blackness and chromaticness

[30]. Based on this insight, proposing fundamental, one-dimensional scales of hue, lightness, brightness, and saturation/chroma can be very useful for a variety of colorimetric applications and for better understanding the principles of human color perception.

FCAM explicitly formulates each perceptual dimension as an independent one-dimensional scale, without assuming any underlying three-dimensional geometry. This approach is theoretically and practically advantageous. It eliminates the need to enforce artificial uniformity through complex non-linear transforms and allows each scale to be modeled, calibrated, and validated separately using psychophysical data relevant to that attribute. This framework facilitates modular implementations as applications may use only those scales that are perceptually relevant, such as hue preservation in gamut mapping or brightness control in HDR display.

3.4 Summary

The structure of FCAM emphasizes independent one-dimensional scales for hue, brightness, lightness, and saturation, allowing each perceptual dimension to be modeled and validated separately. This approach avoids the constraints of traditional multidimensional color spaces and supports flexible, modular implementations. Recent chromatic adaptation models such as vK20 and the Weighted Geometric Mean (WGM) were identified as compatible mechanisms for incorporating adaptation into FCAM. Overall, the FCAM framework provides a theoretically robust and practical foundation for modeling color appearance while accounting for individual differences in human color vision.

Chapter 4

Fundamental Hue Scales

Hue can be described with two types of scales for hue discrimination and hue appearance purposes. A fundamental and physiologically plausible model, called *FHS* for **F**undamental **H**ue **S**cales, with both types of hue scales, built directly from cone fundamentals, was proposed in this study.

The first step of the *FHS* model is a simple conversion of the LMS cone responses into the opponent axes. The opponent axes can be converted into a hue discrimination scale using a rotation matrix that is generated based on five principal hues, or they can be converted into a hue appearance scale using a rotation matrix based on four unique hues. The hue discrimination scale is called FHS_h, and the hue appearance scale is called FHS_H.

The proposed hue model was evaluated in terms of linearity, spacing, and hue quadrature using traditional data sets including the Munsell, NCS, Hung-Berns, and Ebner-Fairchild. In addition to the available data sets, three experiments were completed to evaluate the *FHS* model for stimuli with higher saturation and higher luminance levels. Results showed that the *FHS* is successful in terms of linearity, spacing, and hue quadrature prediction. The *FHS* hue scales are mathematically very simple, physiologically and perceptually plausible, and directly based on cone fundamentals to allow easy generalization to individual observers and perform at least as well as more complicated models.

The derivation and evaluation of *FHS* are described in [16, 31], and they are attached in Appendices 1 and 2.

4.1 Introduction

Hue is one of the psychological/perceptual attributes used to describe color. According to the definition of hue, an area is described as similar to one of the perceptions such as the

unique hues of red, yellow, green, and blue or their combination. It is worth noting that this definition refers to a perceived combination of the fundamental hue perceptions, not a physical system used to mix color stimuli [1, 8, 16].

Two types of hue scales, or specifications, can be defined. The Munsell-type color models that aim to create scales of equal color discrimination, or color differences, and the NCS-type opponent models that aim to specify colors according to their appearance. Two types of hue scale can be developed based on these two systems. Neither of these systems are more correct or more useful than the other. They are simply two different approaches to describe the human perception of hue; a hue scale for color discrimination purposes which is consistent with the Munsell system based on five, equally spaced, principal hues and a hue scale for color appearance consistent with the NCS system based on four unique hues as cardinal axes [17]. The Munsell-type hue scale is similar to a hue-angle metric such as those of CIELAB and CIECAM16. The NCS-type hue scale is akin to a hue-quadrature metric as found as a secondary hue scale such as H in CIECAM16 [11].

The *FHS* model with two scales was proposed for hue discrimination and hue appearance purposes in this study. The aims of the *FHS* model are to have a one-dimensional hue scale based on cone fundamentals and to be mathematically easy to implement and straightforward. The *FHS* model was built directly from cone fundamentals as this is the best way to account for individual differences in color vision [6, 15]. Also, the *FHS* aimed to be one-dimensional scale which is very useful for a variety of colorimetric applications and for better understanding the principles of human color perception.

Hue scales can be specifically important in some applications. For example, in the case of image gamut mapping, if hue perception should be preserved while chroma and lightness change, it is useful not to change the perceptual correlates of hue. At least, the hue name of the color must be the same [32, 33]. Hung and Berns showed that four color appearance spaces do not have accurate representations of hue across changes of lightness or chroma [34]. Xiao et al. showed the same for unique hue loci in the CIECAM02. They evaluated the hue invariance properties in the CIECAM02 under different lightness and chroma settings [35].

Hue linearity and constant hue surfaces were investigated by Wang et al. using a wide color gamut and high dynamic range display. The results showed that some hue scales have similar performance in terms of linearity, they have good linearity on some hues and poor linearity on the other hues [36].

Despite the usefulness of existing hue scales, their dependence on the XYZ-based models and their inconsistent hue invariance across changes in lightness and chroma limit their reliability. These shortcomings, together with the need for a hue representation based on the LMS cone responses, motivated the development of the Fundamental Hue Scales (FHS).

The *FHS* development and its evaluations are described in the following sections.

4.2 Color Vision as A Two-Stage Process

Color vision processes can be simply modeled as a two-stage process, starting with three cone receptors (LMS), and then transferring to opponent-color processes (light-dark, red-green, yellow-blue), but the process is not necessarily simple or a direct linear transformation [17, 37].

The second stage involves opponent processing, which was originally inferred based on Hering's observation [38] that included appearance of hues (that some hues are never perceived to occur together, for example reddish-green or yellowish-blue are not hue perceptions found in nature), simultaneous contrast, afterimages, and color vision deficiencies [1, 39]. The opponent nature of the second stage is widely supported by psychophysical [40] and electrophysiological [41] studies, though it is now recognized that the poles of the axes of this cone-opponent stage do not align directly with Hering's four "opponent colors".

The three cone responses can be transformed to cone-opponent responses in a number of ways, including via linear combinations. A variety of linear matrices have been suggested to model the transformation from three cone types to opponent responses. This is an important transformation within the formulation of all color appearance models [1].

The following subsections explain modeling two stages of color vision in order to have a better understanding of these stages within FHS. The analysis of current transformations helped to develop and propose a new cone to opponent transformation within FHS. Then two new scales for hue, one for discrimination and one for appearance, are proposed based on this transformation.

4.2.1 Modeling the First Stage of Color Vision

The first step of modeling color vision is determination of cone spectral sensitivities. Some methods have been developed to reconstruct the cone spectral sensitivities from CMFs by a simple linear transformation [42]. Asano et al. have also proposed a fundamental model, based on the CIE 2006 physiological system of colorimetry that allows direct formulation of cone fundamentals for individual observers [6].

As the first stage, Ebner and Fairchild used the transformation matrix in Eq. 4.1 for developing the IPT model. This linear transformation converts the XYZ tristimulus values into a description that is very similar to the Hunt-Pointer-Estevez cone primaries, and it is normalized to D65 [43].

$$\begin{bmatrix} L \\ M \\ S \end{bmatrix} = \begin{bmatrix} 0.4002 & 0.7075 & -0.0807 \\ -0.2280 & 1.1500 & 0.0612 \\ 0.0 & 0.0 & 0.9184 \end{bmatrix} \begin{bmatrix} X_{D65} \\ Y_{D65} \\ Z_{D65} \end{bmatrix} \tag{4.1}$$

The matrix transformation in Eq. 4.1 could be replaced by the Hunt-Pointer-Estevez, the Guth, or other proper transformations. If those transformations are used, the calculated LMS values should be normalized as illustrated in Eq. 4.2. The Ebner transformation matrix is normalized to D65 and does not need this step.

$$\begin{aligned} L_{\text{nor}} &= 100 \times \frac{L}{L_{D65}} \\ M_{\text{nor}} &= 100 \times \frac{M}{M_{D65}} \\ S_{\text{nor}} &= 100 \times \frac{S}{S_{D65}} \end{aligned} \tag{4.2}$$

In a more complete formulation of a color appearance model, it would be necessary to first convert any tristimulus specifications to corresponding colors under D65 adaptation using an appropriate chromatic adaptation transform. Once such corresponding colors are available, Eq. 4.1 can be used to convert CIE tristimulus values to LMS values. If LMS values are directly available, then Eq. 4.1 becomes unnecessary.

In this study, the cone spectral sensitivity estimates of Stockman and Sharpe [44] sanctioned by the CIE in its 2006 standard were used, which is available in [45]. These LMS cone spectral sensitivities are specified for mean 'standard' observers with normal cone photopigments and average ocular transparencies [7]. Due to the large variability among color-normal populations, it is suggested to use a vision model for individual observers to predict individual CMFs. Asano and Fairchild proposed an observer model with ten physiological parameters to more accurately model individual CMFs [6]. Stockman and Rider also provided formulae for the three cone spectral sensitivities, all as continuous functions of wavelength. These functions reproduce the tabulated discrete CIE2006 cone spectral sensitivities, and allow the easy computation of non-standard cone spectral sensitivities with individual differences in macular, lens, and photopigment optical densities [7]. Any of these models can be used to calculate LMS cone responses as the input of the FHS model.

4.3 Modeling the Second Stage of Color Vision

As mentioned, the second step is transforming the cone responses to an opponent color space. Ebner and Fairchild suggested a model for coding cone responses to opponent axes and named it IPT. They showed that it successfully predicted the constant hue surfaces. They also provided an extensive data set for constant hue surfaces which was used in this study, and referred to as the Ebner data set. The IPT model is presented in Eqs. 4.3 and 4.4. It applies a power function on L, M and S, and then transforms corrected LMS to opponent space. The Ebner data set is shown in IPT color space in Figure 4.1. The transformations from XYZ to LMS and LMS to IPT as well as the nonlinearity were derived empirically to best describe various data sets. They were not established based on any specific physiological concepts. In IPT, P represents a red-green response and T a yellow-blue response [43].

$$\begin{aligned} L' &= L^{0.43}, & L \geq 0 \\ L' &= -(-L)^{0.43}, & L < 0 \\ M' &= M^{0.43}, & M \geq 0 \\ M' &= -(-M)^{0.43}, & M < 0 \\ S' &= S^{0.43}, & S \geq 0 \\ S' &= -(-S)^{0.43}, & S < 0 \end{aligned} \tag{4.3}$$

$$\begin{bmatrix} I \\ P \\ T \end{bmatrix} = \begin{bmatrix} 0.4000 & 0.4000 & 0.2000 \\ 4.4550 & -4.8510 & 0.3960 \\ 0.8056 & 0.3572 & -1.1628 \end{bmatrix} \begin{bmatrix} L' \\ M' \\ S' \end{bmatrix} \tag{4.4}$$

There are several matrices like Ebner-Fairchild that are used to convert the LMS cone responses into opponent axes such as Hunt-Pointer-Estevez [43], Wyszecki and Stiles [46, 47], Pridmore [37], etc. A transformation provided by Stockman and Brainard was interpreted in [47] as a transformation for cone response to opponent dimensions. It is widely accepted as a traditional transformation representing the basic model of color perception. This transformation is presented in Eq. 4.5. It introduces (L – M) for the red-green opponent axis, and (L + M – S) for the yellow-blue opponent axis [47].

$$T_{SB} = \begin{bmatrix} 1 & 1 & 0 \\ 1 & -1 & 0 \\ 1 & 1 & -1 \end{bmatrix} \tag{4.5}$$

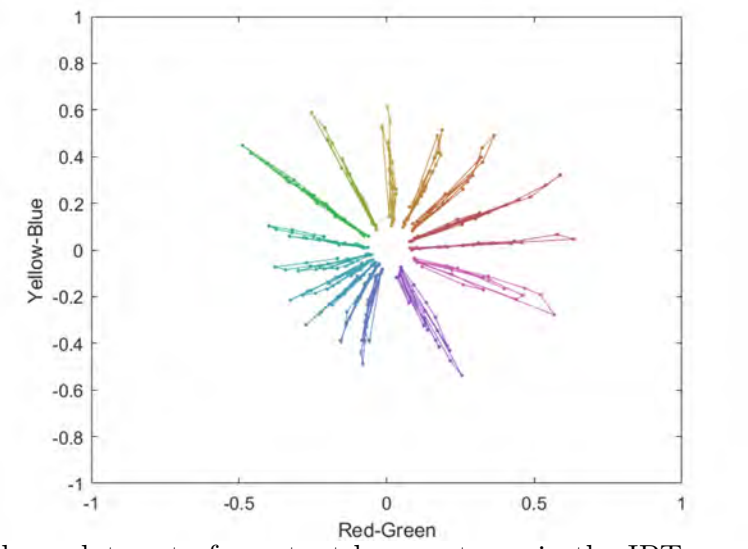

Figure 4.1: The Ebner data set of constant hue contours in the IPT opponent space. Ideal results would be sets of straight lines radiating from the center.

The Ebner data set was used to evaluate Stockman-Brainard transformation. The result is shown in Figure 4.2. As the results show, many hue surfaces overlap and there is inconsistency between the perceived hues and the opponent space values. The middle row of this matrix transformation sums to zero, but the bottom sums to +1. This is the main cause of the inconsistency in the hue predictions. The bottom row would need to be rescaled to something like (0.5 0.5 -1) to represent axes necessary to create a hue scale. It is also likely that some relative scaling between the two axes would be required to more accurately describe hue.

Hunt and Pointer, Wyszecki and Stiles, Pridmore, and other researchers also proposed cone to opponent transformations [47]. These transformations were also evaluated using the Ebner data set. The results are presented in Figure 4.3.

Like IPT, the Hunt and Pointer model has the positive feature that the two chromatic dimensions sum to zero given the appropriate assumption that chromatic adaptation has been accounted for prior to this transformation. Based on the plot, the R-G dimension needs to be scaled up relative to B-Y to more uniformly represent the data, though that will have no impact on the linearity of the hue contours. The R-G dimension in Pridmore model sums to +1 and thus suffers inconsistency issues similar to those found with the transformation attributed to Stockman and Brainard in [47]. The P & T dimensions in IPT transformation matrix summing to zero is what keeps the neutral colors at the origin of the P-T plot, but some transformations proposed for other applications do not have this normalization.

Evaluating these transformations shows that an improved form of cone to opponent

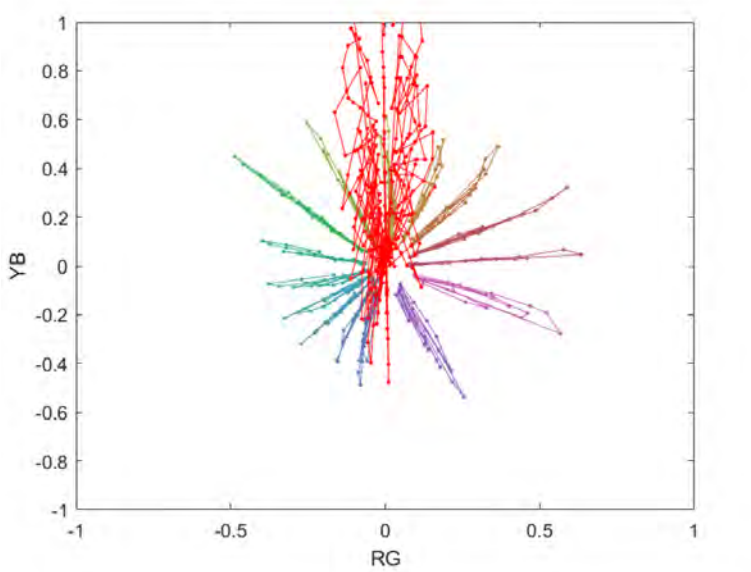

Figure 4.2: The Ebner data set was transformed to opponent axes using two transformations: attributed to Stockman-Brainard in [47] (red) and IPT (colorful).

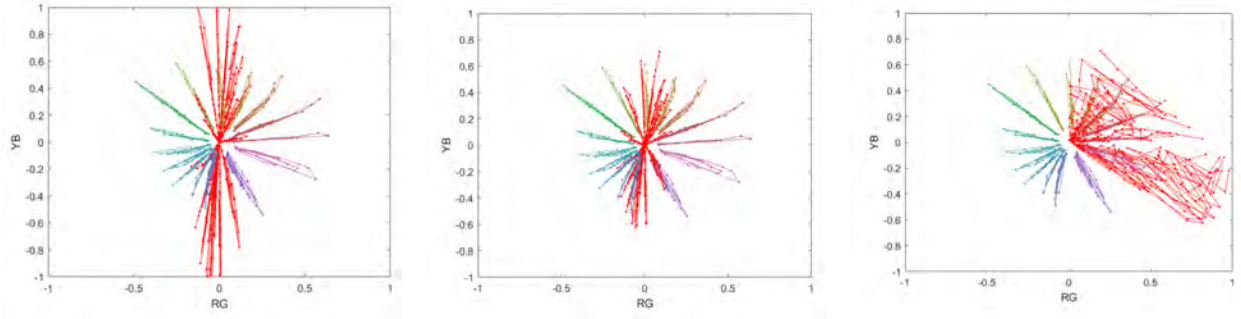

(a) (b) (c)

Figure 4.3: The Ebner data set in (a) Hunt-Pointer opponent axes (red) along with IPT (colorful), (b) Wyszecki and Stiles opponent axes (red) along with IPT (colorful), and (c) Pridmore opponent axes (red) along with IPT (colorful).

transformation is required, and it does appear that a linear cone-to-opponent transformation might be able to predict the constant-hue data. Previously, Jameson and Hurvich proposed that there is a linear relation between chromatic opponent channels and quantal absorption of the three cone photopigments. The data of several studies also supported this idea, but some studies suggest that a nonlinear interaction between the M and L cones is required to fit the yellow lobe of the yellow-blue channel [39]. Development of the new cone to opponent transformation is discussed in the next section. It is the basis of two hue scales, FHS_h for color discrimination and FHS_H for color appearance.

4.4 Initial Model and Initial Data Set

In this section, development of a new transformation that converts cone responses to opponent axes is described. The Ebner and Fairchild transformation was used in this section to transform the XYZ tristimulus values to LMS for all data sets. It is important to note that the corresponding LMS values could be obtained from another model such as CIE 2006 or the Asano model as long as the spectral data of the stimuli are available. The Guth and the Hunt-Pointer-Estevez transformations were used in this section to assess the generalization of the new opponent space.

As a first step, an initial data set was developed using IPT space to understand and explain the relationship between LMS cone responses and perceived hue. Thirty-six equally-spaced hue angles were selected in IPT. For each hue angle, 16 colors with different chroma were selected. The lightness of all stimuli was 0.5 in IPT (I=0.5). All stimuli are shown in Figure 4.4. For each hue angle, there are 16 values for L, 16 values for M and 16 values for S. The stimuli with more chroma have more contrast across the three cone responses.

According to this data set, it can be observed, for example, that when the hue is red, the L cone has the highest amount compared to M and S which are almost zero. For example, the 34th stimulus is red. When perceived hue is yellow, like the 28th stimulus, the amount of L and M cone responses are almost equal each other, and much larger than the S response which is almost zero. For the green stimuli, such as the 20th stimulus, the response of M cone is larger than S and L cones. For the blue hues, such as the 13th stimulus, the amount of the S cone response is the largest and the L cone response is the lowest. The M cone response is also much lower than the S cone and could be largely neglected for simplicity.

This initial data set helps to explain the relationship between the LMS cone responses and perceived hues, and it provides a basis for developing the initial opponent space, and then hue scales.

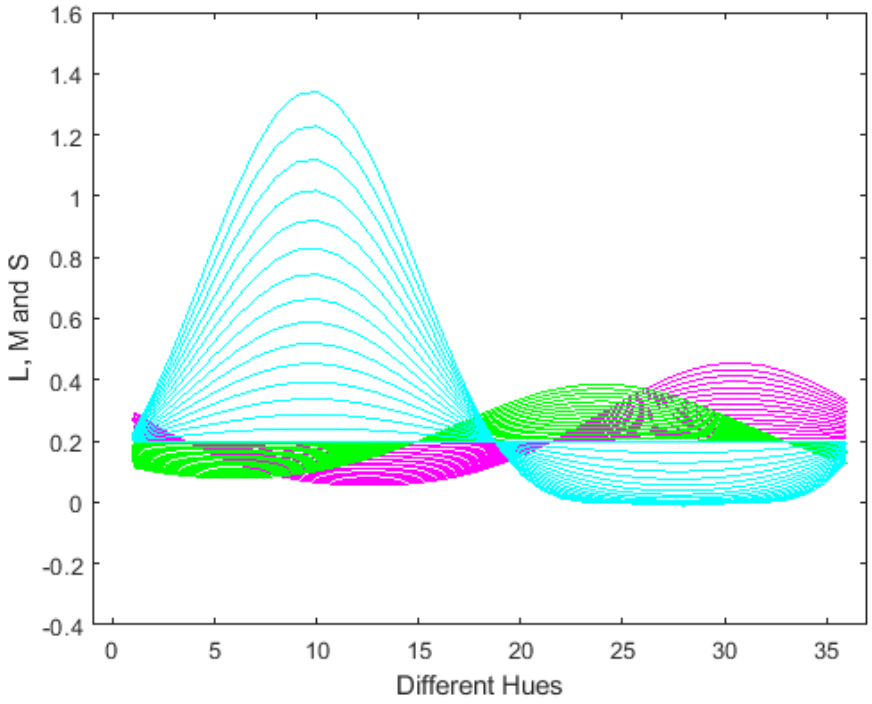

Figure 4.4: The values of L, M and S for different hues.

Based on the initial data set, it can be concluded that for the yellow-blue opponent axis, the L and M cone responses should be opposite to the S response. For yellow hues, L and M are large, and S is small or almost zero. So, $(L+M)$ minus S would be a large positive value for yellow hues. For blue hues, $(L+M)$ is very small or almost zero and S is large. So the $(L+M)$ minus S would be a large negative signal for blue hues. But the $[(L+M)-S]$ formula does not have appropriate scaling for combination of hues. Instead, the $[\frac{L+M}{2}-S]$ should be used to assure that the weighting factors sum to zero. Thus, the yellow-blue opponent dimension could be modeled using Eq. 4.6. It means the average of L and M is a good representation for yellow, and S is a good representation for blue.

$$YellowBlue = \frac{L+M}{2} - S \tag{4.6}$$

For the red-green axis, the L and M responses should be used, without considering the S response. It seems when the hue is red or green, the $(L-M)$ is a good representation for hue. It would be negative for green and positive for red.

For intermediate hues, such as orange, purple, etc., the amount of yellow-blue and red-green axes should be rationale too. According to Figure 4.4, the peak of the S cone response is almost 3 times larger than that of the L and M responses. So, the red-green and yellow-blue axes need to be scaled. For this purpose, the red-green axis should be multiplied by 3.

The red-green opponent axis could be modeled using Eq. 4.7.

$$RedGreen = 3 \times (L - M) \tag{4.7}$$

These two conversions, represented in Eqs. 4.6 and 4.7, that convert cone responses into the opponent axes, became the base of developing the new hue scales that is introduced in the following sections.

4.5 Modeling the Fundamental Hue Scales

In this study, the cone spectral sensitivity estimates of Stockman and Sharpe [44] sanctioned by the CIE in its 2006 standard were used, which is available in [45]. The CIE2006 was used to convert the spectral reflectance into the LMS cone responses. If the spectral reflectance is not available and only the XYZ tristimulus values are available, the Ebner-Fairchild transformation matrix can be used to convert XYZ to LMS. If another transformation such as the Hunt-Pointer-Estevez, the Guth, or other proper transformations are used to convert XYZ to LMS, the adaptation should be considered.

Asano and Fairchild proposed an observer model with ten physiological parameters to more accurately model individual CMFs [6]. Stockman and Rider also provided formulae for the three cone spectral sensitivities, all as continuous functions of wavelength [7]. Any of these models can be used to calculate LMS cone responses as the input of the FHS model.

The main model converts the LMS cone responses into two opponent axes. These opponent axes are called yellow-blue (YB) and red-green (RG). The conversion is presented in Eqs. 4.8 and 4.9. The matrix presentation of *FHS* is provided in Eq. 4.10.

$$YB = \frac{L + M}{2} - S \tag{4.8}$$

$$RG = 3 \times (L - M) \tag{4.9}$$

$$\begin{bmatrix} RG \\ YB \end{bmatrix} = \begin{bmatrix} 3.0 & -3.0 & 0.0 \\ 0.5 & 0.5 & -1.0 \end{bmatrix} \times \begin{bmatrix} L \\ M \\ S \end{bmatrix} \tag{4.10}$$

This step of model is named *FHS*, and it is the basis of two hue scales named FHS_h and FHS_H. It should be noted that the above step was named FHS_h in [16]. As an improvement to have better hue spacing, the above step is considered as the main model, and it is named

FHS in [31]. Then the *FHS* is transformed into two scales which are named FHS_h and FHS_H.

In order to develop the FHS_h scale, the position of stimuli of five principal hues of the Munsell data set were evaluated in the *FHS* opponent space. Based on the evaluation, the *FHS* opponent space is not equally spaced regarding the five principal hues. The axes need to be rotated to have better spacing and better agreement with the position of the five principal hues in the hue circle. Then the hue discrimination scale becomes the hue angle of stimuli in the rotated space, FHS_h.

Also, the yellow-blue and red-green axes in *FHS* are not orthogonal concerning the position of unique hues. So, the opponent axes need to be rotated to have an orthogonal presentation of the unique hues. Then hue appearance can be easily described using the hue-quadrature measure.

For these two purposes, two rotation matrices needed to be designed and applied on the RG and YB axes of Eq. 4.10. The general rotation matrix is presented in Eq. 4.11. A constant amount of θ for all hue surfaces cannot be used in Eq. 4.11, and θ should be a function of hue angle. The position of five principal hues and four unique hues in the *FHS* space should be used to define the rotation matrices of FHS_h and FHS_H.

For the rotation matrix of FHS_h, the hue angle of five principal hues in *FHS* should be determined, which is introduced by h_i in Eqs. 4.12 and 4.13. The desired hue angle for each principal hue is introduced by h'_i. The required angle for rotating each principal hue to make them equally-spaced is the difference between h'_i and h_i calculated by Eq. 4.12. Then the required rotation angle for the combination hues can be found by linear interpolation using Eq. 4.13. The i in Eqs. 4.12 and 4.13 are 1, 2, 3, 4, and 5 for red, yellow, green, blue and purple principal hues, respectively. Each combination hue is between two principal hues, indexed by i and i+1. This model is called FHS_h.

$$\begin{bmatrix} YB' \\ RG' \end{bmatrix} = \begin{bmatrix} \cos(\theta) & \sin(\theta) \\ -\sin(\theta) & \cos(\theta) \end{bmatrix} \times \begin{bmatrix} YB \\ RG \end{bmatrix} \tag{4.11}$$

$$\theta_i = h'_i - h_i \tag{4.12}$$

$$\theta = \frac{(\theta_{i+1} - \theta_i)}{h_{i+1} - h_i} \times (h - h_i) + \theta_i \tag{4.13}$$

For the rotation matrix of FHS_H, the same approach is used. In this case, the hue angle of four unique hues in *FHS* should be determined which is introduced by h_i in Eqs. 4.12 and 4.13. The desired hue angle for each unique hue is introduced by h'_i. The required angle

for rotating each unique hue to make them orthogonal is the difference between h'_i and h_i calculated by Eq. 4.12. Then the required rotation angle for the combination hues can be found by linear interpolation using Eq. 4.13. The i in Eqs. 4.12 and 4.13 are 1, 2, 3, and 4, for unique hues of red, yellow, green, and blue, respectively. Each combination hue is between two unique hues, indexed by i and i+1. This model is called FHS_H.

The hue angle computed from the ratio of YB' to RG' in FHS_h is a Munsell type of hue scale which can be calculated using Eq. 4.14. The hue quadrature computed from the ratio of YB' to RG' in FHS_H is an NCS type of hue scale presented in Eq. 4.15. As hue angle in Eq. 4.14 is between 0 to 360 degrees, in order to have hue quadrature between 0 to 400, the coefficient 400/360 is used in Eq. 4.15.

$$FHS_h = \arctan(\frac{YB'}{RG'}) \tag{4.14}$$

$$FHS_H = \frac{400}{360} \times \arctan(\frac{YB'}{RG'}) \tag{4.15}$$

The position of five principal hues of the Munsell data set in the *FHS* and FHS_h are shown in Figure 4.5. It can be seen that after rotation, five principal hues are equally spaced in FHS_h. The h_i of five principal hues were determined by averaging the hue angle of all stimuli in each principal hue of the Munsell data set in the *FHS* space. The h_i is 18.33, 65.28, 148.00, 219.28 and 282.30 for red, yellow, green, blue, and purple, respectively. The h'_i is 18, 90, 162, 234 and 306 for red, yellow, green, blue and purple, respectively.

It should be mentioned that the spectra of stimuli of the Munsell Book of Color (Glossy Collection) were measured. Only the stimuli with chroma higher than 2 were used as the Munsell data set in this study.

The position of four unique hues of the NCS data set in the *FHS* and FHS_H are presented in Figure 4.6. It is shown that four unique hues are orthogonal in FHS_H. The h_i of four unique hues were determined by the average hue angle of all stimuli in each unique hue of the NCS in the *FHS* space. The h_i is 16.91, 64.82, 146.82 and 228.30 for red, yellow, green and blue, respectively. The h'_i is 0, 90, 180 and 270 for red, yellow, green and blue respectively.

It should be mentioned that the spectra of stimuli of the NCS collection were measured. Only the stimuli with chromaticness higher than 5 were used as the NCS data set in this study.

The structure of the FHS model is presented in the graphical abstract in Figure 4.7 to introduce the model in a easy way.

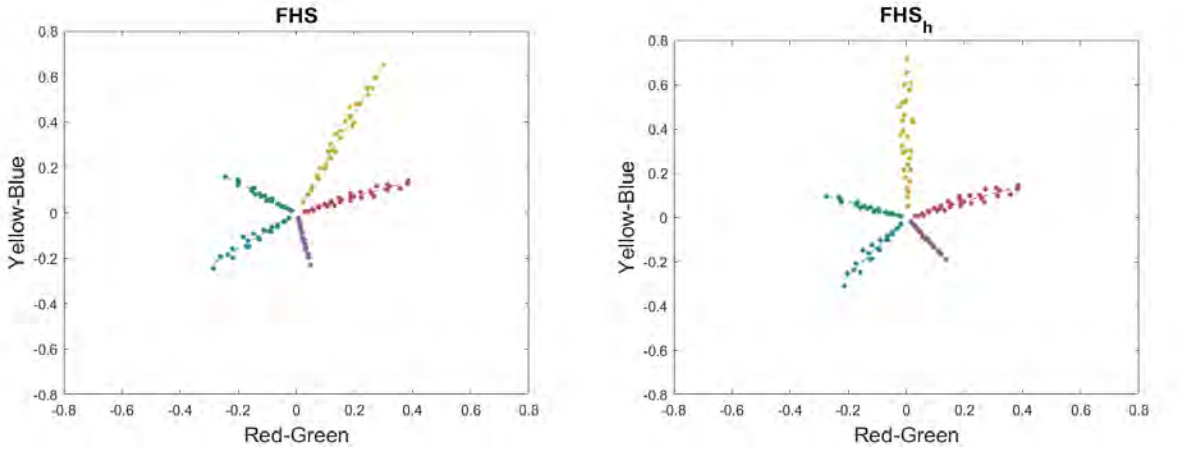

Figure 4.5: The position of stimuli of five principal hues of the Munsell data set in FHS and FHS_h. The hue surfaces in FHS_h (post-rotation) can be compared to FHS (pre-rotation).

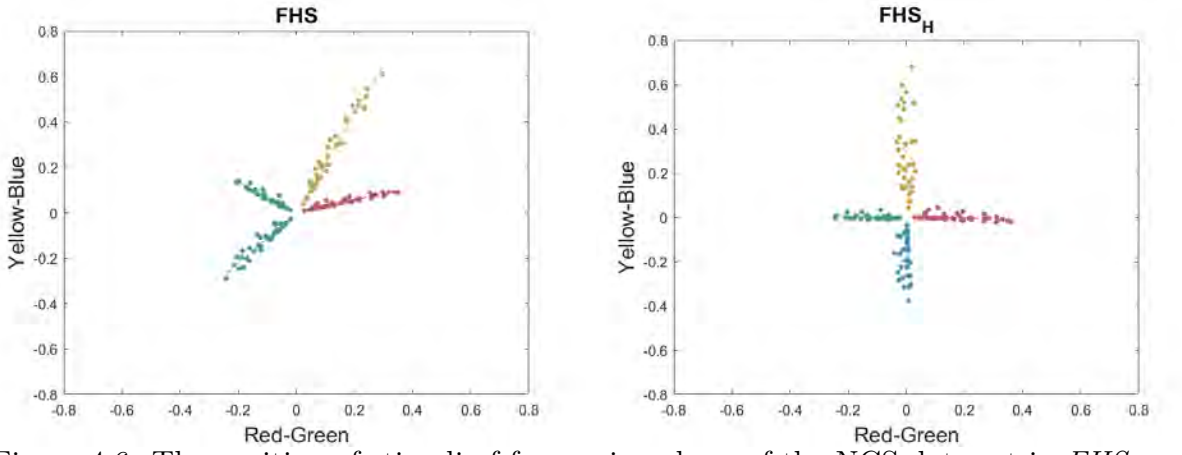

Figure 4.6: The position of stimuli of four unique hues of the NCS data set in FHS and FHS_H. The hue surfaces in FHS_H (post-rotation) can be compared to FHS (pre-rotation).

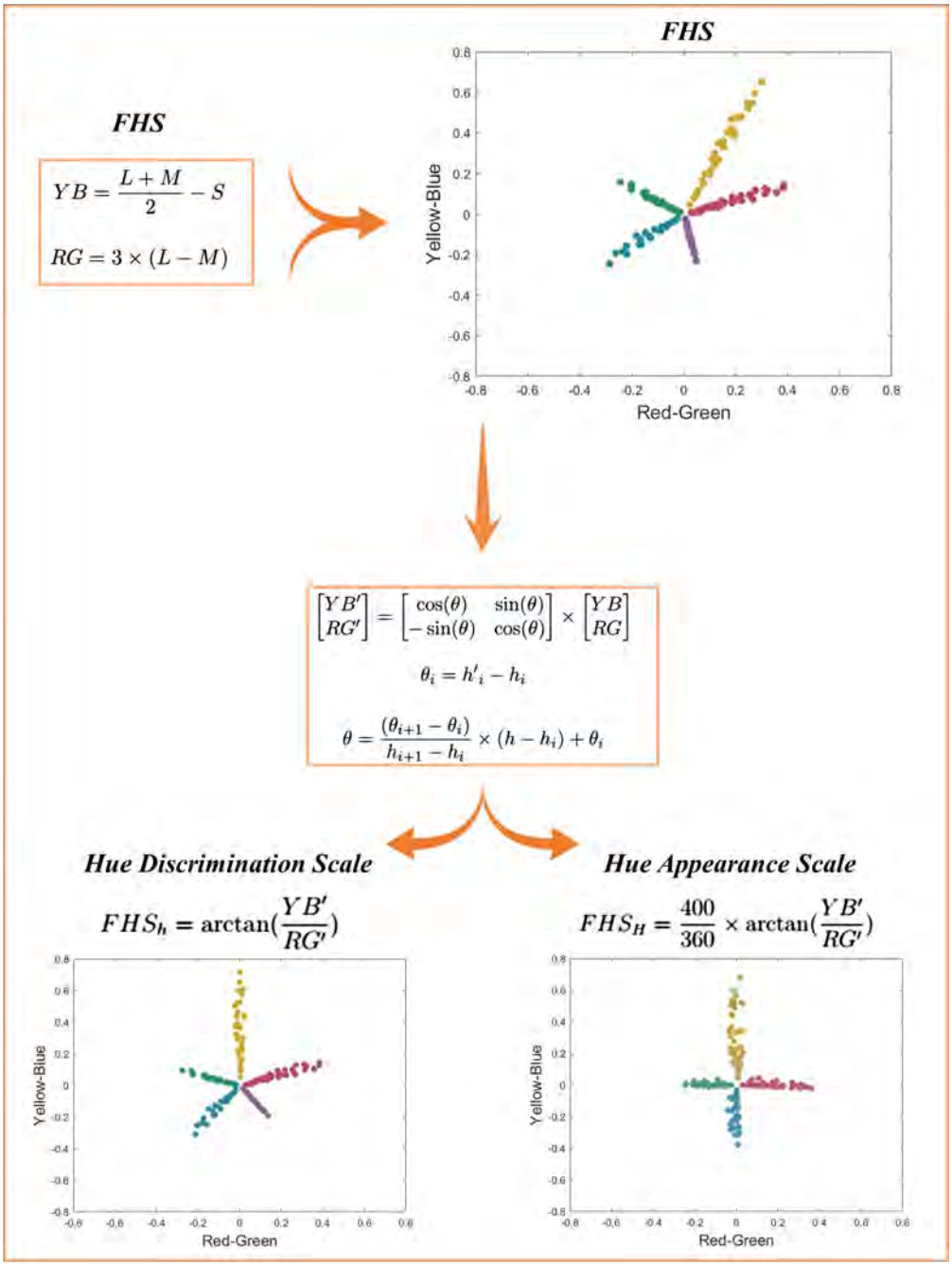

Figure 4.7: The graphical abstract of the *FHS* model.

4.6 Model Evaluation Using Different Data Sets

Hue scales need to be evaluated in terms of linearity, spacing, and agreement with hue appearance. Hue linearity means stimuli with the same perceived hue result in constant model hue output. For example, constant Munsell hue inputs should have equal calculated hue angle. Hue spacing means each constant hue surface as input, on average, results in hue output which is equally spaced from the next hue surface [48]. Also, calculated hue quadrature should have a good agreement with hue appearance description. For example, the assigned hue quadrature to the NCS hue surfaces should be the same as calculated hue quadrature.

4.6.1 Available Data Sets

The linearity of four scales including FHS, IPT, CIECAM16, CIELAB was evaluated using four available data sets including the Munsell, NCS, Hung-Berns and Ebner-Fairchild. The Munsell and NCS were chosen because the stimuli on each hue page of them were defined to have the same hue appearance and they form a constant hue surface. So, these data sets are useful to evaluate the performance of hue scales in term of linearity.

Also, the Hung-Berns [34] and Ebner-Fairchild [32] data sets were used in linearity evaluation because these two data sets have constant hue surfaces, similar to the Munsell and NCS pages. Hung and Berns [34] conducted an experiment using a CRT display and they provided a data set including 132 stimuli that are categorized into 24 loci of constant perceived hue. Ebner and Fairchild [32] conducted a visual experiment using a CRT display, and they provided a data set with 306 stimuli on 15 constant hue surfaces. So, the stimuli in each hue page of the Hung-Berns and Ebner-Fairchild data sets form constant hue surfaces which are useful to evaluate the linearity of hue scales.

The Munsell and NCS stimuli are reflective samples, and the Hung-Berns and Ebner-Fairchild data sets are self-luminous samples. So, it is beneficial to use both types of data sets to evaluate the linearity of the hue scales for reflective samples and self-luminous samples.

The spacing of FHS_h, IPT, CIECAM16, and CIELAB were evaluated using the Munsell data set because it was designed to have equally-spaced hue surfaces. The other above mentioned data sets cannot be used in this step, as they are not designed to have equal space between hue pages.

The NCS data set was used to evaluate the hue quadrature prediction of FHS_H, CIECAM16 and CAM16-Hellwig as this data set was designed based on four unique hues to describe hue appearance. The other data sets were not applicable for hue quadrature evaluation, as they

are not based on four unique hues and equal hue quadrature steps.

It should be mentioned that the spectra of stimuli of the Munsell Book of Color (glossy collection) and the NCS collection were measured using an X-Rite i1 profiler. Only the stimuli of Munsell with chroma higher than 2 and the stimuli of NCS with chromaticness higher than 5 were used as the Munsell and NCS data sets in this study. (All data sets are available in the Supplementary Files.) The measured reflectance of the Munsell and NCS samples were converted into the CIEXYZ tristimulus values for the 2-degree observer to be used in IPT, CIECAM16 and CIELAB. Also, the measured reflectances were converted into the LMS cone responses for the 2-degree observer using the cone spectral sensitivity estimates of Stockman and Sharpe (CIE2006) [44] to be used in the FHS model.

4.6.2 New Data Sets

It should be noted that the mentioned data sets in Section 4.6.1 have limited saturation and luminance, also relatively small color gamut. It is required to evaluate the performance of the FHS model for higher saturation, higher luminance, and in larger gamut as well. The Hung-Berns and Ebner-Fairchild data sets were provided using CRT displays. Considering the larger gamuts of new displays, specifically HDR and WCG displays, it is important to have data sets with larger gamuts. Therefore, the performance of the FHS model was evaluated for the new displays, and for the higher saturation and luminance levels. The FHS model should have a good hue linearity, spacing, and hue quadrature for wider gamuts and higher saturation and luminance.

Three experiments were conducted to generate the required data sets to evaluate linearity of the main scale (FHS), spacing of the discrimination scale (FHS_h), and hue quadrature of the appearance scale (FHS_H). As evaluation of linearity, spacing, and hue quadrature have different requirements, three experiments were conducted which are explained in the following sections.

All experiments were conducted under the same condition and the same setup. A Sony PVM-X3200 display was used to illustrate the stimuli in all experiments. The experiments were implemented using Psychtoolbox on MATLAB, which was controlled using a Windows computer with an Nvidia GeForce RTX 3070 GPU. All stimuli were illustrated on a random noise background that was generated randomly in each trial. The average lightness of background was 50 (J in CIECAM16) with a maximum luminance of 775 cd/m^2. The noise pattern was used to reduce the effect of simultaneous contrast and afterimage. The experiments were done in a darkened room and the display desk was covered with a black fabric to minimize reflections.

4.6.2.1 Constant Hue Surface Experiment for Linearity Evaluation

The first experiment was conducted using the method of adjustment. The aim of this experiment was to find constant hue surfaces to assess the linearity of *FHS* scale. In this experiment, there were two samples in each trial: a test sample and a target sample. Observers were asked to adjust the hue angle of the test stimulus to match its hue with the hue of the target sample. Eight hue angles for the target sample were chosen from the NCS data set including four unique hues and four intermediate hues. For each of these eight hue angles, twelve test stimuli with a variety of luminance and saturation were generated, different from those of the target sample. The luminance and saturation of the test stimuli were chosen in a way to have well-distributed test stimuli. In this experiment a total of 96 stimuli were examined.

The experiment was performed in a darkened room and the desk was covered by a black fabric to eliminate unwanted reflections. The distance between observer and the display was 120 cm, which was an empirically comfortable distance for observers, they did not need to move their heads to compare test and target stimuli in this distance. The sample size was adjusted to be 4° FOV. The experiment was repeated three times in three sessions, and 96 stimuli were examined in each session. The stimuli were presented in random order. Observers should adjust the hue angle with left and right buttons until the hue of the test sample matches the hue of the target. A screenshot of a trial is presented in Figure 4.8 along with a photo of the experimental setup. There were five small samples on top row of the screen as guidance. If observers wanted to know what hue they will see, by pressing the left and right buttons, they can look at those stimuli. For example, in Figure 4.8, if a observer wants to go greener, they should press left button. Seven observers participated in this experiment who were students or faculty of Munsell Color Science Laboratory at RIT. They all had normal color vision. Totally, there were 96 stimuli. The experiment was repeated three times in three sessions.

4.6.2.2 Equally Spaced Experiment for Spacing Evaluation

The second experiment was conducted to assess the spacing between the constant hue surfaces in the FHS_h scale. In this experiment, observers were asked to adjust the hue difference between two samples to be equal to the hue difference of a target pair. The target pair was the same in all trials to be sure that the hue difference of the target stimuli was identical in all trials. The hue angle of the five principal colors and five intermediate colors from the Munsell data set were chosen for test stimuli. It should be noted that only the hue angle is chosen based on five principal and five intermediate hues of the Munsell data set, but the

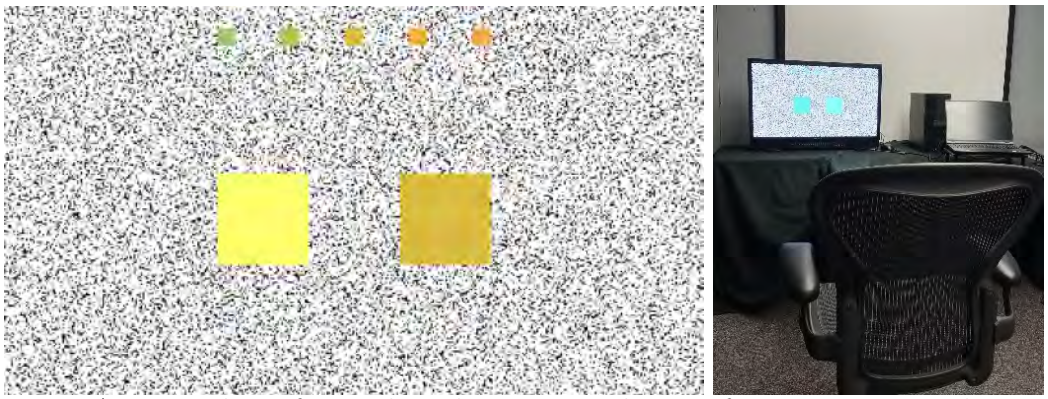

Figure 4.8: A screenshot of a trial in the constant hue surface experiment along with a photo of the setup (the setup was the same for all experiments).

luminance and saturation of samples are different from those of Munsell samples. There were nine stimuli with different luminance and saturation in each hue angle, so a total of 90 samples were judged by each observer. The experiment was repeated three times for each observer and there was a rest between each repetition. Eight observers participated in this experiment who were students or faculty of Munsell Color Science Laboratory. They all had normal color vision. The experimental setup was the same setup in Section 4.6.2.

A screenshot of a trial is shown in Figure 4.9. The position of the target pair was fixed at the left side of the screen, and the test pair was at the right side in all trials. The test pair were presented randomly. The color attributes of two test samples were equal at the beginning, then observer can change the hue angle of top sample of the test pair until its hue difference with the bottom sample becomes equal to the hue difference of the target pair. Then they can go to the next stimuli. There was a small cyan circle in the middle of the screen which observers look at when moving their eyes between pairs. It provides a short pause when moving eyes from one sample to another, this short rest for eyes reduces the after-image effect sometimes caused by direct comparison of one stimulus pair with the other without resulting in fixation on the noise background.

Totally, in the second experiment, there were 90 pairs. Eight observers participated. The experiment was repeated three times in three session.

4.6.2.3 Intermediate Hue Experiment for Hue Quadrature Evaluation

The third experiment was conducted using the method of adjustment to evaluate the hue quadrature of FHS_H scale. This experiment had two steps. The first step was running an experiment to find the unique hues of each observer. Unique hues were defined by Hering as hues of four fundamental chromatic percepts regardless of saturation and lightness. Unique

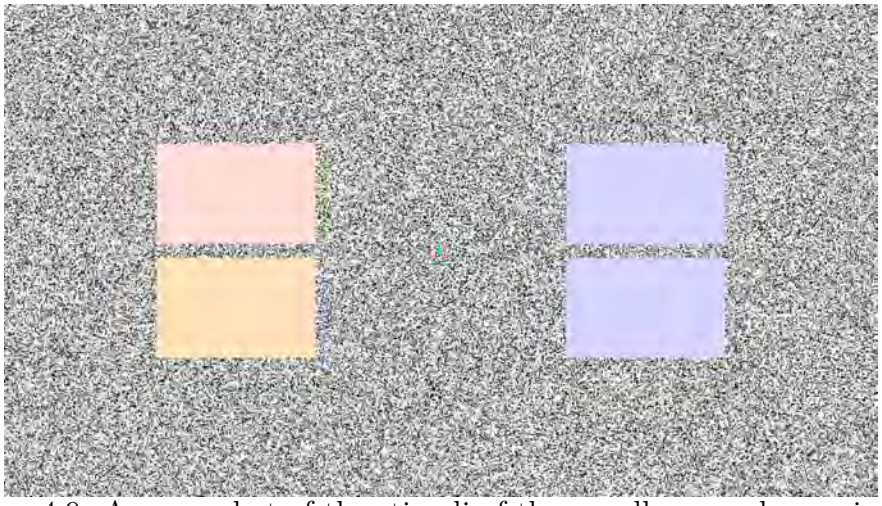

Figure 4.9: A screenshot of the stimuli of the equally spaced experiment.

yellow and unique blue are defined as colors perceived without redness or greenness. Unique red and unique green are defined as colors for which the yellow-blue opponent channel is at equilibrium. Experimentally, unique hues are obtained by asking observers to adjust or select the stimulus that contains neither of other adjacent unique hues [35].

In this step of experiment, there was a sample in the middle of the screen and observers were asked to adjust the hue angle of sample by left/right button until they find their own unique hues. The luminance and saturation of samples were fixed. A screenshot of a trial is shown in Figure 4.10(a). There were three small circles at the bottom of the screen for guiding observers; the central hue is the requested hue in each trial, the left/right hue indicates the hue appearance resulting if they press left/right button. In this step, 24 stimuli were examined by observers, six stimuli with different luminance and saturation for each unique hue. The trials were repeated three times for each observer.

The second step was another experiment to find the intermediate hues based on the unique hues of each observer from the first step. A screenshot of a trial is shown in Figure 4.10(b) in which observers were asked to adjust the hue angle of the central sample until the perceived hue of it is an equally-mixed (intermediate) of those two unique hues at left and right. It should be noted that unique hues of each observer from the first step were averaged for each observer, and four unique hue angles were calculated for each observer. Those four hue angles were used to generate the samples at left and right for this experiment. So, the samples at left and right had specific hue angles for each observer but luminance and saturation were the same for all observers. Twenty-four stimuli, six stimuli for each intermediate hue, were examined by observers with three repetitions. Ten observers participated in this experiment who were students or faculty of Munsell Color Science Laboratory. They all had normal

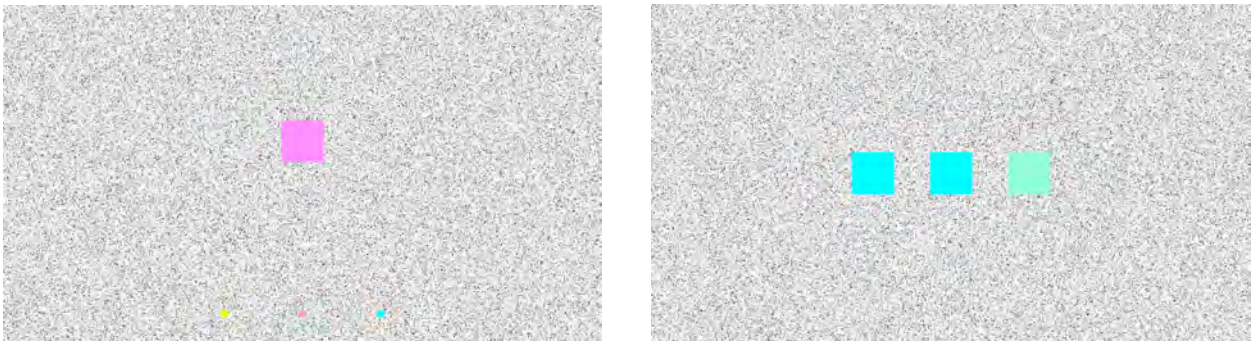

(a) (b)

Figure 4.10: Two screenshots of the hue quadrature experiment; a) The sample in the first step of experiment, b) The samples in the second step of experiment.

color vision.

Totally, in the third experiment, there were two steps. There were 24 samples in each step. Ten observers participated in the first step, then the same observers completed the second step based on their own unique hues. The experiment was repeated three times in three session for each step.

4.7 Results

The results of model evaluation using available data sets and new data sets are presented in this section and analyzed in Section 4.8.

4.7.1 Results of Evaluation with Available Data Sets

The results of evaluation using available data sets are presented in the following subsections in terms of linearity, spacing and hue quadrature prediction.

4.7.1.1 Results of Linearity with Available Data sets

The linearity of four scales including FHS, IPT, CIECAM16, CIELAB was evaluated using four available data sets including the Munsell, NCS, Hung-Berns and Ebner-Fairchild. The standard deviation of the hue angles of the stimuli having the same hue appearance is a metric that has been used to characterize the hue linearity. It quantifies the variations of the hue angles from the average [36]. The standard deviation (SD) of stimuli in each hue surface of all available data sets are calculated for different hue scales. The results are presented in Figures 4.11-4.14. Each figure shows the SD of hue angles of hue surfaces for a data set which were calculated using four hue scales. Also, the stimuli of eight hue surfaces of the

NCS data set and ten hue surfaces of the Munsell data set are presented in Figures 4.15 and 4.16 using four hue scales to show the linearity of each hue scale.

It can be seen in Figures 4.11-4.14 that there are considerable overlaps among hue scales for all data sets. These overlaps show similar performance of hue scales in terms of linearity. All hue scales have good linearity for some hue surfaces and poor linearity for other surfaces. This poor linearity can be related to weakness of hue scales in modeling those regions, or it can be related to some systematic errors in the data sets. For example, blue-green hues in the NCS data set in Figure 4.11 have ups and downs for adjacent hue surfaces and all hue scales have very good linearity for one hue surface and moderate linearity for the next hue surface. It seems to be due to the method of producing samples of these pages as there are less samples on those hue surfaces with very good linearity. There are 23, 14, 12 and 23 samples in B20G, B40G, B60G, and B80G pages in the NCS atlas that was used, respectively. When there are fewer samples on a hue page, there is less variation among luminance and saturation on that page, which causes less variation in the predicted hue angles. On the other side, there are 39, 39, 44 and 35 samples in B10G, B30G, B50G and B70G pages, respectively. More samples on a page means more luminance and saturation levels on that page which can cause larger variation in the predicted hue angles. The same overlaps and similar performance can be seen for other data sets as well, especially the Munsell data set. The third reason that may cause poor linearity of some hue surfaces of all data sets is larger variation among observations for those hue surfaces. As determining stimuli with the same hue appearance is more difficult and more challenging for some hues, which can cause larger hue variation of those hue surfaces. For example, there are larger SDs in blue hues in Figures 4.11-4.14, which shows poor linearity of those hues in all four data sets. This can be due to larger variation among individual's observations in constant hue surfaces for blue hues.

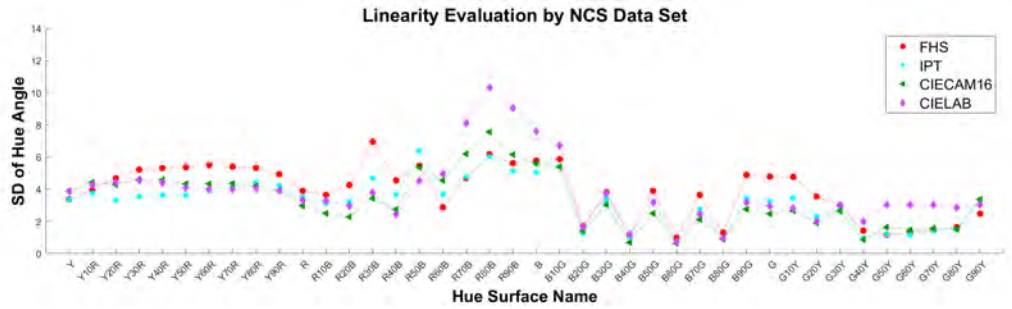

Figure 4.11: Results of linearity evaluation using the NCS data set. Abscissa is the hue surface name. Ordinate is the standard deviation of hue angles of the stimuli in each hue surface. Each plot presents the SDs calculated for a hue scale.

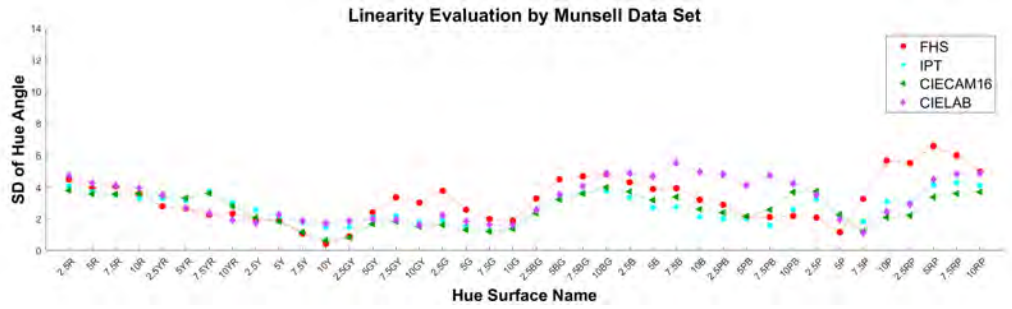

Figure 4.12: Results of linearity evaluation using the Munsell data set. Abscissa and ordinate are those of Figure 4.11. Each plot presents the SDs calculated for a hue scale.

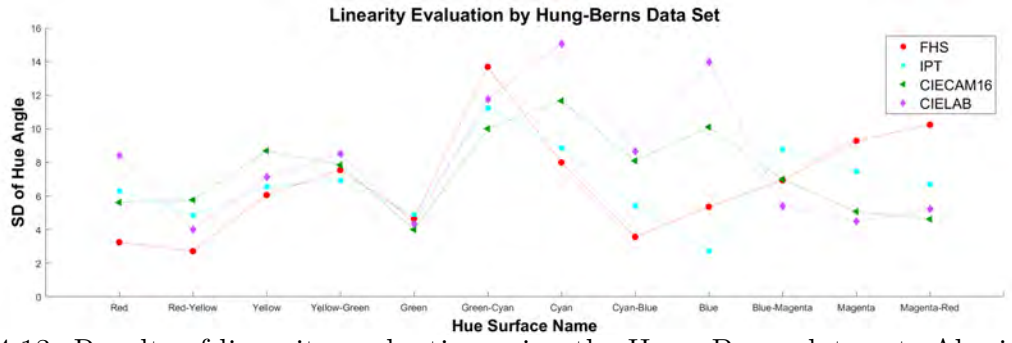

Figure 4.13: Results of linearity evaluation using the Hung-Berns data set. Abscissa and ordinate are those of Figure 4.11. Each plot presents the SDs calculated for a hue scale.

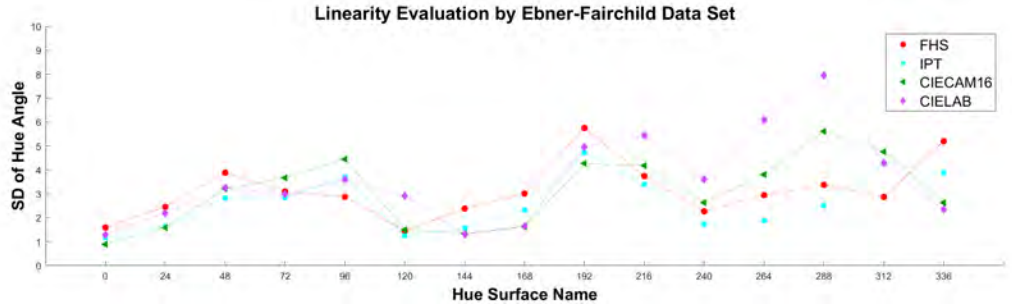

Figure 4.14: Results of linearity evaluation using the Ebner-Fairchild data set. Abscissa and ordinate are those of Figure 4.11. Each plot presents the SDs calculated for a hue scale.

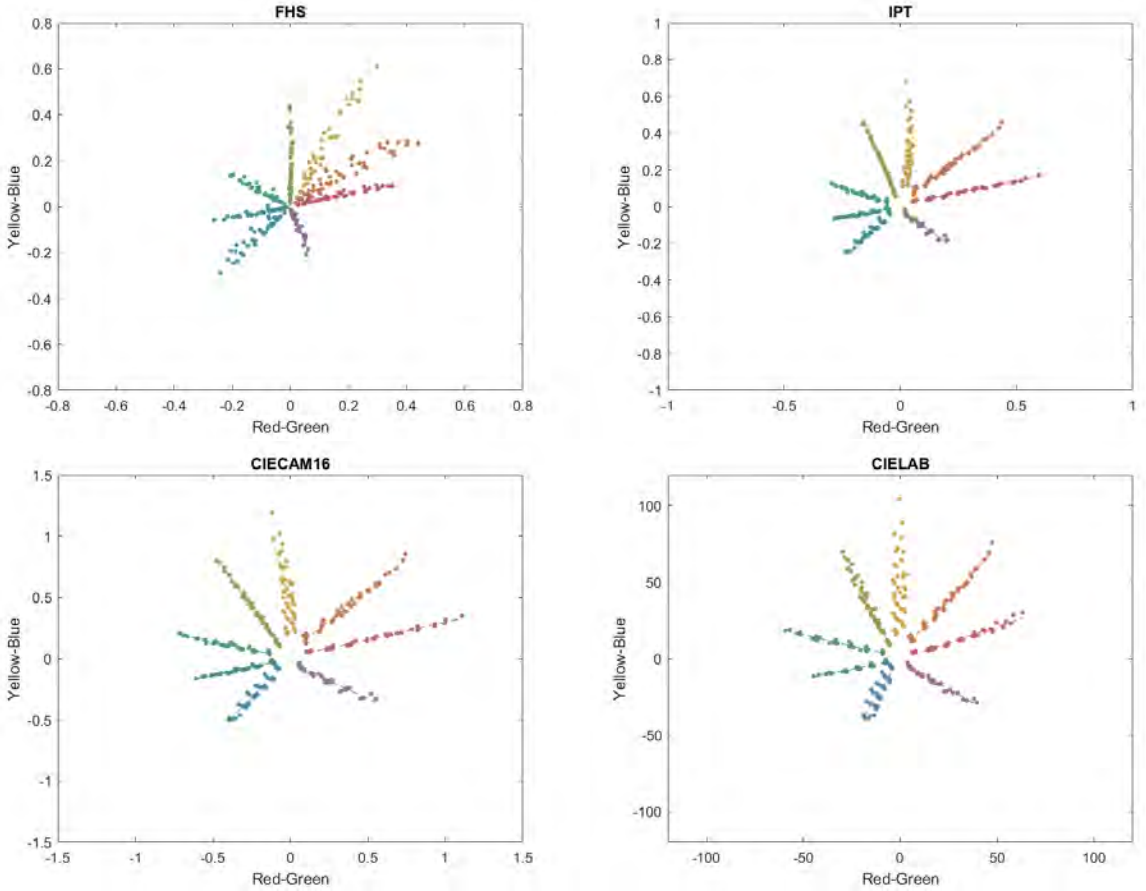

Figure 4.15: The stimuli of eight hue surfaces of the NCS data set plotted in four hue scales. The colors of plots are approximated from the stimuli.

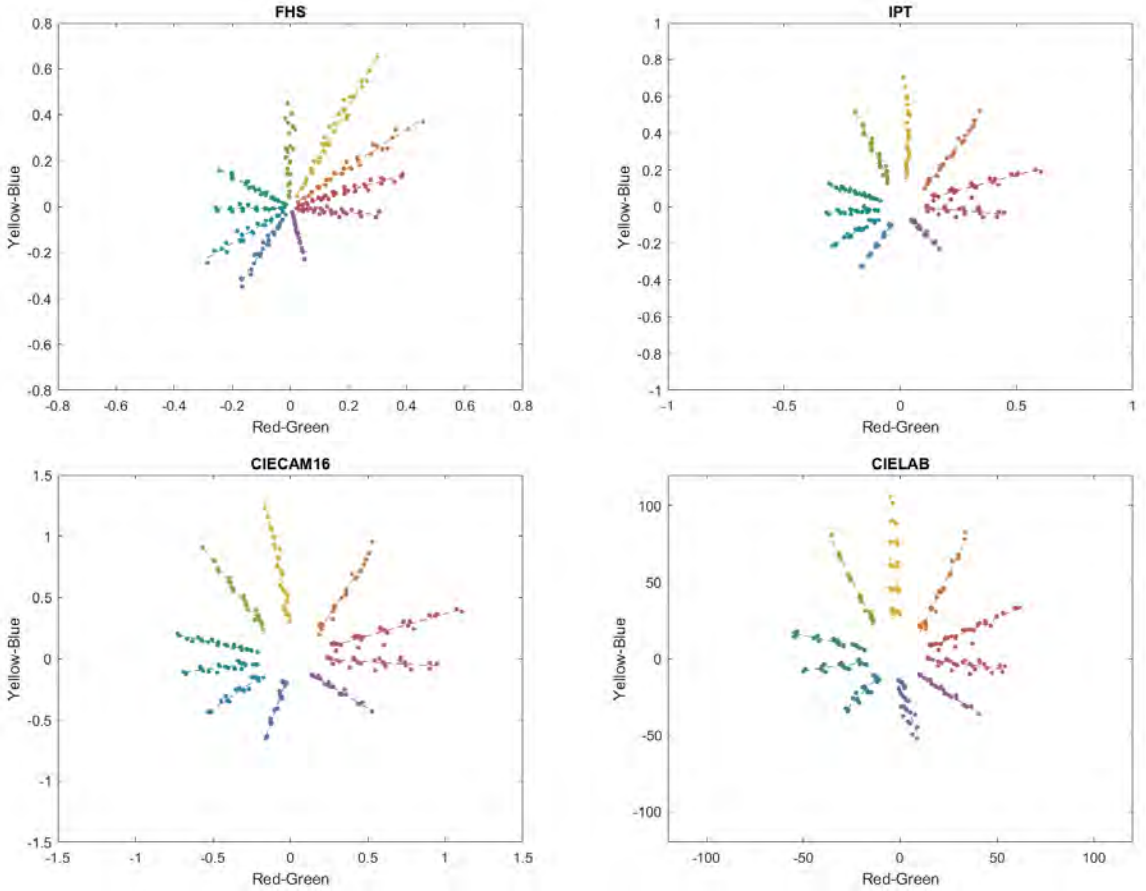

Figure 4.16: The stimuli of ten hue surfaces of the Munsell data set plotted in four hue scales. The colors of plots are approximated from the stimuli.

4.7.1.2 Results of Spacing with Available Data sets

The spacing of the FHS_h, IPT, CIECAM16, and CIELAB scales was evaluated using the Munsell data set because it was designed to have hue surfaces which are equally spaced from the adjacent hue surfaces.

In this evaluation, the assigned hue angle to each hue surface of the Munsell data set was considered as a reference hue angle. For example, the hue angle of 2.5R page is 9 degrees, 5R page is 18 degrees and so on. The hue angle difference between a reference and predictions of four hue scales was calculated for stimuli on that page. If a scale has a successful spacing, the hue angle difference between predictions and reference points should be almost zero. If there is good spacing but assigning hue angles is different from those of Munsell pages, then hue differences between predictions and references are not zero, but similar value for all hue surfaces. The results are presented in Figure 4.17. There is a horizontal line in each plot to make comparison easy. Each sample is presented with a point. As it is shown in the plots, the hue angles of some samples are larger than the reference hue angle and some hue angles are smaller. It means none of the hue scales have spacing as good as the Munsell pages. This poor spacing can be due to poor linearity of some hue surfaces, as linearity has an effect on spacing.

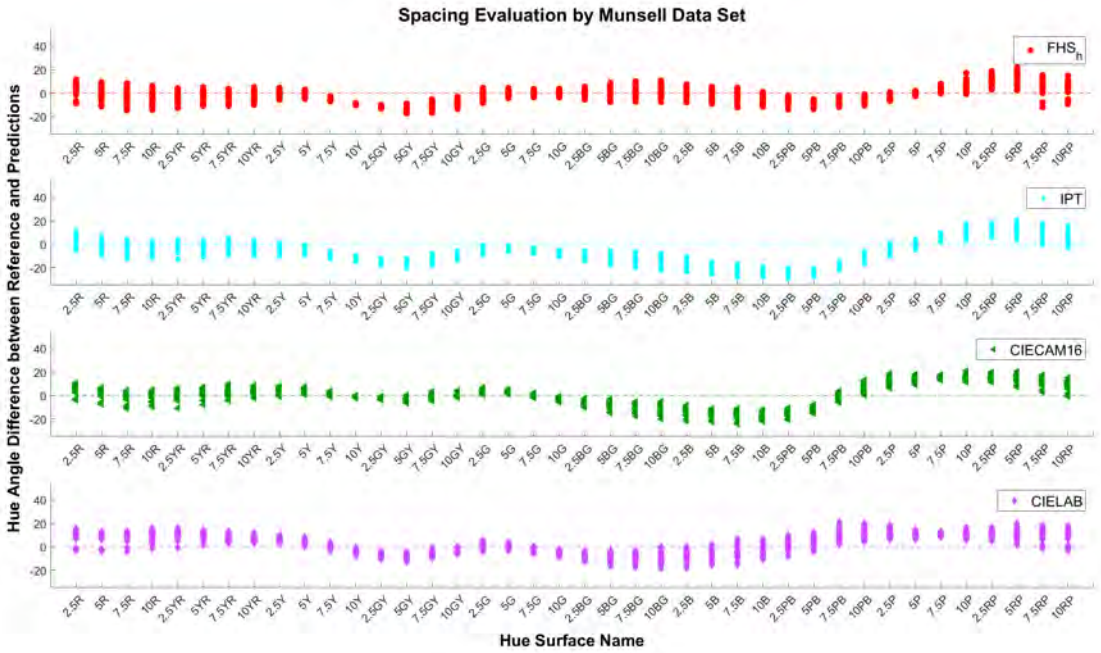

Figure 4.17: Results of spacing evaluation using the Munsell data set. Abscissa is the hue surface name. Ordinate is the hue angle difference between reference and predictions.

The root mean square error (RMSE) of the hue angle differences between the stimuli and corresponding reference angle were calculated for each hue surface of the Munsell data set which is presented in Figure 4.18. RMSE measures the average difference between the model's prediction values and the actual values. In this case, the actual values were considered to be the reference angle of each hue page. And, the model prediction is the predicted hue angle.

Also, the stimuli of the ten hue surfaces of the Munsell including the five principal and the five intermediate hues are presented in Figure 4.19 only for the FHS and FHS_h. The spacing of scales in Figure 4.19 can be compared with the other scales in Figure 4.16.

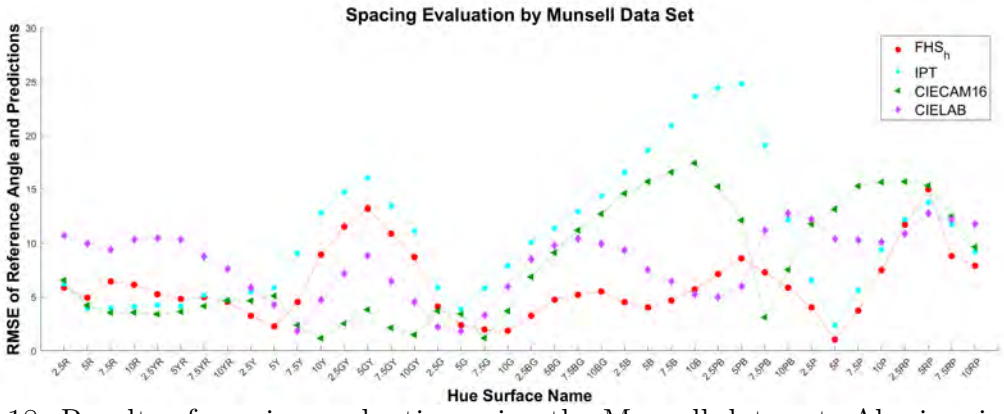

Figure 4.18: Results of spacing evaluation using the Munsell data set. Abscissa is the hue surface name. Ordinate is the RMSEs of reference hue angle and predictions. Each plot presents the RMSEs calculated by a hue scale.

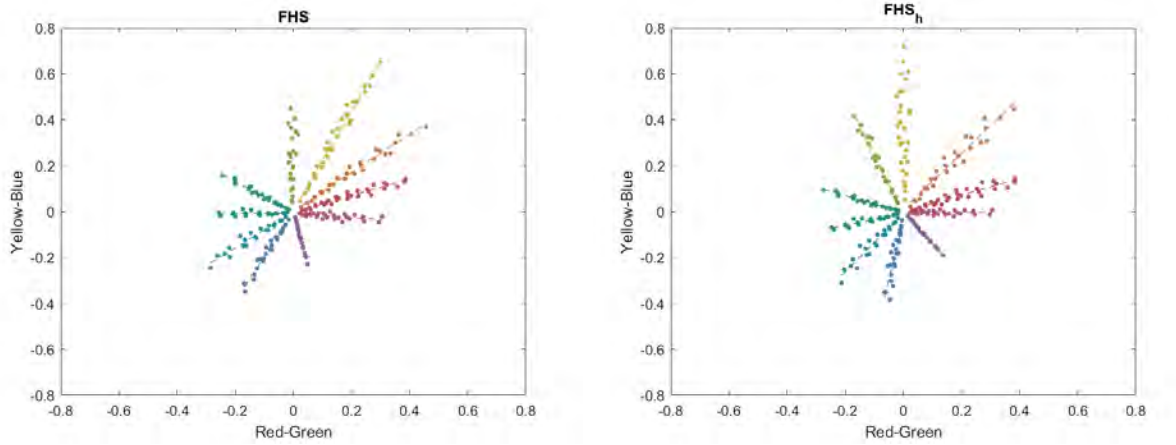

Figure 4.19: The stimuli of ten hue surfaces of the Munsell data set are plotted in the FHS and FHS_h. The spacing between hue surfaces can be compared in two scales.

4.7.1.3 Results of Hue Quadrature Evaluation with Available Data sets

The NCS data set was used to evaluate the hue quadrature prediction as this data set was designed based on four unique hues for hue appearance specification. The RMSE of predicted hue quadrature for each hue surface was calculated considering the assigned hue quadrature of the NCS pages as the reference hue angle. RMSE measures the average difference between the model's prediction values and the actual values. In this case, the actual values were considered to be the assigned hue quadrature of each hue page of the NCS. And the model prediction is the hue quadrature by FHS_H. In this comparison only FHS_H, CIECAM16, and CAM16-Hellwig [19] were used because CIELAB and IPT were not designed with hue quadrature prediction included. The RMSE of predicted hue quadrature for each hue surface using different hue scales are shown in Figure 4.20. Also, the stimuli of eight hue surfaces of the NCS including four unique hues and four intermediate hues are presented in Figure 4.21 only for the FHS and FHS_H. The position of hue surfaces can be compared to other hue scales in Figure 4.15.

As it can be seen in Figure 4.20, there are similar performance among different hue scales for some hue surfaces. But there is a big difference between FHS_H and other scales in green-yellow hues. The FHS scale does not have good spacing in green-yellow region, therefore the rotation matrix of hue quadrature cannot assign proper values on those hues. The poor spacing of the FHS in green-yellow hues can be seen in Figures 4.17 and 4.18. For the same reason, the hue quadrature prediction by the FHS_H of red-blue hues is poor. Another reason for having poor hue quadrature prediction for some hues is poor linearity on those regions. So, good linearity and good spacing is required for having successful hue quadrature prediction.

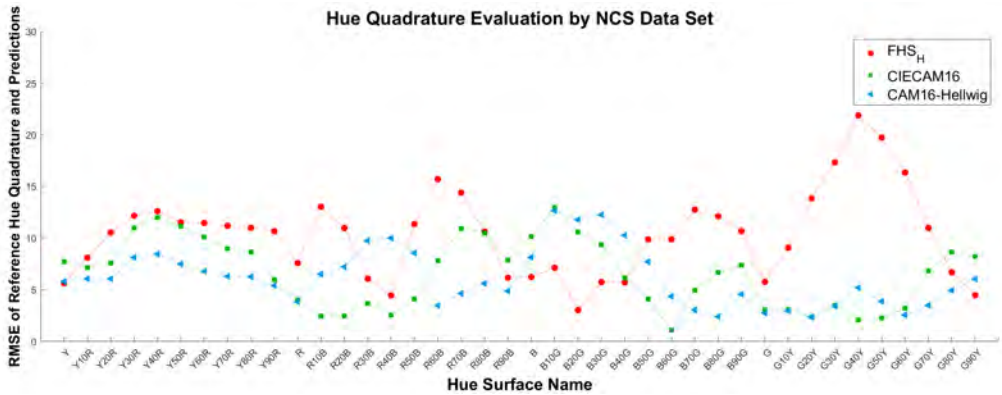

Figure 4.20: Results of hue quadrature evaluation using the NCS data set. Abscissa is the hue surface name. Ordinate is the RMSEs of reference hue quadrature and predictions. Each plot presents the RMSEs calculated by a hue scale to evaluate them individually.

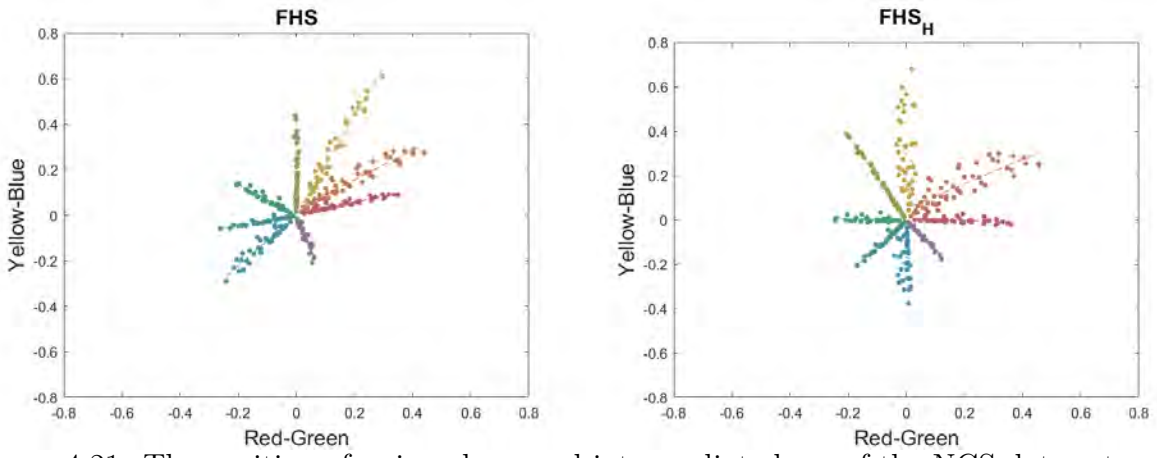

Figure 4.21: The position of unique hues and intermediate hues of the NCS data set can be compared in the *FHS* and FHS_H scales.

4.7.2 Results of Evaluation with New Data Sets

The result of visual experiment which was conducted to assess the linearity of hue scales is presented in Figure 4.22 using different hue scales. It can be seen in Figure 4.22 that all hue scales have similar performance in terms of linearity. They all have poor linearity in blue-green hue, and *FHS* and IPT have poor linearity in red-blue hue, too. Also, the constant hue surfaces are plotted in Figure 4.23 using different hue scales.

It should be noted that each point in Figures 4.22 and 4.23 is the average of adjusted samples by all observers. In this experiment, observers adjusted the hue angles of samples to find the constant hue surfaces. Each observer did the experiment three times. The adjusted hue angle by each observer over three repeats were averaged for each observer and then the hue angles of all observers were averaged. The average hue angle along with luminance and saturation was used in inverse CIECAM16 to calculate the CIEXYZ tristimulus values. Then the tristimulus values were used as input for all hue scales. The standard deviation (SD) of hue angles of stimuli in each hue surface is calculated to show the linearity of hue prediction in Figure 4.22, and the average hue angles in different scales are presented in Figure 4.23.

The result of the second visual experiment, which was conducted to evaluate the spacing between hue surfaces, is shown in Figures 4.24 and 4.25. The RMSE of the hue angle difference between the reference pair and the test pair is presented in Figure 4.24. The hue angle difference of the test pair is compared to the hue angle difference of the reference pair in Figure 4.25. The horizontal line in each plot of Figure 4.25 is the hue angle difference of the reference pair that is calculated by that hue scale.

It should be mentioned that each observer did the experiment three times and the average hue angles of each observer for all samples were calculated. Then the averages of hue angles

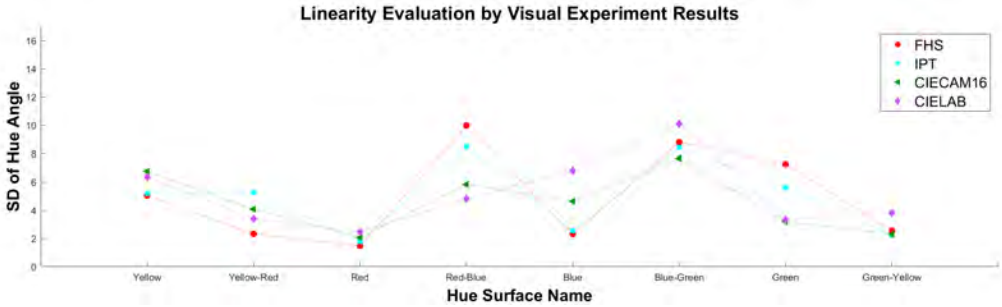

Figure 4.22: Results of linearity evaluation using visual experiment data. Abscissa is the hue surface name. Ordinate is the standard deviation of hue angles of the stimuli in each hue surface. Each plot presents the SDs calculated by a hue scale to evaluate them individually.

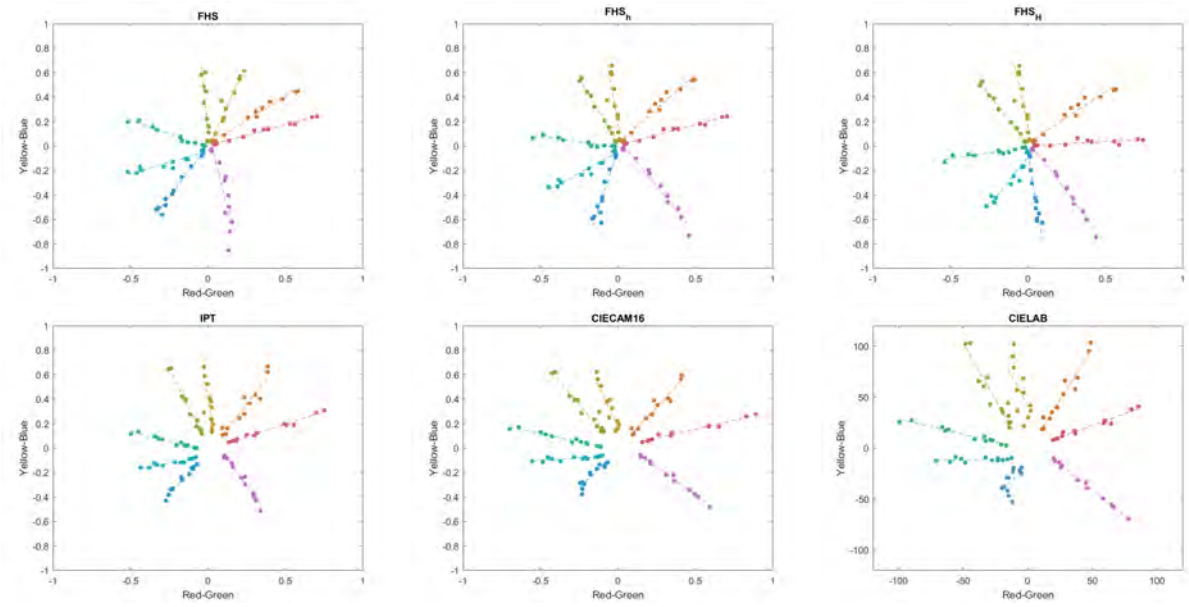

Figure 4.23: Results of constant hue surface experiment for linearity evaluation are presented in different hue scales.

of all observers were calculated. The average hue angles along with luminance and saturation were used in the inverse CIECAM16 to calculate the XYZ tristimulus values of all samples, and they were used as the input for all hue scales. Then the hue angle difference of test pair was calculated. Finally, the hue angle difference of the test pair was compared with the hue angle difference of the reference pair in Figures 4.24 and 4.25.

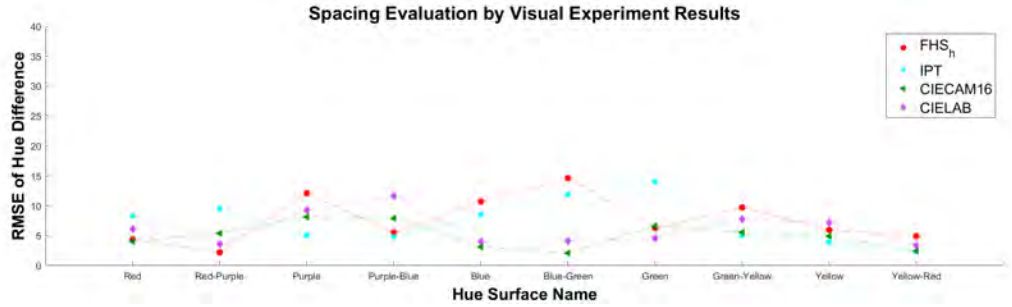

Figure 4.24: Results of spacing evaluation using the visual experiment data. Abscissa is the hue surface name. Ordinate is the RMSEs of reference hue angle and predictions. Each plot presents the RMSEs calculated by a hue scale to evaluate them individually.

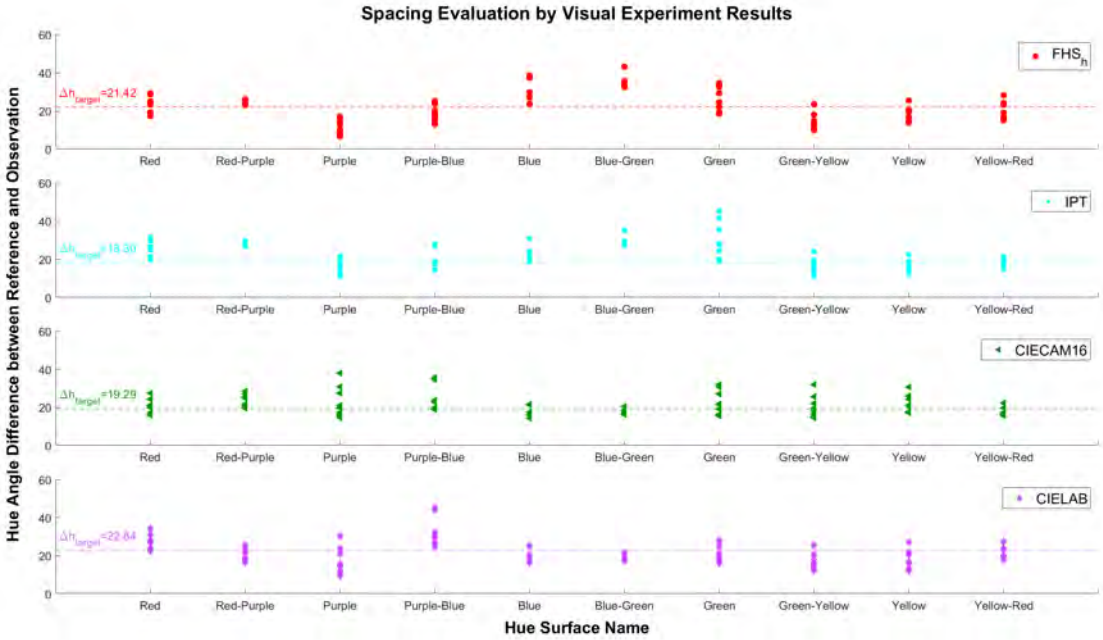

Figure 4.25: Results of spacing evaluation using the visual experiment data. Abscissa is the hue surface name. Ordinate is hue angle difference between reference and predictions.

The result of the third visual experiment, which had two steps to evaluate hue quadrature, is shown in Figures 4.26 and 4.27. Each observer did both steps. The unique hues of each observer in the *FHS* scale are presented in Figure 4.27(a). There are large variations in

unique hues among observers. The rotation matrix of FHS_H was determined for each observer based on their specific unique hues. Then the unique hue surfaces were plotted in the FHS_H scale for each observer, which is presented in Figure 4.27(b). As the rotation matrix was determined for each observer, the rotated hue surfaces are all orthogonal in the FHS_H scale. The intermediate hues of each observer are plotted together in Figure 4.27(c). As the intermediate hues are plotted based on the unique hues of each observer, they can be compared together. It can be seen in Figure 4.27(c) that there are large variations in intermediate hues among observers.

It should be mentioned that each observer did both steps, and there were three repetitions in each step. The average hue angles of each observer for all samples were calculated. Then the averages of hue angles of all observers were calculated. The average hue angles along with luminance and saturation were used in the inverse CIECAM16 to calculate the XYZ tristimulus values of all samples, which were used as the input for the FHS_H, CIECAM16, and CAM16-Hellwig. Then the RMSEs between reference intermediate angle and predictions were calculated. The result is shown in Figure 4.26. There are considerable similarities between three models except for red-blue hues.

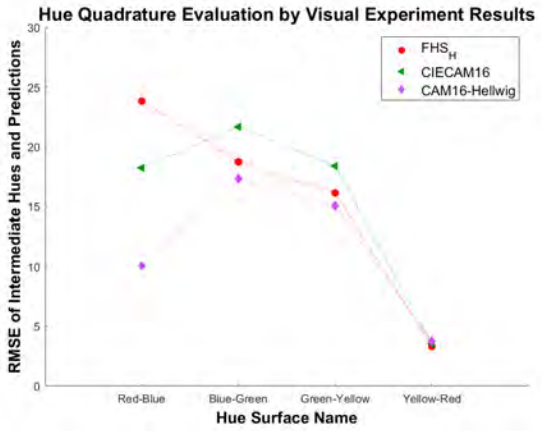

Figure 4.26: Results of hue quadrature evaluation using the visual experiment. Abscissa is the hue surface name. Ordinate is the RMSEs of intermediate hues and predictions. Each plot presents the RMSEs calculated by a hue scale.

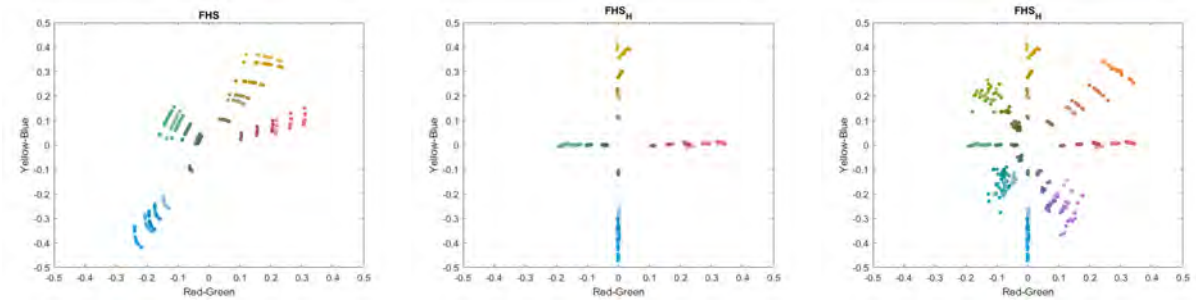

(a) (b) (c)

Figure 4.27: Results of hue quadrature experiment; a) unique hues of all observers in the FHS scale, b) unique hues of all observers in the FHS_H scale, and c) intermediate hues of all observers which are calculated based on their own unique hues.

4.8 Data Analysis

The reported results in Section 4.7 are discussed and analyzed in the following subsections.

4.8.1 Linearity of Different Scales

Linearity of different scales was evaluated using the standard deviation. This evaluation was done using four available data sets and one visual experiment for four hue scales. The performance of these four scales was compared using one-way ANOVA for each data set. The one-way ANOVA was between FHS, IPT, CIECAM16, and CIELAB scales, and it was conducted separately for each of the five data sets of the NCS, Munsell, Hung-Berns, Ebner-Fairchild, and visual experiment. The SDs of hue angles on constant hue surfaces of each data set were used to compare linearity of different scales using ANOVA. The significance level was 0.05 in this ANOVA test. So, if the p-value is less than or equal to the significance level, the linearity of hue scales are significantly different for that data set.

The results of this statistical analysis are reported in Table 4.1. The linearity of four scales including FHS, IPT, CIECAM16, and CIELAB are not significantly different for any data sets. The average of SDs of each hue scale for all data sets are presented in Table 4.2. The FHS scale shows good hue linearity for all data sets because it is not developed based on optimization for a specific data set.

It can be seen in Figures 4.11-4.14 and Figure 4.22 that there are considerable overlaps among hue scales for all data sets. It can be due to weakness of all hue scales in modeling some hue regions, or poor designation of stimuli on those hue surfaces, or big variation among observers who participated in data collection. All of these reasons can be true because modeling some hue regions has specific difficulties. Also, providing stimuli of constant hue

surfaces is more difficult for some hue angles which can cause having less samples in some pages, consequently smaller variation and better linearity for those pages like the B40G and the B60G pages of the NCS data set with 14 and 12 samples. On the other hand, larger variation among observers for some hue surfaces can cause poor linearity of those regions. For example, observers had larger variations in blue-green and red-blue hues in the conducted visual experiment.

Table 4.1: The results of ANOVA comparing the linearity of four hue scales.

Data Set	Source	SS	Df	MS	F	Prob>F
NCS	Column	13.638	3	4.545931	1.54	0.207
	Error	461.277	156	2.95691		
	Total	474.915	159	-		
Munsell	Column	13.357	3	4.45231	3.16	0.0264
	Error	219.883	156	1.40951		
	Total	233.24	159	-		
Hung-Berns	Column	14.403	3	4.80094	0.54	0.6584
	Error	392.302	44	8.91596		
	Total	406.705	47	-		
Ebner-Fairchild	Column	6.756	3	2.25202	1.08	0.3661
	Error	117.053	56	2.09023		
	Total	123.809	59	-		
Visual Experiment	Column	1.379	3	0.45981	0.06	0.9781
	Error	199.117	28	7.11131		
	Total	200.496	31	-		

Table 4.2: Average of SDs for evaluating the linearity of four hue scales.

Data Set	*FHS*	IPT	CIECAM16	CIELAB
NCS	3.89	3.27	3.29	3.83
Munsell	3.22	2.70	2.60	3.24
Hung-Berns	6.78	6.73	7.38	8.08
Ebner-Fairchild	3.13	2.64	3.08	3.59
Visual Experiment	4.97	4.94	4.57	5.14

4.8.2 Spacing of Different Scales

The spacing evaluation was done using the Munsell data set and the visual experiment result. The spacing performance of FHS_h, IPT, CIECAM16, and CIELAB scales was compared using the one-way ANOVA, and it was conducted separately for two data sets of the Munsell and visual experiment. The RMSEs of the hue angle differences between the stimuli and corresponding reference angle of constant hue surfaces of each data set were used to compare spacing of different scales using ANOVA. The significance level was 0.05 in this ANOVA test. So, if the p-value is less than or equal to the significance level, the spacing of hue scales are significantly different for that data set.

The results are presented in Table 4.3. The results showed that there is no significant difference between four scales for the visual experiment results, but there is a significant difference between scales for the Munsell data set. The average of RMSEs of four scales for both data sets are presented in Table 4.4. The comparison among the groups showed that there is a significant difference between the FHS_h and IPT. The FHS_h is significantly better in terms of spacing.

The results show that the FHS_h has the best performance in terms of spacing for the Munsell data set. The rotation matrix that was developed based on five principal hues of the Munsell data set helps to rotate the hue surfaces to make them equally-spaced. The FHS_h has poor performance in terms of spacing for the visual experiment data. Based on the results, the main weakness is in the blue-green and purple hues, which can be seen in Figure 4.24. The FHS_h has poor linearity on those hues too. So, the poor linearity of those hues may cause larger RMSE in spacing evaluation.

Table 4.3: Results of ANOVA for spacing evaluation of all hue scales for two data sets.

Data Set	Source	SS	Df	MS	F	Prob>F
Munsell	Column	434.15	3	144.715	6.65	0.0003
	Error	3393.11	156	21.751		
	Total	3827.26	159	-		
Visual Experiment	Column	43.386	3	14.4619	1.38	0.2649
	Error	377.607	36	10.4891		
	Total	420.993	39	-		

Table 4.4: Average of RMSEs of spacing evaluation of all hue scales for two data sets.

Data Set	FHS_h	IPT	CIECAM16	CIELAB
Munsell	6.08	10.72	8.01	8.20
Visual Experiment	7.65	7.34	5.02	6.15

4.8.3 Hue Quadrature of Different Scales

The RMSEs of hue quadrature predictions of FHS_H, CIECAM16 (H), and CAM16-Hellwig (H) were compared using one-way ANOVA. The ANOVA was conducted separately for two data sets; the NCS and visual experiment. The RMSEs of the differences between the predicted hue quadrature and assigned hue quadrature of constant hue surfaces of each data set were used to compare hue quadrature predictions of different scales using ANOVA. The significance level was 0.05 in this ANOVA test. So, if the p-value is less than or equal to the significance level, the hue quadrature prediction of hue scales are significantly different for that data set.

The result is presented in Table 4.5. The analysis showed that there is a significant difference in hue quadrature prediction for the NCS data set. The average of RMSEs of three scales for the NCS data set is reported in Table 4.6. The comparison among groups showed that there is a significant difference between the FHS_H and CIECAM16, also between the FHS_H and CAM16-Hellwig for the NCS data set. The hue quadrature prediction of FHS_H is significantly worse than those scales for the NCS data set. But there is no difference between CIECAM16 and CAM16-Hellwig in terms of hue quadrature prediction.

The results in Table 4.5 showed that there is no significant difference between hue scales for the visual experiment results. It can be seen in Figure 4.27 that there are considerable overlaps between scales. But it should be noted that there are large variations in intermediate hues among observers and it seems observers had different preferences for choosing the intermediate hues.

Table 4.5: Results of one-way ANOVA for hue quadrature evaluation of three hue scales.

Data Set	Source	SS	Df	MS	F	Prob>F
NCS	Column	371.59	2	185.794	15.05	1.5e-06
	Error	1444.54	117	12.346		
	Total	1816.13	119	-		
Visual Experiment	Column	41.988	2	20.994	0.35	0.7122
	Error	536.016	9	59.5574		
	Total	578.004	11	-		

Table 4.6: Average of RMSEs for hue quadrature evaluation of three hue scales.

Data Set	FHS_H	CIECAM16	CAM16-Hellwig
NCS	10.08	6.59	6.15
Visual Experiment	15.51	15.46	11.55

4.8.4 FHS Performance for 2° and 10° observers

The Munsell and NCS data sets were used to evaluate the performance of the *FHS* model for 2° and 10° field-of-view (FOV) in terms of linearity, spacing and hue quadrature. Only the Munsell and NCS were used in these comparisons because their stimuli reflectance was available. The hue angle of stimuli on each Munsell page and each NCS page was calculated using 2° and 10° cone fundamentals. The resulting hue angles for 2° and 10° observers were used to calculate the SDs of each constant hue surface of the Munsell and NCS data sets to compare their linearity using the *t-test*.

Also, RMSEs of hue difference between hue angle reference and predicted hue angle were calculated for the Munsell data set to compare the spacing of 2° and 10° observers using the *t-test*. Then, RMSEs of differences between assigned hue quadrature and predicted hue quadrature were calculated for the NCS data set to compare the hue quadrature performance of 2° and 10° observers using the *t-test*.

The stimuli of eight hue surfaces of the NCS data sets and ten hue surfaces of the Munsell data set calculated for both 2° and 10° observers are illustrated in Figure 4.28. It can be seen that there is a small shift between 2° and 10° observers on all hue surfaces which is due to different hue angles calculated by 2° and 10° cone fundamentals.

The comparisons in this section can be summarized in this way:

- The performance of the *FHS* for 10° observer was compared with 2° in terms of linearity using the Munsell and NCS data sets.
- The performance of the FHS_h for 10° observer was compared with 2° in terms of spacing using the Munsell data set.
- The performance of the FHS_H for 10° observer was compared with 2° in terms of hue quadrature prediction using the NCS data set.

The calculations were completed using CIE2006 cone fundamentals for 2° and 10° observers. The results showed that there are no significant differences between the performance of the *FHS* for 2° and 10° observers in terms of linearity, spacing and hue quadrature. The analysis was performed using *t-test*. The results are reported in Table 4.7.

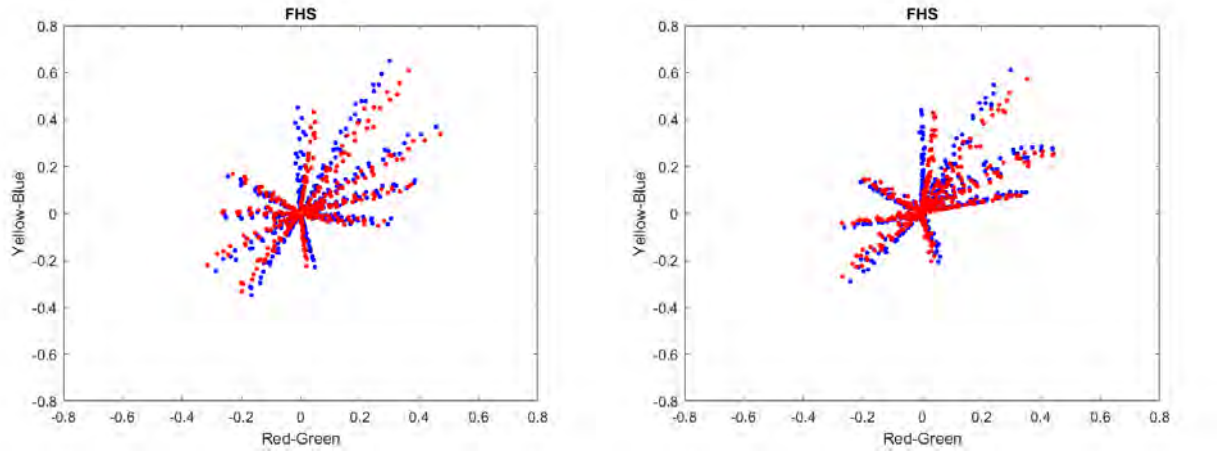

(a) (b)

Figure 4.28: Results of different field-of-view, blue stimuli are calculated by 2° CIE2006 cone fundamentals and red stimuli are calculated by 10° CIE2006 cone fundamentals; a) five principal and five intermediate hues of the Munsell data set in the *FHS* scale, b) four unique and four intermediate hues of the NCS data set in the *FHS* scale.

Table 4.7: Results of Comparing the performance of the *FHS* for 2° and 10° observers.

Evaluation	Data Set	df	SD	*p*-value	CI	*tstat*
Linearity	Munsell	39	0.5717	0.1811	[-0.0597, 0.3059]	1.3617
Linearity	NCS	39	6.8173	0.3003	[-1.0489, 3.3117]	1.0496
Spacing	Munsell	39	53.9177	0.5076	[-11.5424, 22.9450]	0.6688
Hue Quadrature	NCS	39	8.6745	0.5744	[-3.5510, 1.9974]	-0.5664

4.9 Conclusion and Discussion

FHS model was introduced in this chapter. The *FHS* model includes two scales, a hue discrimination scale named FHS_h and a hue appearance scale named FHS_H. The *FHS* model was evaluated in terms of linearity, spacing, and hue quadrature prediction using four available data sets and three visual experiments. The *FHS* was evaluated for hue linearity. The FHS_h was evaluated for hue spacing and the FHS_H was evaluated for hue quadrature.

The *FHS* was compared to the IPT, CIECAM16 and CIELAB in terms of linearity using the Munsell, NCS, Hung-Berns, and Ebner-Fairchild data sets, and the results of the first visual experiment. The results showed that the *FHS* is successful in terms of linearity and there are considerable similarities between the *FHS* performance and other hue scales. Therefore, although the FHS model is a simple model, it achieves hue linearity at the level of other hue scales that are more complicated.

Based on the results of hue linearity comparisons among different models, it seems all

hue scales have a good linearity for some hues and not for other hues. It can be due to weakness of hue scales in modeling some hue regions, or larger variation among individual observations for those hue regions, or some systematic errors on generating stimuli of those hue surfaces.

The FHS_h was compared to the IPT, CIECAM16 and CIELAB in terms of spacing using the Munsell data set and the results of the second visual experiment. The FHS_h has good spacing, and the results showed that it has the best spacing in some hue regions compared to other scales.

The FHS_H was compared to the CIECAM16 and CAM16-Hellwig in terms of hue quadrature prediction using the NCS data set and the results of the third visual experiment. The FHS_H was worse than other hue scales for the NCS data set, but there were no significant differences between hue scales for the results of the third visual experiment. The FHS_H can be improved to have a better prediction of the hue quadrature by improving hue linearity. This improvement can be achieved by optimizing the matrix transformation in Eq. 4.10, specifically for a particular data set for some applications.

The linearity of the model is very important as poor linearity can cause poor spacing and poor hue quadrature predictions. So, it is beneficial to improve the model to have better linearity. The hue linearity can be potentially improved by optimizing the main *FHS* matrix, which converts the LMS cone responses into the opponent axes. This matrix can be optimized for a specific data set. In this study, it was aimed to have a matrix transformation that has good performance for all data sets instead of having excellent performance for one data set and poor performance for the others. So, it was preferred to have the current matrix without further improvement or optimization, but researchers can optimize this matrix transformation for their purposes and for their specific data set. Also, the FHS_H can have a better prediction of the hue quadrature by improving the FHS_H rotation matrix and considering more hue surfaces to build the rotation matrix. For example, instead of four unique hues, researchers can use eight hue surfaces to build the rotation matrix of FHS_H. It was preferred to use only four unique hues for the rotation matrix of FHS_H, and five principal hues for the rotation matrix of FHS_h, to make an easy process, as the performance of the model with these rotation matrices was as good as other models.

It can be concluded that the formulated *FHS* hue scales are mathematically very simple, physiologically and perceptually plausible, and directly based on cone fundamentals to allow easy generalization to individual observers, and perform at least as well as more complicated and abstract colorimetric models in most situations.

Chapter 5

Fundamental Lightness and Brightness Scales

Modeling lightness and brightness has some complexities, as they are not a simple functions of luminance, and they are affected by some color appearance phenomena. Several XYZ-based metrics were developed to model lightness and brightness which carry disadvantages of the XYZ-based system. This study aims to develop one-dimensional brightness and lightness scales directly built on cone fundamentals to account for the underlying physiology of the human visual system and individual differences. The proposed lightness and brightness scales are called *FLS* for **F**undamental **L**ightness **S**cale, and *FBS* for **F**undamental **B**rightness **S**cale, respectively. The Helmholtz–Kohlrausch effect was included in the scales using the G_0 luminance, and the Bartleson–Breneman effect was modeled using an optimized power function, and the Stevens effect was included using terminal brightness. Evaluation of the FLS and FBS scales were completed using seven data sets. In comparison to other models, the FLS and FBS have a good performance on all data sets.

5.1 Introduction

Brightness and lightness are important attributes in color appearance models. Brightness is defined as a perceptual attribute related to the amount of light that is emitting or reflecting from a surface or light source. Lightness is the brightness of an area judged relative to a white or highly transmitting area that is similarly illuminated. The main distinction is that brightness refers to the perception of absolute amounts of light, but lightness is a relative perception [1, 8].

During recent decades, there have been many studies to model brightness and lightness.

Modeling these two attributes has some complexities, as these attributes are not simple functions of luminance, which is a physical measure [18, 19]. Two stimuli with equal luminance can be said to be equally bright under special circumstances, such as having identical spectral distributions or at least being judged to be equal in color and having identical surrounds [20].

The precise relationship between brightness/lightness and luminance has been studied using variety of a visual experiments. Based on these studies, perceived brightness increases with the logarithm or with some power (less than 1.0) of stimulus luminance [21]. Additionally, stimuli with greater purity appear brighter than stimuli with less purity if they are of the same luminance. This effect is known as the Helmholtz–Kohlrausch effect (the H-K effect) [19].

Considering these relations and appearance phenomena, several XYZ-based metrics were developed to model lightness and brightness such as L^* in the CIELAB, J and Q in the Hunt model [10], J and Q in the CIECAM97, CIECAM02, and CIECAM16 models [11], J_{HK} and Q_{HK} in the Hellwig22 and Hellwig23 models [12, 19], High23 model [13] and Kim19 model [14].

These models are based on the current CIE colorimetric system. The current CIE colorimetric system is based on the CIE XYZ trichromatic system that was the best choice at the time that it was developed. The XYZ-based system has some disadvantages. For example, the $\bar{x}(\lambda)$ function has a bimodal form that has no direct physiological analogue. Also, the $\bar{x}(\lambda)$, $\bar{y}(\lambda)$, $\bar{z}(\lambda)$ functions are defined based on some experiments conducted for a group of observers in limited geographical regions. It is now appropriate to develop a new system that can account for the underlying physiology of the human visual system and also accounts for the individual differences [3].

Recently, a technical report was published by CIE [3] as a road map toward a new colorimetry based on cone fundamentals, considering the normal variations of cone fundamentals due to age, field of view, and individual diversity. "Cone fundamentals are defined in the CIE publication as the spectral sensitivity functions of the long- (L-), medium- (M-), and short- (S-) wavelength sensitive cones, measured in the corneal plane" [3]. There is a large variability among color-normal populations. Individual's cone fundamentals and human color vision differs from person to person making fundamental lightness and brightness scales that account for individual differences beneficial in many color-critical applications [6, 7].

This chapter introduces one-dimensional brightness and lightness scales that are built directly based on cone fundamental responses. The proposed lightness scale is called *FLS* for **F**undamental **L**ightness **S**cale, and the proposed brightness scale is called *FBS* for

Fundamental **B**rightness **S**cale.

Some color appearance phenomena were included into the FLS and FBS scales such as the Helmholtz–Kohlrausch effect, the Stevens Effect, and the Bartleson–Breneman effect. Development and evaluation of the FLS and FBS scales are explained in the following sections.

5.2 Model Development

At the first step, a small data set was generated that included stimuli with different luminance levels. A simple model, which was a power function, was developed using this data set. The constants of this model were optimized in comparison with L* in CIELAB. The initial model is introduced in Eq. 5.1. A is the Achromatic response that is essentially a luminance metric, though not identical with CIE luminance, and it can be calculated using Eq. 5.2.

$$Lightness = \frac{(A)^{\frac{1}{3}} - 0.2026}{0.01266} \tag{5.1}$$

$$A = \begin{bmatrix} 2.0 & 1.0 & \frac{1}{20} \end{bmatrix} \times \begin{bmatrix} L \\ M \\ S \end{bmatrix} \tag{5.2}$$

Then, this initial model was improved in the next steps to be a physiologically plausible model, and to account for the Helmholtz–Kohlrausch effect, the Stevens effect, and the Bartleson–Breneman effect. The approaches for improving this model and incorporating these effects into the proposed lightness and brightness scales are explained in the following subsections. The development of lightness scale is explained first, then the brightness scale is defined based on that.

5.2.1 Modeling the Helmholtz–Kohlrausch effect

Brightness and lightness as visual perception attributes have been modeled using luminance, which is a physical metric. Luminance is calculated by integrating spectral radiance multiplied by the luminous efficiency function [49, 50]. But the perceived brightness and lightness are not simple functions of luminance, and they depend on other parameters as well. For example, the Helmholtz-Kohlrausch effect, or the H-K effect, shows that brightness depends on saturation and hue. The H-K effect conveys that the brightness-to-luminance ratio is not equal across the chromaticity diagram, and more saturated colors appear to be brighter with

a hue dependency [51, 52].

Much research has been done to model the H-K effect, specifically based on the visual experiments and brightness matching data sets. One approach for modeling brightness and lightness of chromatic stimuli is to use 'brilliance'. This is a perceptual attribute introduced by Evans, and it is a combination of brightness and saturation. Brilliance can be considered as the perceived brightness that incorporates the H-K effect [53, 54]. Evans examined a series of monochromatic stimuli on a neutral background, and he was the only observer in this experiment [54]. He adjusted the luminance of the stimulus until it appeared in a mode between object color and self-luminous color, which he called 'fluorence' [53, 55]. The transition to fluorence is a perception that can be equivalent to a color with zero gray content, known as G_0. The G_0 luminance defines the luminance of the 'equal chromatic brightness' and can be determined for the entire chromaticity diagram [53, 56]. The significance of G_0 was introduced in several studies [57–59]. The luminance of the stimulus in the G_0 state can be considered as an anchor for each chromaticity coordinate. So, the luminance of a specific chromaticity can be normalized to its G_0 luminance, instead of normalizing to a white luminance [5]. Fairchild and Heckaman provided a framework to use the G_0 luminance in lightness and brightness modeling [5]. Li and Lee used MacAdam's optimal colors as anchors, which is almost the same concept of using the G_0 luminance as anchor [60]. Aghamohammadi et al. [61] used these concepts to estimate the G_0 luminance based on optimal colors.

In this study, the G_0 luminance is used to account for the H-K effect in the proposed brightness and lightness scales. A function was provided by Aghamohammadi et al. [61] to calculate the LMS cone responses of G_0. This function was used in this study to calculate the corresponding LMS_{G_0} for each sample. The following steps were taken to account for the H-K effect using the G_0 concept.

The achromatic response of the LMS_{G_0} was calculated using Eq. 5.2, and it was named A_{G_0}. Then, the normalized achromatic response of each sample was calculated using Eq. 5.3, and it was named A_{HK}, to note that the achromatic response is normalized to A_{G_0} for the same chromaticity of the stimulus to account for the H-K effect.

$$A_{HK} = \frac{\begin{bmatrix} 2.0 & 1.0 & \frac{1}{20} \end{bmatrix} \times \begin{bmatrix} L \\ M \\ S \end{bmatrix}}{A_{G_0}} \tag{5.3}$$

The calculated achromatic response using Eq. 5.3 was used in the next steps to optimize the constants of the final model.

5.2.2 Modeling Different Surround Conditions

Bartleson and Breneman examined the perceived contrast of elements in complex stimuli (images) and its variation with luminance level and surround. They conducted matching and scaling experiments and showed that the perceived contrast of images increased when the image surround was changed from dark to dim to light. The dark surround of an image causes dark areas to appear lighter while having little effect on light areas, so the contrast of the image changes [1]. This phenomena is known as the Bartleson–Breneman effect that conveys the image contrast changes with surround luminance.

To account for the Bartleson–Breneman effect, the power of achromatic response which is 1/3 in Eq. 5.1, should be defined for different surround conditions. Three surround conditions including 'dark', 'dim', and 'average' are usually defined in different color appearance models to account for the Bartleson–Breneman effect. Usually, 'dark' is surround condition with luminance of approximately zero, 'dim' is considered as surround with luminance greater than zero but less than 20% of the reference white, and 'average' is surround with luminance greater than 20% of reference white [1]. Based on the definition of this effect, the magnitude of power should be larger for the surround of higher luminance (average), and it should be smaller for the surround of lower luminance (dark) [62, 63].

The second parameter that should be improved is the offset value, which should be larger for the surround of lower luminance (dark) and it should be smaller for the surround of higher luminance (average). Additionally, the offset is subtracted from the achromatic response in Eq. 5.1, which cannot be physiologically accepted as it causes negative lightness for zero achromatic response. So, the offset should be added to the achromatic response. Also, the denominator should be adjusted based on the offset to converge at the highest lightness for all three surround conditions, including 'dark', 'dim', and 'average'. So, two constants, including power and offset, should be optimized in the final model to predict lightness for three surround conditions. Considering these parameters, the general form of the lightness model should be like Eq. 5.4, then 'c' and 'd' should be optimized for different surround conditions.

For each surround condition, 'c' and 'd' were optimized using the Munsell and NCS data sets in such a way that the RMSE between the lightness prediction of the proposed model and Hellwig23 [12] should be minimized. This optimization step is detailed in Section 5.2.4. 'c' and 'd' can be optimized for any specific viewing condition and for any data set. This feature makes the proposed model useful for any application.

$$Lightness = \frac{(A_{HK})^c + d}{1 + d} \tag{5.4}$$

5.2.3 Modeling the Stevens Effect

The Stevens effect refers to an increase in brightness (or lightness) contrast with increasing luminance. In this context, contrast is the rate of change in perceived brightness (or lightness) with respect to luminance, and luminance means the adapting luminance. The adapting luminance is the luminance of white point (for example Y_w in terminal brightness). The Stevens effect applies to all viewing situations, and it states that, as the luminance level increases, dark colors will appear darker and light colors will appear lighter [1, 64].

The classic psychophysical experiment conducted by Stevens and Stevens showed that the perceived brightness grows as a power function of adapting luminance with an exponent. The exponent increases from a value for the dark-adapted eye to a higher value for the light-adapted eye [64]. Some models, such as Hunt and CIECAM16, have included the Stevens effect in brightness and lightness predictors. The effect of luminance level on the overall slope of the brightness function is an important effect that should be included in the lightness and brightness predictions.

In this work, the Stevens effect is modeled using the terminal brightness, a concept adopted from [5, 64]. First, the power and offset in Eq. 5.4 should be optimized to account for the Bartleson–Breneman effect, then the Stevens effect will be included in using the terminal brightness locus. The terminal brightness locus is defined by Stevens and Stevens as the perceived brightness of a stimulus when an observer is adapted to the luminance of the stimulus itself. It defines how bright white appears as a function of adapting luminance. Terminal brightness is calculated using Eq. 5.5.

$$Q_{tbl} = 0.6 \times [log10(Y_w + 1)]^{0.65} + 0.0572 \tag{5.5}$$

Where Y_W is the absolute luminance of diffuse white in cd/m^2. Q_{tbl} is defined to be 1.0 at an adapting luminance of 100 cd/m^2. It should be noted that the offset in Eq. 5.5 is slightly changed to make the Q_{tbl} equal to 1.0 for an adapting luminance of 100 cd/m^2. The offset is 0.061 in [64].

In this model, terminal brightness was used for two purposes. First, to be multiplied by the power 'c' in Eq. 5.4 to change the magnitude of power to account for the Stevens effect based on adapting luminance. Second, to be used as the white scale in brightness calculation, which is explained in Section 5.2.4.

Terminal brightness was chosen to model the Stevens effect, because it has a good prediction for available data sets. The prediction of the model for different data sets is explained in Section 5.3. Also, terminal brightness has the adapting luminance in its formula, and it is

1.0 for 100 cd/m^2, less than 1.0 for lower luminance, and more than 1.0 for higher luminance, which makes it appropriate to model the Stevens effect by providing a meaningful coefficient.

5.2.4 Introducing the FLS and FBS

To include the H-K effect, the Stevens effect, and the Bartleson–Breneman effect into the lightness model, the general form of the equation should be like Eq. 5.6. The A_{HK} is the achromatic response that is normalized to A_{G_0} to account for **the H-K effect**. Two constants, c and d, introduce the nonlinear relationship between achromatic response (or luminance) and perceived lightness. Also, c and d change for different surround conditions to account for **the Bartleson–Breneman effect**. Then, terminal brightness is multiplied by 'c' to account for **the Stevens effect**. Finally, the lightness prediction is multiplied by 100 to scale the values between 0 and 100.

$$FLS = (\frac{(A_{HK})^{(Q_{tbl} \times c)} + d}{1 + d}) \times 100 \tag{5.6}$$

The A_{HK} was introduced in Eq. 5.3, and terminal brightness, Q_{tbl}, was introduced in Eq. 5.5. Two constants, c (power) and d (offset), were optimized compared to the prediction of a model introduced by Hellwig et al. in [12]. This model is referred to as **Hellwig23** in the rest of this chapter. So, the constants of the FLS model were optimized to have a lightness prediction similar to J_{HK} of Hellwig23 for different surround conditions. The Hellwig23 model was chosen for this step because it was developed based on several data sets to account for the H-K effect, and it has a good performance compared to other models [12].

The Munsell and NCS data sets were used in the optimization step. The spectral reflectance of stimuli of the Munsell Book of Color (glossy collection) and the NCS collection were measured in [31] and used here. The RMSE between the lightness prediction of the FLS and Hellwig23 was used as a metric that should be minimized for all surround conditions and both data sets. The average RMSEs that were minimized to optimize the constants of the FLS model are reported in Table 5.1. The optimized constants for the FLS model are introduced in Table 5.2.

The constants, 'c' and 'd', in Table 5.2 can be optimized for a specific data set, or a specific application, or different viewing conditions. This feature makes the FLS model useful and flexible for different applications.

As an overview, the general form of Eq. 5.4 comes from psychophysical studies that show the perceived brightness grows as a power function of adapting luminance with an

exponent. The exponent increases from a value for the dark-adapted eye to a higher value for the light-adapted eye (the Stevens effect), also the exponent increase with the surround luminance (the Bartleson–Breneman effect). So, two constants, 'c' and 'd' were used in Eq. 5.4 to represent the Bartleson–Breneman effect, and 'Q_{tbl}' was defined to model the Stevens effect. The magnitude of power, 'c', should increase with the surround luminance, and the offset value, 'd', should decrease with the surround luminance, to model the psychophysical results. It should be noted that 'c' and 'd' are two constants that are optimized based on psychophysical scaling results to form a mathematical model. They are not defined to fit a specific data set perfectly, they are defined to work well for a variety of viewing conditions and for different data sets.

Figure 5.1 shows the FLS model with optimized constants for three surround conditions and different adaptive luminance that converges to one point. Figure 5.1 shows that the FLS successfully models the Bartleson and Breneman effect and the Stevens effect. In other words, the FLS predicts that the contrast increases when the surround changes from dark to dim to average, also the contrast increases with adapting luminance.

Table 5.1: The average RMSEs in the optimization step.

Data Set	Dark	Dim	Average
Munsell	3.90	4.06	4.84
NCS	3.58	3.77	4.51

Table 5.2: The optimized constants for the FLS model introduced in Eq. 5.6.

	Dark	Dim	Average
c	$\frac{1}{2.8}$	$\frac{1}{2.5}$	$\frac{1}{2.25}$
d	0.004	0.003	0.002

In this study, the brightness scale is built based on the lightness scale from Eq. 5.6, and it is named FBS, short for **F**undamental **B**rightness **S**cale. The FBS is introduced in Eq. 5.7.

$$FBS = FLS \times Q_{tbl} \tag{5.7}$$

It can be seen in Eq. 5.7 that the relationship between lightness and brightness is linear. A nonlinearity between lightness and brightness can be seen in CIECAM16 model, which

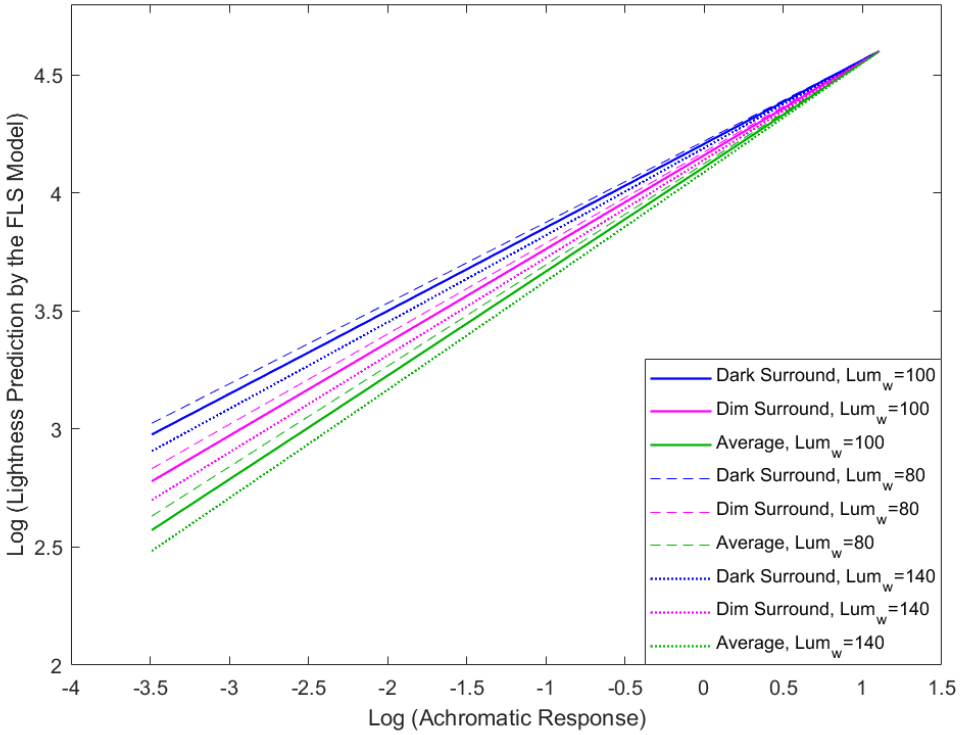

Figure 5.1: The FLS model converges to one point for three surround conditions at different adapting luminance.

comes from CIECAM02 and CIECAM97. These three models calculated lightness J first, then brightness Q, and considered a nonlinearity in Q calculation. It seems the nonlinearity in brightness calculation in CIECAM97, CIECAM02, and CIECAM16 comes from the Hunt model, and these three models did not consider that the Hunt model calculates the brightness first, then lightness. The nonlinear relationship between lightness and brightness has little theoretical evidence. To clarify this point, the CIE definitions of lightness and brightness can help. CIE states *'Brightness is an attribute of a visual sensation according to which an area appears to emit more or less light. Lightness is the brightness of an area judged relative to the brightness of a similarly illuminated area that appears to be white or highly transmitting'* [1]. These definitions imply a linear relationship between brightness and lightness. Supporting this, Hellwig et al. [18] conducted a simple experiment showing that the stimulus chosen as halfway between black and white in terms of brightness is the same stimulus chosen as halfway in terms of lightness. However, CIECAM16 fails to reflect this observation, instead predicting that the same stimulus would not be selected for both tasks. Based on the theoretical definitions and experimental evidence, the relationship between brightness and lightness is considered linear in this study.

The brightness formulae in CIECAM97, CIECAM02, CIECAM16, and Hellwig23 are function of constant 'c'. The constant 'c' is the same constant in Eq. 5.6 that accounts for different surround conditions. It means the ratio of brightness to lightness is a function of the surround condition, and it is larger for the average surround condition than the dark surround condition. This needs to be proven by some psychophysical experiment or theoretical evidence. In this study, it is assumed that the ratio of brightness to lightness is constant for all surround conditions, and it is only a function of the luminance of the white point. The luminance of the white point is included in the brightness formula using terminal brightness 'Q_{tbl}'.

The CIECAM97, CIECAM02, CIECAM16, and Hellwig23 models also have a scalar in the brightness calculation, which may be defined to scale the brightness range and make it similar to the brightness prediction in the Hunt model. The FBS model does not have this scalar. So, the FBS should be scaled, in case of direct comparison to other models. The FLS and FBS scales are introduced in the graphical abstract in Figure 5.2.

5.3 Model Evaluation

To evaluate the FLS performance, seven data sets were used, including the DIN data set, and the data sets provided by Sanders and Wyszecki [65], Wyszecki [66], Fairchild and Pirrotta [67], Xie [68], High [13], and Hellwig [12]. The evaluation was performed in two main steps based on the data sets:

- First, the FLS prediction was evaluated using the DIN data set. The DIN data set was used as a ground truth to check the accuracy of the FLS in comparison with the Hellwig23, especially in terms of the H-K effect prediction.

- Second, the data sets resulting from brightness matching experiments provided by researchers over several decades were used to evaluate the FLS model in comparison with other lightness models. These data sets include different viewing modes, different surround conditions, and a variety of adapting luminance.

These two evaluations are introduced in the following subsections. It should be mentioned that the FBS was not evaluated separately. As the FBS is a function of the FLS and the luminance of the white point. So, if the FLS successfully predicts the lightness of stimuli, then the FBS prediction is successful as well. It should be noted that the FBS has a different range compared with the other brightness models. In case of direct comparison between the FBS and other brightness models, they should be scaled to have the same range of magnitudes.

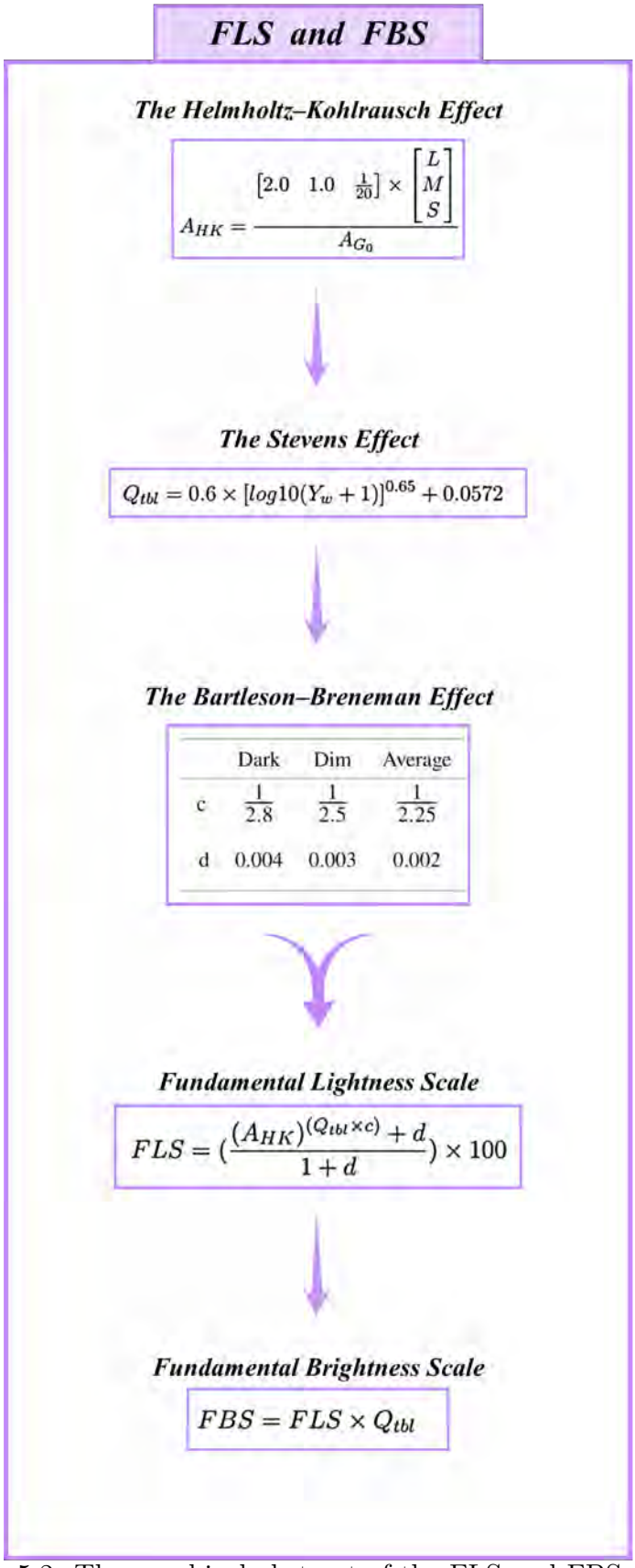

Figure 5.2: The graphical abstract of the FLS and FBS scales.

5.3.1 Evaluation using the DIN Data Set

The DIN data set was used to assess the accuracy of the FLS in comparison with the Hellwig23 model. In the optimization step in **Section 5.2.4**, it was observed that the FLS underestimates the lightness of yellows and greens and overestimates the lightness of reds, blues, and purples compared to the Hellwig23 model.

The lightness difference between the FLS and Hellwig23 for five principal hues of the Munsell data set, and four unique hues of the NCS data set, are presented in Figures 5.3 and 5.4, respectively. These pages from the Munsell and NCS data sets were selected as some examples to show the underestimation and overestimation of the FLS compared to the Hellwig23.

The main aim of the Hellwig23 model was to include the H-K effect in the lightness prediction accurately. It should be explored whether Hellwig23 has underestimation in the lightness prediction of reds, blues, and purples, or the FLS has overestimation for these hues, also, whether Hellwig23 overestimated the lightness of yellows and greens, or the FLS underestimated the lightness of these hues. The different prediction between the Hellwig23 and FLS seems to be related to the method of modeling the H-K effect. So, a ground-truth was needed to assess the accuracy of the FLS and Hellwig23. The DIN data set was used as a ground truth to answer these questions because the darkness attribute in the DIN data set accounts for the H-K effect, so it is an appropriate data set for this comparison.

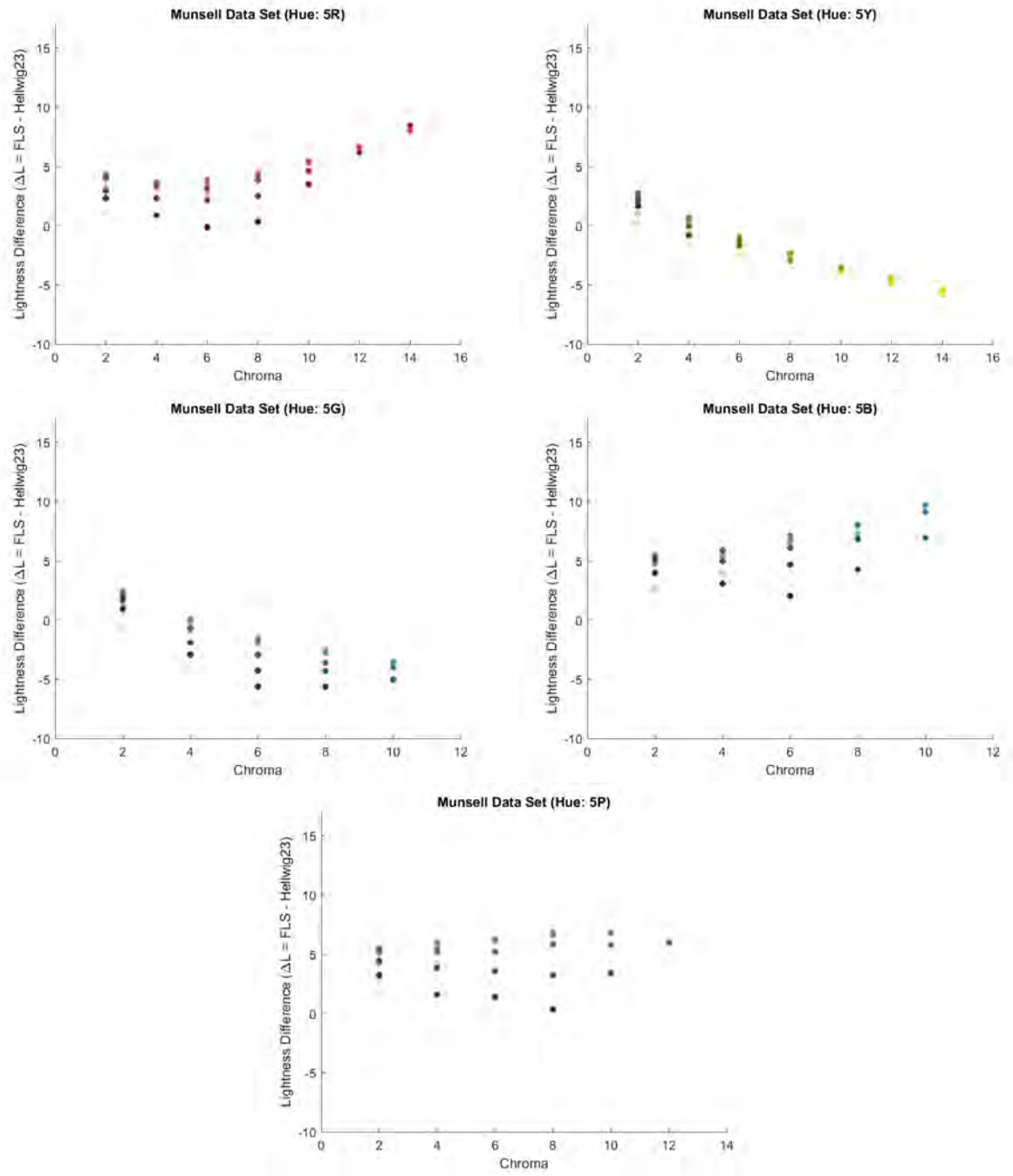

Figure 5.3: The lightness difference between FLS and Hellwig23 for all stimuli of the five principal hues of the Munsell data set. The colors of plots are approximated from the stimuli.

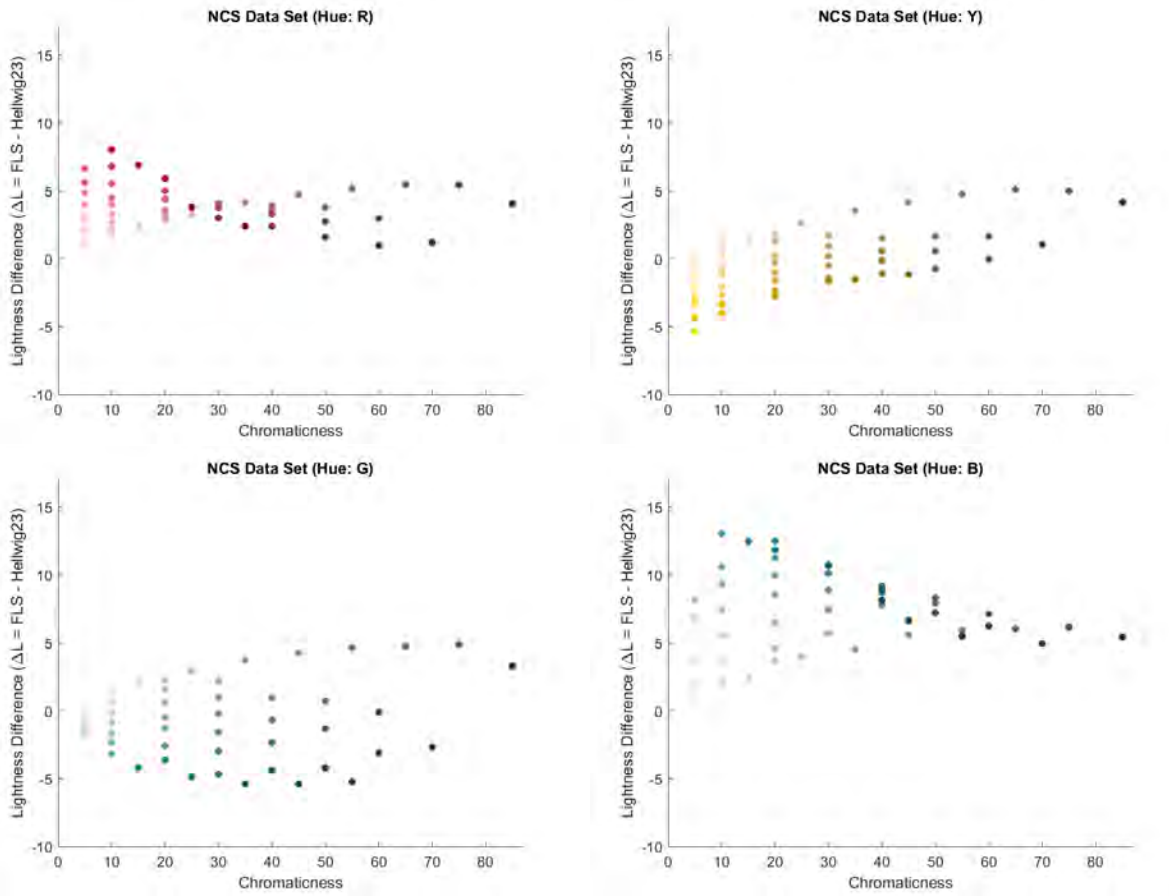

Figure 5.4: The lightness difference between FLS and Hellwig23 for all stimuli of four unique hues of the NCS data set. The colors of plots are approximated from the stimuli.

DIN is a color order system that was created by Manfred Richter for technical applications. The dimensions of this color order system are hue 'T', saturation 'S', and darkness 'D'. Psychophysical experiments were conducted to define perceptually-equidistant hues at S = 6 and D = 1. Then, observers defined saturation in 6 equidistant steps towards the white-point for each hue, and finally extrapolated to cover a larger gamut. Darkness, D, is defined relative to the optimal color Y_0, the brightest color for each chromaticity. This definition is meant to incorporate the Helmholtz-Kohlrausch effect in the darkness attribute. But it was later discovered that there is a slight drop in brightness as saturation increases at constant darkness. The calculation for darkness is given in Eq. 5.8. There are 10 darkness levels for every hue and saturation [69, 70].

$$D = 10 - 6.1723log(40.7\frac{Y}{Y_0} + 1) \tag{5.8}$$

Rather than defining formulas for hue and saturation, DIN uses a look-up table which is described in the DIN 6164 standard document [71]. The data set provided in this standard was used here, but only stimuli with saturation less than 8, as it was mentioned that there is a slight drop in brightness as saturation increases at constant darkness [70]. This specific definition of darkness, D, in the DIN data set helped to assess the accuracy of the FLS prediction, and compare the FLS with the Hellwig23.

Therefore, the lightness prediction by the FLS and Hellwig23 was compared with the darkness of each stimulus. The lightness prediction by the Hellwig23 and FLS for some pages of the DIN are presented in Figures 5.5-5.9. The standard deviation, SD, of the lightness prediction for stimuli with constant darkness is a good scale to assess lightness models. The stimuli with constant darkness in the DIN data set should have the same calculated lightness.

So, the SD of lightness prediction by the Hellwig23 and FLS of constant darkness stimuli on each page of the DIN was calculated. Then, the average of the SDs of each page was calculated. The statistics of the SDs are reported in Table 5.3.

Table 5.3: The statistics of the SDs of constant darkness stimuli in the DIN data set.

Model	Mean (SDs)	SD (SDs)	Min (SDs)	Max (SDs)
FLS	0.51	0.36	0.15	1.31
Hellwig23	1.91	0.53	1.27	3.29

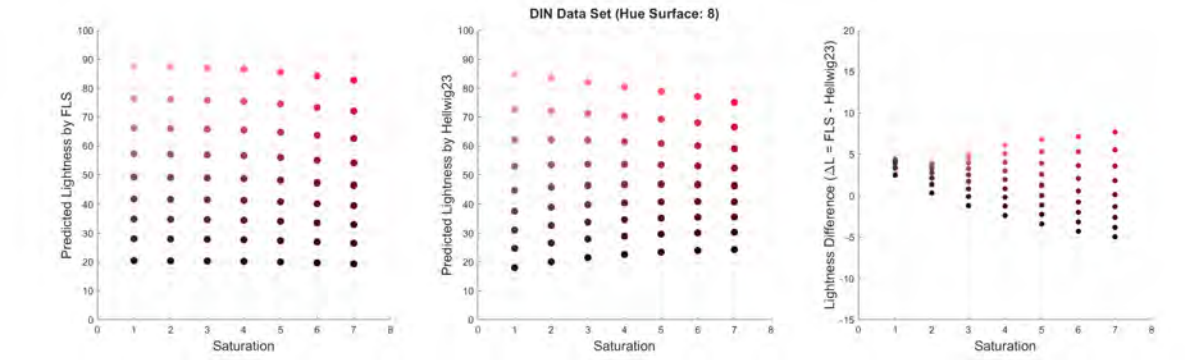

Figure 5.5: Left: The lightness prediction by the FLS. Middle: The lightness prediction by the Hellwig23. Right: The lightness difference between the FLS and Hellwig23. Stimuli of the 8th hue surface of the DIN data set.

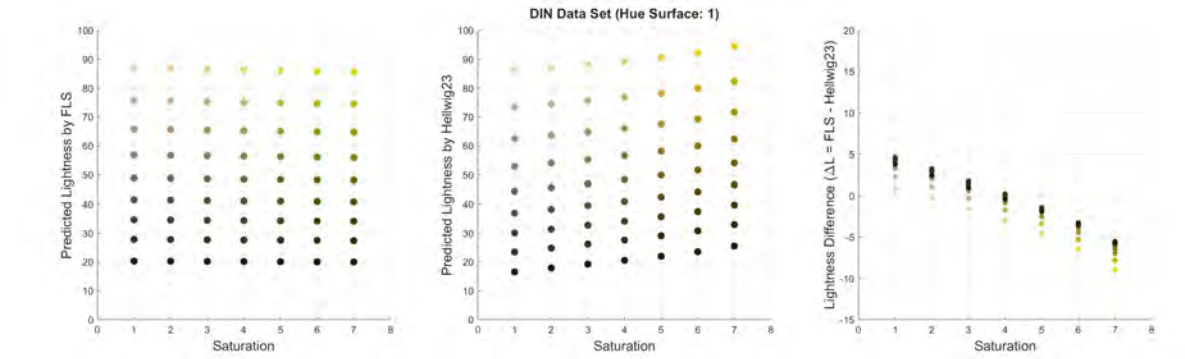

Figure 5.6: The same as Figure 5.5 for the 1st hue surface of the DIN data set.

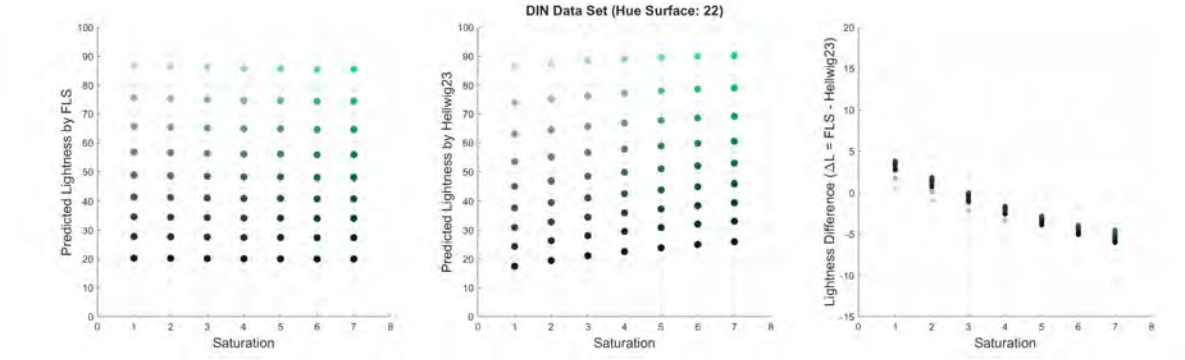

Figure 5.7: The same as Figure 5.5 for the 22nd hue surface of the DIN data set.

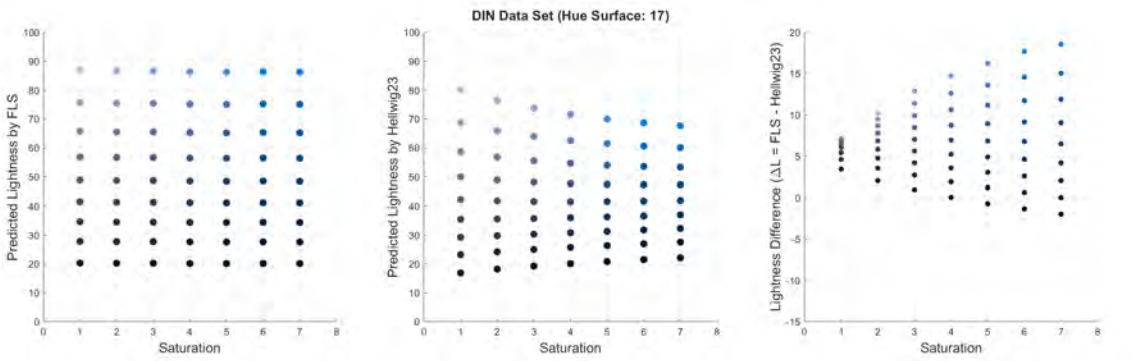

Figure 5.8: The same as Figure 5.5 for the 17th hue surface of the DIN data set.

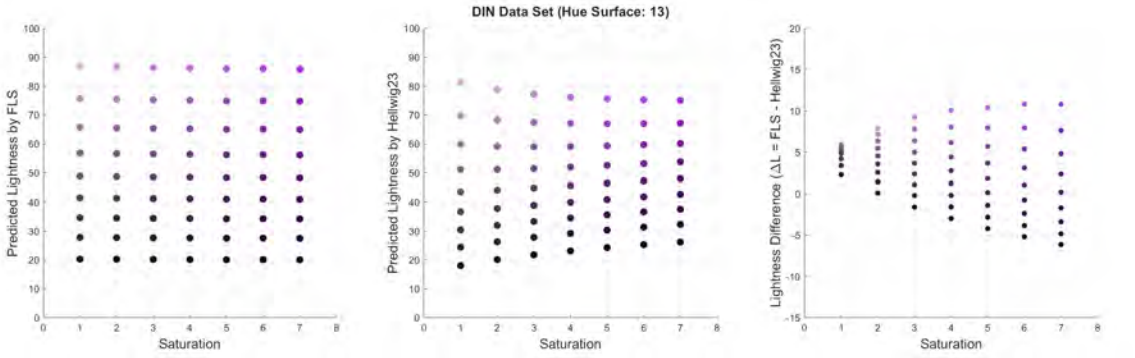

Figure 5.9: The same as Figure 5.5 for the 13th hue surface of the DIN data set.

5.3.2 Evaluation using Brightness Matching Data Sets

Direct brightness matching is a standard method to measure the brightness of stimuli in a manner sensitive to the Helmholtz-Kohlrausch effect. This method has been used in several studies to evaluate the performance of lightness and brightness models. Six brightness matching data sets provided by researchers were used in this study to evaluate the performance of the FLS model. The features of these six data sets are provided in Table 5.7.

The performance of the FLS was compared with the CIELAB, Fairchild91 [67], CIECAM16 [11], Kim19 [14], Hellwig22 [19], Hellwig23 [12], and High23 [13] models. The RMSEs of the lightness prediction between the test and reference stimuli were used as a metric to compare different models. A perfect lightness model should assign the same lightness to both test and reference stimuli. The results are reported in Table 5.5.

Table 5.4: The features of six brightness matching data sets.

Data Set	No. Stimuli	Lightness Range	White Lum. (cd/m^2)	Background Lum. Factor	Surround	Match Criteria	Viewing Mode
Hellwig23 [12]	236	30-90	400, 500	18	Dark	Brightness	Emissive
High23 [13]	74	80-100	120	20	Dim	Lightness	Emissive
Xie21 [68]	15	100	50, 100, 200	18	Dark	Zero-grayness	Emissive
Fairchild91 [67]	36	30-70	382	20	Average	Lightness	Reflective
Wyszecki67 [66]	43	50	159	30	Average	Lightness	Reflective
Sanders63 [65]	96	50	100	20	Unknown	Brightness	Emissive

Table 5.5: The RMSEs of lightness prediction between the test and reference stimuli.

Data Set	*FLS*	Hellwig23	Hellwig22	Kim19	CIECAM16	High23	Fairchild91	CIELAB
Hellwig23	9.1	6	11.3	5.6	14.3	7.4	8.7	14.6
High23	3.7	2.3	3.1	4.5	6.0	1.7	2.3	5.2
Xie21	11.7	9.9	12.6	7.0	17.5	9.7	13.7	21.7
Fairchild91	6.2	11.2	3.4	6.8	4.6	4.9	4.6	4.9
Wyszecki67	2.7	4.7	1.6	4.2	4.6	1.9	1.2	4.8
Sanders63	7.4	6.2	1.8	7.3	4.9	6.5	2.1	5.9

The RMSEs of different models were analyzed using one-way ANOVA. The one-way ANOVA was between different lightness models. The RMSEs of the test and reference were used to compare different models. The significance level was 0.05 in this ANOVA test. So, if the p-value is less than or equal to the significance level, the performance of models for different data sets are significantly different. The results of the one-way ANOVA is reported in Table 5.6.

Table 5.6: The results of the one-way ANOVA to compare different models.

	Sum of Square	DF	Mean Squares	F	p-value
Factor 1	101.59	7	14.512	0.70357	0.66888
Error	825.07	40	20.627		
Total	926.66	47			

The Hellwig23 data resulted from an innovative experiment. It includes three categories, 236 pairs in total. Each pair includes a test and a reference. The first category is presented in Figure 5.10 to visualize the lightness prediction by the FLS and Hellwig23 models. Also, the results of four hue surfaces from the second category including 0°, 90°, 180°, and 270° hue angles (h in CIECAM16) are presented in Figures 5.11 and 5.12 to compare the performance

of the FLS and Hellwig23 models.

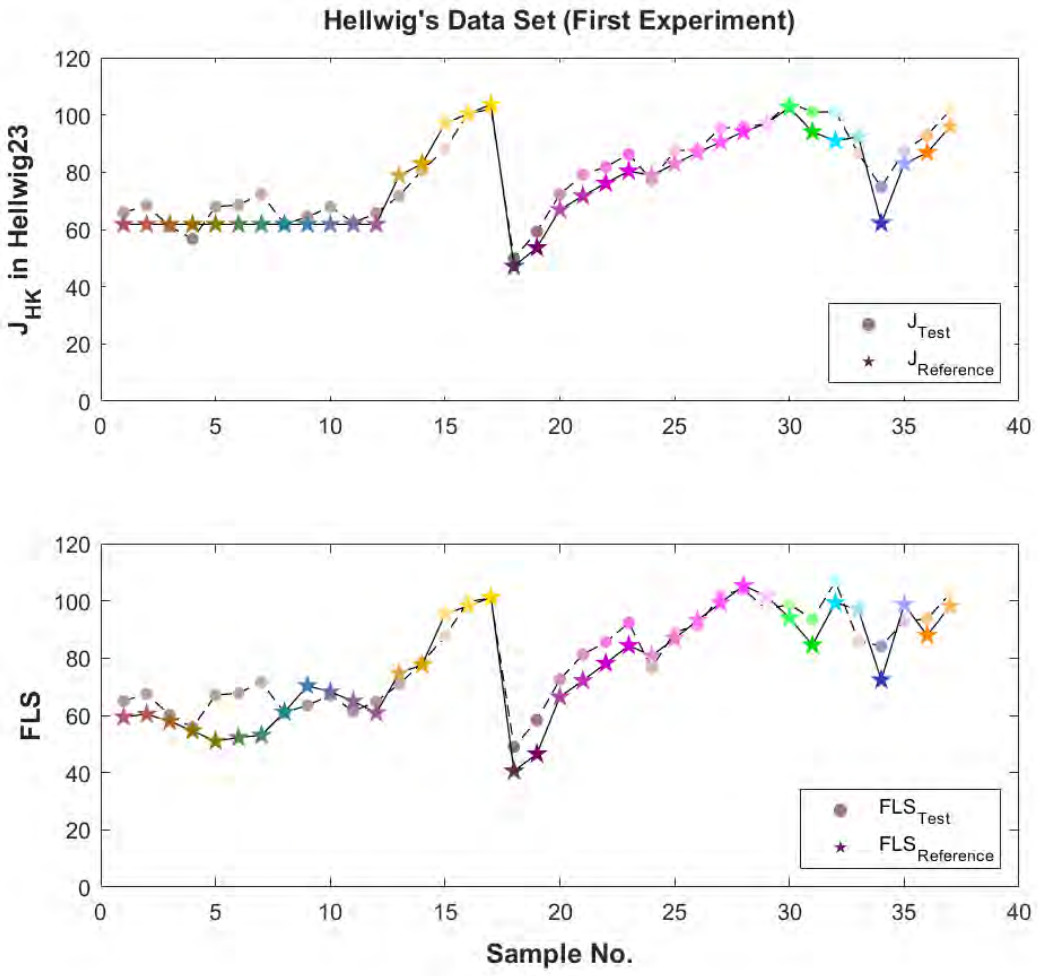

Figure 5.10: The lightness prediction for the test and reference stimuli using the FLS and Hellwig23 models for the first category of the Hellwig23 data set.

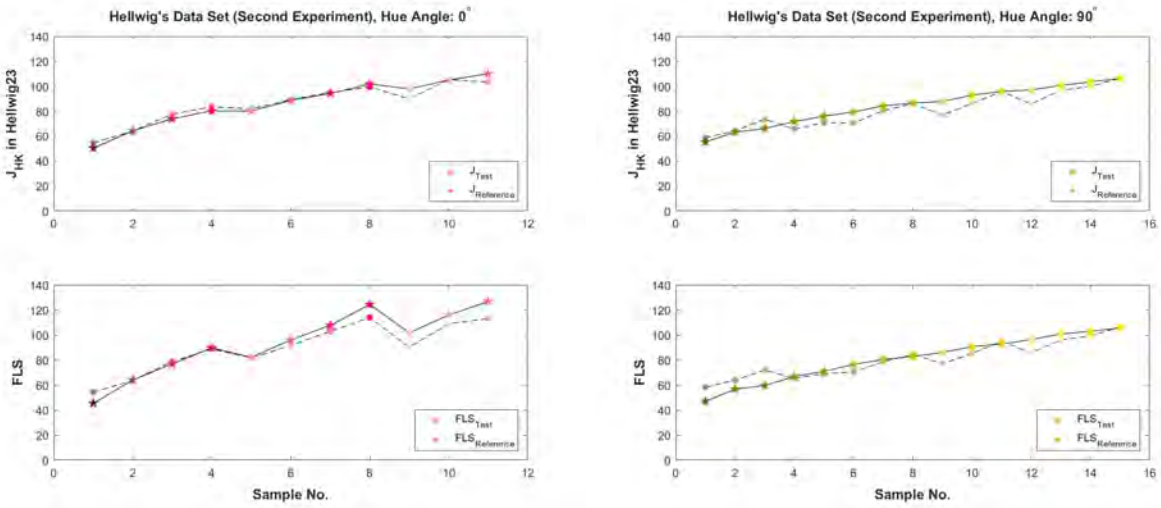

Figure 5.11: The lightness prediction for the test and reference stimuli using the FLS and Hellwig23 models for two hue surfaces (0° and 90°) of the second category of the Hellwig23 data set.

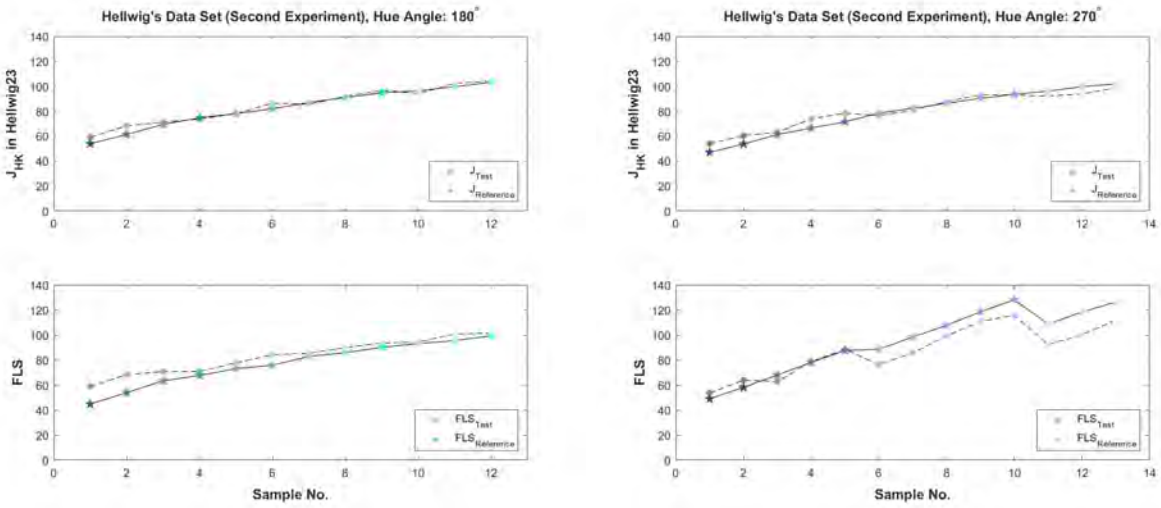

Figure 5.12: The lightness prediction for the test and reference stimuli using the FLS and Hellwig23 models for two hue surfaces (180° and 270°) of the second category of the Hellwig23 data set.

5.4 Data Analysis

It was observed in **Section 5.3.1** that the FLS overestimates lightness of reds, blues, and purples, and it underestimates lightness of yellows and greens compared to the Hellwig23 model. The DIN data set was used as a ground truth to evaluate the lightness prediction of the FLS and Hellwig23 for the constant darkness stimuli. Five pages of the DIN data set are presented in Figures 5.5-5.9. The stimuli with constant darkness are lined up in the FLS plot, but the Hellwig23 has overestimation and underestimation for constant darkness samples. The SDs of lightness prediction using the FLS and Hellwig23 models for constant darkness stimuli are reported in Table 5.3. The results show that the FLS has smaller SDs compared to the Hellwig23. So, the FLS has a better prediction for the DIN data set, and a better prediction of the H-K effect compared to the Hellwig23.

The statistical analysis between different models using the one-way ANOVA is reported in Table 5.6. The results show that there is no significant difference between lightness models. It means that none of the models is better than the others for all data sets. Six data sets were used in this comparison to be sure to have different luminances, different viewing modes, different surround conditions, and different adapting luminance.

Based on the results, some models work better for several data sets. The Hellwig22 model has the best performance for the reflective data sets. The Hellwig23 has a good performance on newer data sets including the Hellwig23 and High23 data sets. The Kim19 model has a good performance on all data sets.

The FLS has a good performance on the Hellwig23 and High23 as newer data sets. It can be seen in Figures 5.10-5.12 that the FLS has its worst prediction on the highly saturated and low-chroma samples of the Hellwig23 data set. It can be due to G_0 optimization for these stimuli. Also, the SPD of the white point for the Hellwig23 data set was reconstructed from the XYZ tristimulus values of the white that it can be another source of error. It is desired to have the SPD of the white point.

It can be concluded that the FLS is not significantly better than other models for these six brightness matching data sets. But it has a good performance for all data sets, although it is a simple model compared to other models. This is a good feature that the FLS works well for a variety of data sets and different luminance ranges and different viewing conditions. Also, the constants of the FLS can be optimized for a specific data set or viewing condition. This makes the FLS a flexible model for different applications.

5.5 The Effect of Stimulus Size on the Perceived Brightness/Lightness

There are some complexities in modeling brightness and lightness, as these attributes are not simple functions of the amount of light emitted by a stimulus. Brightness and lightness depend on other parameters as well. One of these parameters is the stimulus size, which was found to be important in standardization and quantification of brightness for displays, especially for HDR displays [24]. The effect of stimulus size on perceived brightness was known from early studies and early models of brightness scales [26].

Most research shows that as the display size increases, the size effect becomes larger. It is important for display manufacturers to precisely reproduce or to enhance the source images on different sizes of display [72], [73], [74], [75]. It is worth noting that standard color appearance models, such as CIECAM16, are generally recommended to only be used for 2° stimuli [76], [77]. Thus, there is a need to develop color appearance models for different stimuli sizes. There have been some attempts to understand and model the effect of stimulus size on perceived brightness/lightness, saturation, and hue. In these studies, large samples have been reported to appear brighter than small samples [24], [64]-[74]. It was also reported that the magnitude of the size effect is not a function of hue, but it is a function of luminance level of stimuli [24], [74]. It seems the size effect on perceived brightness is due to the nonuniform distribution of photoreceptors (rods and cones) across the human retina. This leads to different color vision in the peripheral retina compared to color vision in the fovea [64], [75]. The details of these studies are reviewed in [78]. The paper is attached in Appendix 3. In this study, a model was developed to incorporate the size effect on the perceived lightness/brightness in the Hellwig23 model. The conducted experiments and the proposed model are introduced briefly here, and more detail can be found in Appendix 3 [78].

Three pilot experiments were conducted to evaluate the size effect. A final experiment was designed based on the results of the pilot experiments. In the first pilot experiment, the shape of the target and test stimuli was evaluated. Based on the results, it was decided to have circular shape in the experiments of this study. Seven observers participated in the first pilot experiment.

The second pilot experiment was conducted using the forced choice method to assess the effect of different size categories on the perceived lightness/brightness. There were five categories of sizes in this experiment. The results showed when the size-difference between the target and test stimuli increases, the magnitude of size effect on the perceived bright-

ness/lightness increases. Six observers participated in this experiment.

The third experiment was performed using the method of constant stimuli. This experiment was done using the samples of the second experiment and the same observers. It was conducted to assess the difference between the two methods of experiment. Based on the result, the method of constant stimuli was chosen for the main experiment.

The main experiment was conducted only for one category of size. The test sample was decided to be one degree of visual field, and the target sample was 10° FOV, so it was 10 times larger than the test. Fourteen observers participated in this experiment. The result is shown in Fig 5.13. The x axis is the target lightness (J in Hellwig23), and the y axis is the observation. The observation was calculated for each stimulus using the psychometric function [79]. The lightness predictions by the Hellwig23 model were significantly smaller than the observations. The results showed that the stimuli size has a considerable effect on the perceived brightness. The bigger stimulus appears brighter than the smaller stimulus.

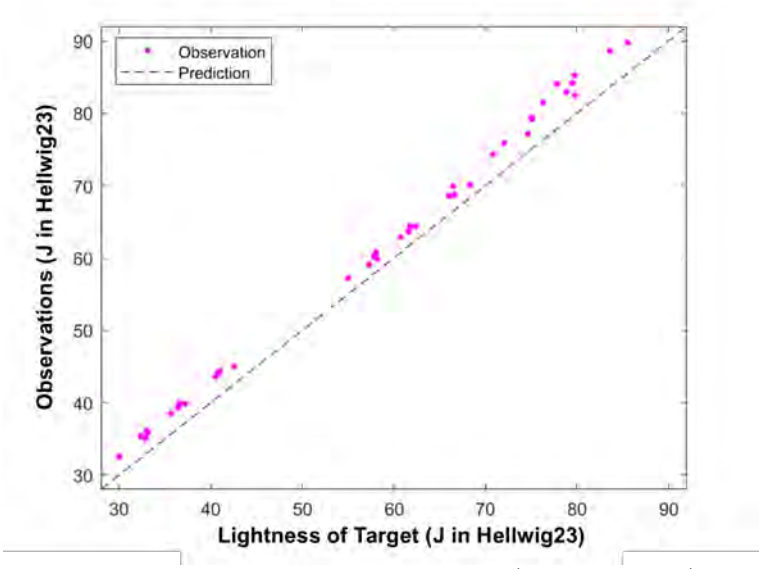

Figure 5.13: The perceived lightness for all samples (observations) is compared to the predicted lightness by Hellwig23.

The lightness difference between the target and the observation was analyzed considering the luminance effect, the saturation effect and hue. Based on the data analysis, the magnitude of the size effect on perceived brightness/lightness is a function of luminance level of stimuli, but it is not a function of hue and saturation of stimuli. Similar results were reported in other studies [24], [64]-[74].

According to the data analysis, a power function model was proposed. It is a very simple model to implement, and it can be applied as an optional step in the last step of the lightness calculation. This model has the best performance compared to the current models which

incorporated size effect into the lightness calculations. This model was evaluated only for one category of size-difference. It can be evaluated for other categories of size-difference in future studies. The model development is briefly discussed here.

5.5.1 Model Development

Based on the results of the second pilot experiment, with decreasing the size difference between target and test stimuli, the magnitude of size effect on perceived brightness decreases. This effect can be modeled with a linear formula like Eq. 5.9. It should be noted that the sample with a field-of-view (FOV) of one-degree, was assumed as a reference sample. So, the calculated lightness for a one-degree sample is the same as CIECAM16 or Hellwig23. The lightness of the bigger sample can be calculated by the equations below. Eq. 5.9 was developed based on the data set of this study. It can be generalized using Eq. 5.10 for other sizes, once it is approved for samples which are bigger than 10-degrees.

$$SE = \frac{FOV_{test} - 1}{9} \tag{5.9}$$

$$SE = \frac{FOV_{test} - 1}{FOV_{target} - 1} \tag{5.10}$$

The next step is considering the effect of different luminance levels on the magnitude of size effect. The effect of size on perceived brightness in low luminance and high luminance is higher compared to the medium luminance level. To model this effect the formula in Eq. 5.11 is proposed. In this formula, as the stimulus luminance goes lower or higher than 50, the 'f' would be larger, which represents the results for luminance effect. There is a constant '60' in denominator, which was chosen based on the best fitting of the model with the observations. These two constants, 50 and 60, can be influenced by the background luminance. To generalize these constants, more experiments should be done with different luminance for the background. If these values are functions of the background luminance, they can be replaced with variables which are representatives of the background luminance.

$$f = \frac{100}{|J - 50| + 60} \tag{5.11}$$

The final formula was decided to be a power function as it is simple to implement and can be applied to the lightness calculation at the last step as an optional choice based on the applications. This formula is presented in Eq. 5.13. The 'k' in this power function would be calculated using Eq. 5.12.

$$k = 1 + \frac{SE}{f \times J} \tag{5.12}$$

$$J' = J^k \tag{5.13}$$

The performance of the proposed model was compared with the Hellwig23 and three models that were introduced in [72], [73], [75], [76] and were developed to account for the size-effect on the perceived lightness/brightness. The RMS, average and SD of lightness difference between these models and observations are reported in Table 5.7. There is no significant difference between those models and Hellwig23. Those three models introduced in [72], [73], [75], [76] can slightly increase the lightness. The large difference between observation and predictions of those three models can be due to two reasons. First, these three models were developed based on a dataset that was for very light color stimuli and that had a lack of darker samples. So, these models might not be easily used for other lightness levels. The second reason is that the models were optimized by decreasing the color difference. So, these models are not specifically for lightness, as decreasing color difference is not equal to lightness matching in all cases. The proposed model in this study has a much better performance, with lowest mean and SD, and the best RMS. This performance can be due to developing the model based on a data set with various samples that had different lightness, hue, and saturation levels. On the other hand, the model was not developed only based on a data fitting, it was developed based on analyzing the effect of each parameter on the perceived brightness.

The size effect was only implemented on the Hellwig23 model in the current study. Once it is generalized for different sizes, and optimized for the FLS model, it can be applied on the FLS and FBS at the last step of calculation.

Table 5.7: The RMS, average and SD of lightness difference between different models and observations.

Model	Mean	SD	RMS
Proposed Model	0.65	0.52	0.83
Hellwig23	3.15	1.10	3.33
First polynomial (Gao)	3.11	1.24	3.35
Second polynomial (Gao)	3.03	1.56	3.41
Correction Matrix (Xiao)	3.08	1.31	3.34

5.6 Conclusion and Discussion

Two one-dimensional scales, named FLS and FBS, were proposed directly based on cone fundamentals to predict lightness and brightness attributes. These scales account for the Helmholtz–Kohlrausch effect, the Stevens effect, and the Bartleson–Breneman effect. The H-K effect was modeled using G_0 luminance. The Bartleson–Breneman effect was modeled using optimized constants as a power, 'c', in Eq. 5.6, for different surround conditions. The Stevens effect was included in using terminal brightness, Q_{tbl}, as a coefficient to adjust the power magnitude in Eq. 5.6.

The FBS is defined in Eq. 5.7 based on the FLS and the white point. The FBS was not evaluated separately as it is defined based on the FLS. So, evaluating the performance of the FLS should be sufficient for the FBS as well.

It was shown using the DIN data set that the FLS has better performance than the Hellwig23, especially for the H-K effect prediction. Based on the results of the evaluation using the brightness matching data sets, the FLS does not have the best performance in any of the data sets. In comparison to other models, the FLS has a good performance for all data sets.

It was aimed to optimize the FLS to work well for all data sets and in all viewing conditions. So, the FLS was not optimized to work perfectly for a specific data set. In case someone needs to use it for a specific data set or a specific viewing condition, the constants in Eq. 5.6 can be optimized for that specific application. Also, to better estimate G_0 luminance, it is recommended to have the SPD of the white point instead of the reconstructed SPD.

In a parallel study, a model was proposed to incorporate the effect of stimulus size into the brightness and lightness models. The proposed model was successfully implemented for the Hellwig23. The size effect can be defined for the new model in the same way that it was defined for the Hellwig23.

In future studies, modeling the Stevens effect can be improved. It was modeled using the terminal brightness in this research. A model can be defined using more data sets with a variety of adapted luminance to be used instead of Q_{tbl}, or to refine its definition.

There are a number of models for the lightness and brightness prediction. We would recommend the Hellwig23 (the Hellwig-modified CIECAM16) for someone interested in being close to a standardized model, and the FLS and FBS for someone wanting an LMS-based model with more flexibility, simplicity, and accuracy.

Chapter 6

Fundamental Saturation Scale

Modeling saturation presents notable challenges, as saturation is not a direct function of chromaticity coordinates alone and is influenced by hue as well. Current saturation scales are typically derived from XYZ-based color spaces or chromaticity diagrams, which inherit the limitations of tristimulus-based representations. This study introduces a one-dimensional saturation scale constructed directly from cone fundamentals to better align with the underlying human visual perception. The proposed scale, termed the *FSS* for **F**undamental **S**aturation **S**cale, computes saturation based on excitation purity in the l–m chromaticity diagram and incorporates a scaling factor derived from classical saturation data reported by Wright [80]. By grounding saturation computation in fundamental CMFs and established perceptual scaling, the FSS provides a physiologically motivated alternative to conventional XYZ-based saturation metrics.

6.1 Introduction

Saturation is a perceptual attribute in color appearance models, and it is defined as "*colorfulness of an area judged in proportion to its brightness*". Saturation of a stimulus with a given chromaticity remains constant for all luminance levels in a given viewing condition within the range of photopic vision, except when brightness is very high [1].

Saturation can be defined as relative colorfulness and it is different from chroma, as it is the colorfulness of a stimulus relative to its own brightness. Chroma is defined as "*colorfulness of an area judged as a proportion of the brightness of a similarly illuminated area that appears white or highly transmitting*". So, chroma is only a related color attribute, but saturation is both an unrelated and related color attribute. It is also required to define colorfulness, as saturation and chroma are both defined based on colorfulness. Colorfulness

is defined as "*an attribute of a visual sensation according to which the perceived color of an area appears to be more or less chromatic*" [1].

Saturation can be described as a shadow series. As stimuli under shadow cast presents the same saturation, although they become darker under deeper shadow. It can also be seen in different sides of a cube that is illuminated by a single light source. Different sides have the same saturation, although some sides appear to be darker. An example is presented in Figure 6.1 to show this effect [1].

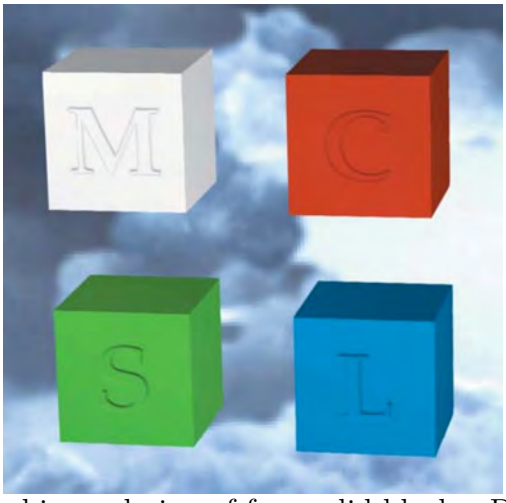

Figure 6.1: A computer graphic rendering of four solid blocks. Different sides of cubes have approximately constant saturation [1].

6.1.1 Saturation Scales

A brief review on some saturation scales is provided in this section. In the Nayatani et al. color appearance model, saturation is derived first and then colorfulness and chroma are introduced based on saturation. Nayatani et al. defined saturation based on Euclidean distance from the origin on an opponent axes, including red-green and yellow-blue, similar to the chroma calculation in CIELAB [1].

The Hunt model defines an overall chromatic response, M, based on Euclidean distance from the origin for yellow-blue and green-red responses. Then, the saturation correlate is calculated from M and the adapted cone signals [1, 10].

Saturation in CIECAM02 is formulated based on the chroma and colorfulness correlates. First, chroma is calculated, then colorfulness is defined as chroma scaled by the luminance-level adaptation factor. Finally, saturation is defined as the square root of colorfulness relative to brightness. The saturation formulation in CIECAM02 is analogous to the CIE

definition of saturation as the colorfulness of a stimulus relative to its brightness. The saturation correlate was defined in the same way in the CIECAM16 model [1, 11].

Hellwig and Fairchild introduced an improved correlate of saturation based on the CIECAM16, to address threefold dependencies of saturation on background luminance in the CIECAM16. In their model, colorfulness is calculated first, then chroma and saturation are defined independently using the achromatic white signal and brightness, respectively [18].

Despite their differences, most existing saturation scales are ultimately rooted in the CIE XYZ colorimetric system. As discussed previously, color appearance attributes derived from XYZ-based models inherit limitations associated with the XYZ color matching functions (CMFs), which are not directly tied to the physiological responses of the human visual system. Consequently, modeling saturation based on fundamental CMFs offers the potential to develop a more physiologically plausible and perceptually meaningful saturation scale. This motivation forms the basis for the saturation model proposed in the following sections. The proposed saturation scale is rooted to the excitation purity, so it is beneficial to review excitation purity and its formulae.

6.1.2 Excitation Purity as a Scale for Saturation

Saturation is a fundamental perceptual attribute, and it can be described as the degree to which a color differs from a neutral of the same lightness, ranging from achromatic to highly vivid appearances. In traditional colorimetry, one of the earliest correlates of saturation is excitation purity, defined as the ratio of the distances from the given white to the chromaticity and to the spectral locus or line of purples within a chromaticity diagram. Excitation purity quantifies the proportion of chromatic content relative to an achromatic reference [1, 8].

Although excitation purity is not a perceptually uniform measure (as it is defined within a chromaticity diagram), it provides a conceptually clear basis for scaling saturation when chromaticity is represented independent of luminance. In particular, excitation purity captures the intuitive notion that saturation increases monotonically as a stimulus chromaticity moves away from the white point along a constant hue direction toward the spectrum locus. This property became a motivation in this study to propose a fundamental saturation scale based on excitation purity [1, 8].

Excitation purity depends only on chromaticity coordinates and the selected white point, and it can be computed in any chromaticity diagram derived from a tristimulus space such as xy and $u'v'$ chromaticity diagrams, or from a cone fundamental space such as lm chromaticity diagram [1, 8].

6.1.2.1 CIE *xy* Chromaticity Diagram

The CIE x,y chromaticity diagram is derived from the CIE XYZ tristimulus values and it is a widely used chromaticity representation in color science and engineering. The chromaticity coordinates are defined in Eqs. 6.1, 6.2, and 6.3 [1, 8].

$$x = \frac{X}{X + Y + Z} \tag{6.1}$$

$$y = \frac{Y}{X + Y + Z} \tag{6.2}$$

$$z = 1 - (x + y) \tag{6.3}$$

The x,y diagram provides a standardized framework for specifying chromaticities of lights and object colors, defining device gamuts, and identifying dominant wavelengths. Despite its widespread use, the x,y chromaticity diagram is perceptually non-uniform; it means that equal distances in the diagram do not correspond to equal perceived color differences [1, 8].

6.1.2.2 CIE $u'v'$ Chromaticity Diagram

The CIE 1976 u',v' chromaticity diagram was introduced to reduce non-uniformity of the x,y chromaticity diagram. The coordinates are defined in Eqs. 6.4 and 6.5 [1].

$$u' = \frac{4X}{X + 15Y + 3Z} \tag{6.4}$$

$$v' = \frac{9Y}{X + 15Y + 3Z} \tag{6.5}$$

Because of its improved hue linearity, the u',v' diagram is commonly used in modern color appearance modeling. Saturation is frequently computed in this space using excitation purity defined along constant hue directions extending from the white point toward the spectrum locus [1, 5].

6.1.2.3 CIE *lm* Chromaticity Diagram

Chromaticity diagrams may also be constructed directly from cone fundamentals, providing a representation closely tied to the earliest stages of human visual processing. Using LMS cone fundamentals, chromaticity coordinates can be defined using Eqs. 6.6, 6.7, and 6.8.

$$l = \frac{L}{L + M + S} \tag{6.6}$$

$$m = \frac{M}{L + M + S} \tag{6.7}$$

$$s = 1 - (l + m) \tag{6.8}$$

Cone-based *l,m* chromaticity diagrams are particularly attractive for saturation modeling because excitation purity computed in this space corresponds directly to relative cone-excitation [1, 15].

6.2 Model Development

The purpose of the Fundamental Saturation Scale (FSS) is to define a saturation metric that is both physiologically grounded and perceptually meaningful. Classical excitation purity provides a geometrically well-defined measure of saturation based on chromaticity distance from a reference white point. However, it does not account for variations in perceived saturation as a function of hue. To address this limitation, the proposed FSS combines excitation purity computed in the *l,m* chromaticity diagram with a hue-dependent perceptual scaling factor derived from Wright's experimental observations [80]. In this formulation, saturation is defined in a fundamental-based chromaticity diagram and subsequently adjusted by a perceptual scaling factor to better reflect human perception.

6.2.1 Construction of the *l,m* Chromaticity Diagram

The FSS is defined within the *l,m* chromaticity diagram constructed from the CIE 2006 cone fundamentals. This representation directly reflects the responses of the L-, M-, and S-cones and therefore corresponds to the earliest stage of human color vision. The chromaticity coordinates are defined based on Eqs. 6.6, 6.7, and 6.8.

The spectrum locus in the *l,m* chromaticity diagram was computed for monochromatic stimuli spanning the visible range from 390 nm to 760 nm in 5 nm intervals using the CIE 2006 cone fundamentals.

6.2.2 Definition of the Reference White Point

A reference white point is required for the computation of excitation purity. In this work, the white point was defined using the Equal Energy (EE) illuminant, which assigns equal radiant power to all wavelengths and provides a neutral reference.

L_{EE}, M_{EE}, and S_{EE} represent the cone excitations produced by the EE illuminant. The chromaticity coordinates of the white point are then given by:

$$l_n = \frac{L_{EE}}{L_{EE} + M_{EE} + S_{EE}}, \tag{6.9}$$

$$m_n = \frac{M_{EE}}{L_{EE} + M_{EE} + S_{EE}}. \tag{6.10}$$

These coordinates (l_n, m_n) are considered as the origin from which saturation is measured in the l,m chromaticity diagram.

6.2.3 Hue Angle Definition in the *l,m* Chromaticity Diagram

To associate each chromaticity with a perceptual hue, a hue angle was computed for spectrum-locus points. The hue angle definition follows the conventional formulation used in CIELAB and is adapted here to the l,m chromaticity plane.

For a chromaticity point (l, m), the hue angle h is defined relative to the white point as

$$h = Arctan(\frac{l - l_n}{m - m_n}) \tag{6.11}$$

where *Arctan* denotes the inverse tangent function. Using this formulation, hue angles were computed for all spectrum-locus points between 390 nm and 760 nm, establishing a mapping between chromaticity coordinates and hue angle within the cone-based chromaticity representation.

6.2.4 Calculation of Excitation Purity

For a given stimulus chromaticity **S** and a reference white point **N**, the corresponding hue angle for that stimulus can be calculated. Then, based on that hue angle, the corresponding point **L** on the spectrum locus along the same hue direction can be found. Having these data, excitation purity p_e is defined geometrically using Eq. 6.12 [1, 8]. The lm chromaticity diagram is presented in Figure 6.2 to show the position of stimulus, white point, and the corresponding point on the spectrum locus.

$$p_e = \frac{\|\mathbf{S} - \mathbf{N}\|}{\|\mathbf{L} - \mathbf{N}\|} \tag{6.12}$$

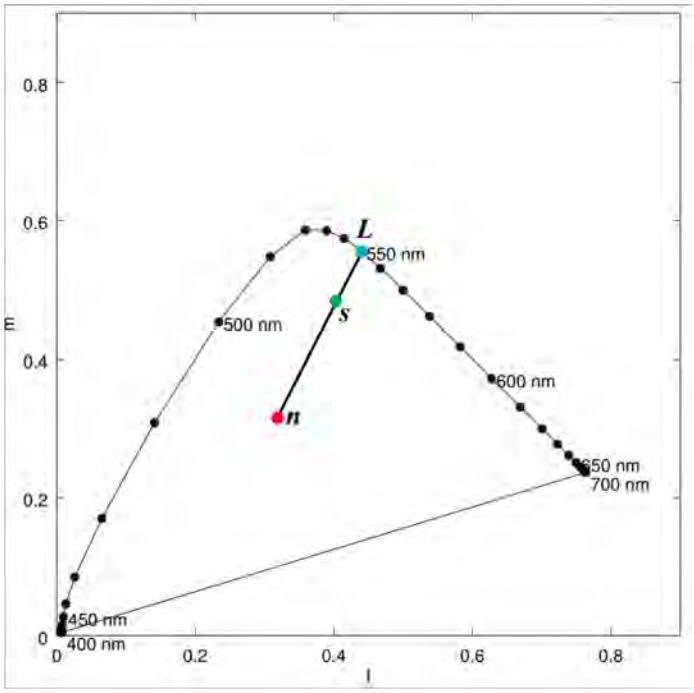

Figure 6.2: A representation of the l,m chromaticity diagram.

where distances are Euclidean distances computed within the selected chromaticity diagram (x,y, or u',v', or l,m). By definition, excitation purity is zero at the white point and unity at the spectrum locus [1, 8]. Explicit form of excitation purity introduced in Eq. 6.12 for each of the x,y, and u',v', and l,m chromaticity diagrams are provided in Eqs. 6.13, 6.14, and 6.15, respectively. By definition, $p_e = 0$ at the white point and $p_e = 1$ at the spectrum locus.

$$p_e(x, y) = \frac{\sqrt{(x_s - x_n)^2 + (y_s - y_n)^2}}{\sqrt{(x_L - x_n)^2 + (y_L - y_n)^2}} \tag{6.13}$$

$$p_e(u', v') = \frac{\sqrt{(u'_s - u'_n)^2 + (v'_s - v'_n)^2}}{\sqrt{(u'_L - u'_n)^2 + (v'_L - v'_n)^2}} \tag{6.14}$$

$$p_e(l, m) = \frac{\sqrt{(l_s - l_n)^2 + (m_s - m_n)^2}}{\sqrt{(l_L - l_n)^2 + (m_L - m_n)^2}} \tag{6.15}$$

6.2.5 Hue-Dependent Scaling Based on Wright's Data

Psychophysical observations reported by Wright indicate that when the calculated excitation purity is identical, the perceived saturation is not constant across different hues. Colors of different hues may appear more or less saturated despite having equal excitation purity. To account for this effect, Wright introduced a hue-dependent scaling factor that modulates excitation purity to better align with human perception of saturation [80].

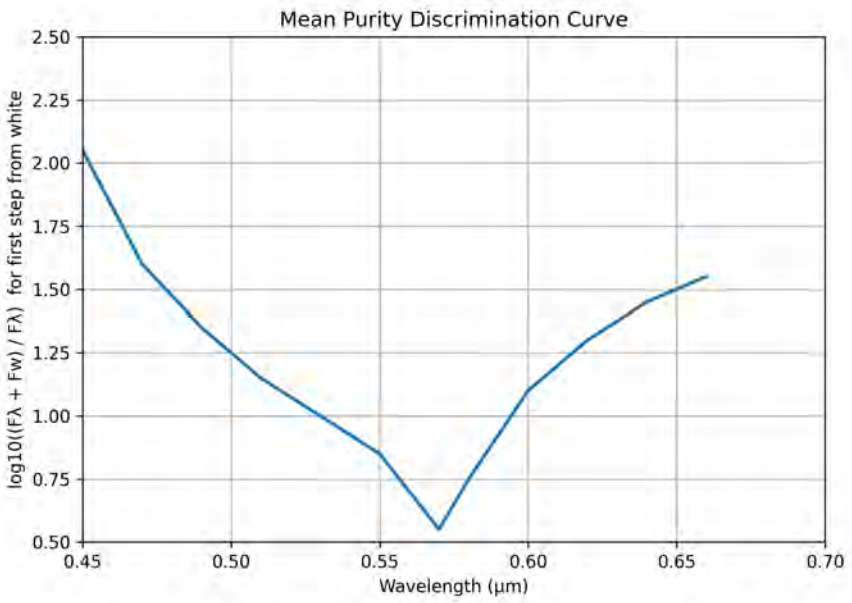

Figure 6.3: Mean purity discrimination curve as a function of wavelength, derived from data in Fig. 92 in [80].

In the present work, this hue-dependent scaling factor was extracted from Wright's experimental data that was published in [80] and organized as a lookup table (LUT). In order to extract this LUT, the mean sensitivity data are found in Figure 93 on Page 166 of Wright's book [80]. That plot was copied and enlarged and values were read off manually. Data were extrapolated down to 390 nm and up to 760 nm smoothly. Purple data were computed via linear interpolation. It should be noted that for arbitrary hue angles, the scaling factor is obtained by interpolation within the LUT.

The logarithmic Wright's data were then converted to linear sensitivity weightings and normalized to have a peak of 1.00. It is named k_h. This scaling factor was used to convert relative saturation (excitation purity) to an absolute saturation scale where the purples still go up to 100 but the green wavelengths only peak at about 16. Better data should be developed in the future studies if more accurate saturation scales on an absolute basis are needed.

6.2.6 Fundamental Saturation Scale

The Fundamental Saturation Scale is the excitation purity computed in the *l,m* chromaticity diagram multiplied by the hue-dependent scaling factor, k_h. For a given sample, FSS can be calculated using Eq. 6.16. It is multiplied by 100 to scale it in a range similar to CIECAM16 and Hellwig-CAM16.

$$FSS = k_h \times p_e \times 100 \tag{6.16}$$

Thus, the computation of FSS proceeds as follows: the sample is first expressed in *l,m* chromaticity coordinates, excitation purity is computed relative to the EE white point and the corresponding spectrum-locus chromaticity. The corresponding spectrum-locus chromaticity is calculated by interpolating sample hue angle. The appropriate scaling factor is obtained by interpolating hue angle in Wright's LUT, and finally excitation purity is multiplied by this scaling factor to yield the FSS value.

6.2.7 Fundamental Colorfulness and Chroma Scales

A simple linear definition was used in this step to introduce the fundamental colorfulness and chroma scales. Saturation can be described as the colorfulness of a stimulus relative to its own brightness. So, colorfulness can be defined as saturation multiplied by its own brightness. Therefore, a simple linear function of saturation like Eq. 6.17 can be formulated to calculate the fundamental colorfulness scale. As colorfulness is denoted by M in some color appearance models, the fundamental colorfulness scale was named FMS.

$$FMS = FSS \times FBS \tag{6.17}$$

Saturation is defined as chroma divided by lightness. So, chroma can be defined as saturation multiplied by lightness [1]. Based on these definitions, the fundamental chroma scale, FCS, can be formulated by Eq. 6.18.

$$FCS = FSS \times FLS \tag{6.18}$$

These are preliminary models of colorfulness and chroma, and the graphical abstract of the proposed scales are presented in Figure 6.4. They can be improved based on recent studies that have explored the effect of different parameters on perceived colorfulness and chroma. Park and Murdoch investigated how perceived colorfulness changes when color stimuli are presented at high luminance levels. They introduced limitations of traditional

color appearance descriptions, which are often developed under moderate luminance conditions, and showed that perceived colorfulness does not scale linearly with brightness. Their results indicate that high-brightness stimuli tend to appear more colorful than predicted by conventional models, highlighting the influence of luminance on chromatic perception. The study provides experimental evidence that perceived colorfulness depends on both chromatic content and stimulus brightness [81].

6.3 Model Evaluation

The proposed saturation scale, FSS, was evaluated using the DIN data sets. Its performance was compared with that of the CIECAM16 and Hellwig-CAM16 [18] models, which are among the most recently developed and widely used color appearance models. The DIN data set was selected for evaluating the FSS scale because of its structure. The dimensions of this color order system are hue 'T', saturation 'S', and darkness 'D'. Psychophysical experiments were conducted to define perceptually-equidistant hues at S = 6 and D = 1. Then, observers defined saturation in 6 equidistant steps towards the white-point for each hue, and finally extrapolated to cover a larger gamut [69, 70]. The fundamental colorfulness and chroma scales were not evaluated directly as they are a function of saturation, so evaluating saturation scale can show their performance as well.

Six pages of the DIN data set are presented in Figures 6.5-6.10 to show the performance of different saturation scales. Stimuli with the same saturation level in a hue surface are assigned with the same number in the DIN data set. An ideal saturation scale must predict the same saturation level for all stimuli with the same assigned saturation level.

Different plots in Figures 6.5-6.10 show that the predicted saturation by FSS has an excellent alignment with assigned saturation. The FSS predicted an almost constant saturation for all stimuli with the same assigned saturation. Therefore, stimuli with the same assigned saturation are aligned in a straight line in the FSS plots. The CIECAM16 and Hellwig-CAM16 didn't predict the same saturation value for constant-saturation stimuli, and they have over-estimation or under-estimation in their prediction for darker stimuli. Stimuli with the same saturation would be underestimated by the CIECAM16 if they are darker, and would be overestimated by Hellwig-CAM16 if they are darker.

Standard deviation (SD) of the saturation prediction by different scales in each saturation level can be a good metric to compare the performance of different scales. As predicted saturation must be the same for the constant-saturation stimuli, then lower SD shows a better performance.

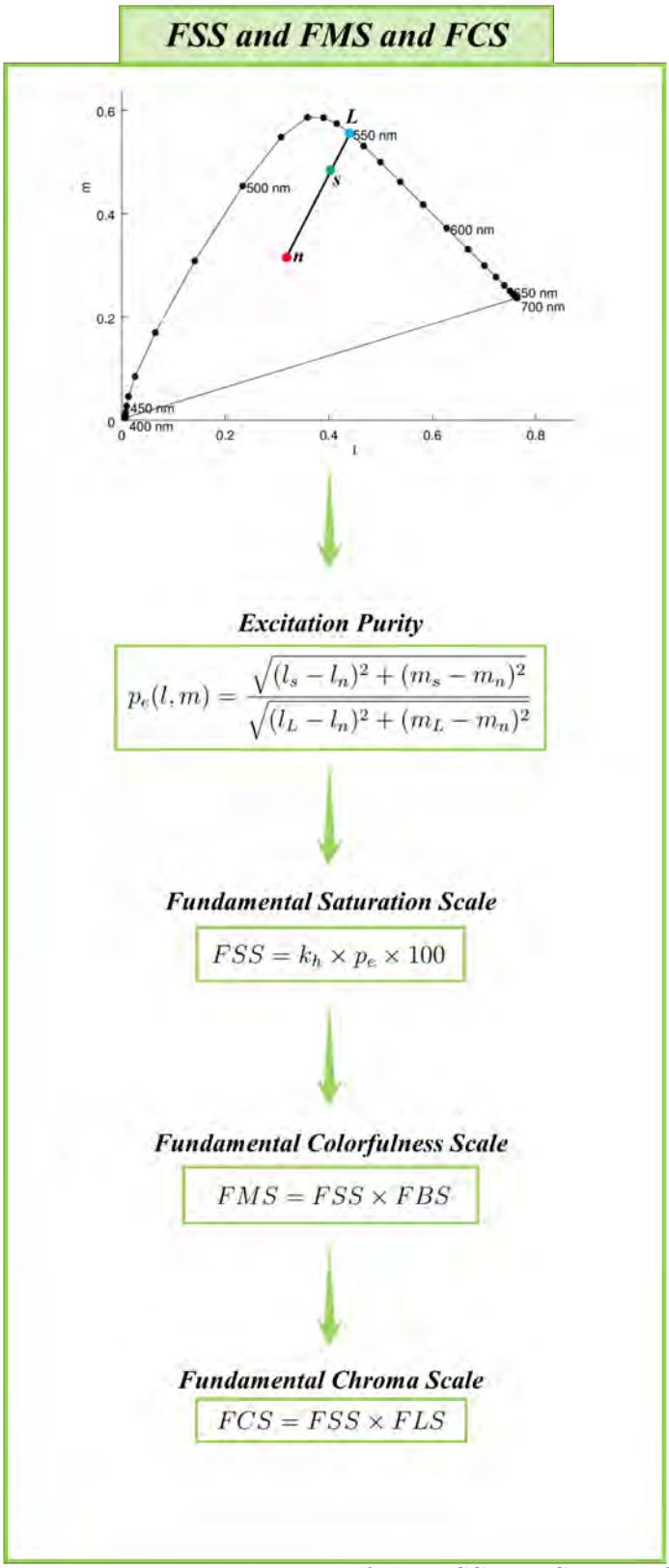

Figure 6.4: The graphical abstract of the FSS, FMS and FCS scales.

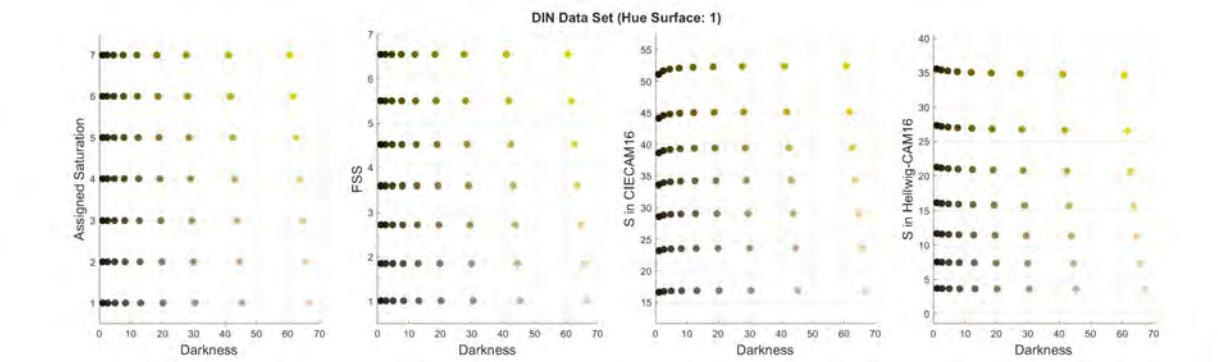

Figure 6.5: Predicted saturation for stimuli in the 1st page of the DIN data set. From left; First: The assigned saturation in the DIN system. Second: The predicted saturation by FSS. Third: The predicted saturation by CIECAM16. Fourth: The predicted saturation by Hellwig-CAM16 introduced in [18].

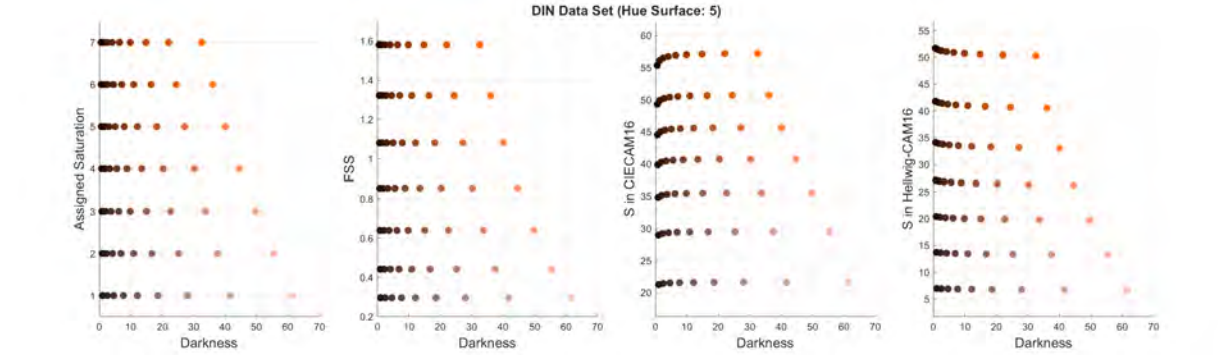

Figure 6.6: Predicted saturation for stimuli in the 5th page of the DIN data set. Plots are in the same order as Figure 6.5.

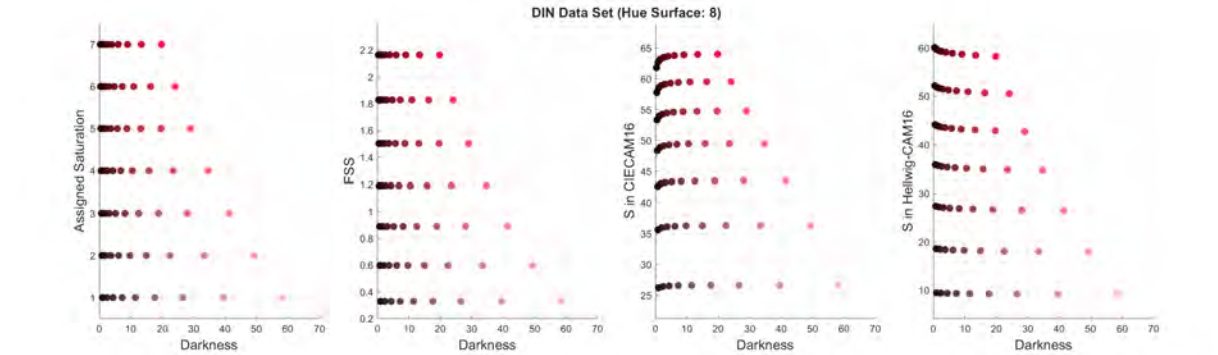

Figure 6.7: Predicted saturation for stimuli in the 8th page of the DIN data set. Plots are in the same order as Figure 6.5.

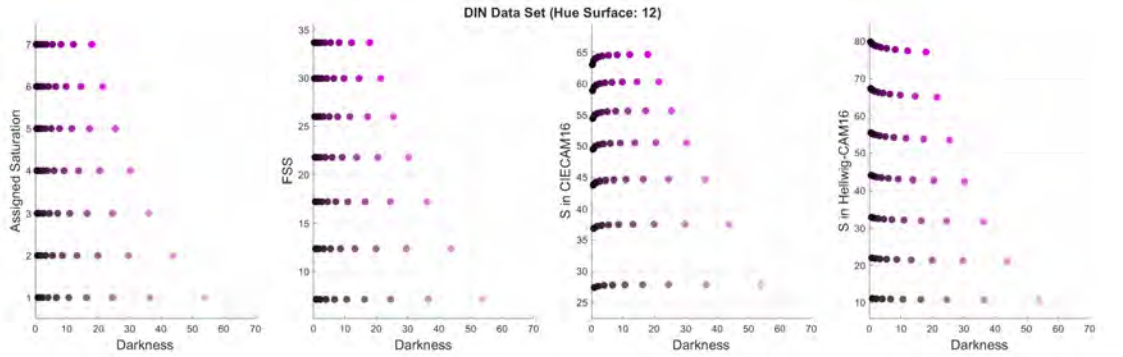

Figure 6.8: Predicted saturation for stimuli in the 12th page of the DIN data set. Plots are in the same order as Figure 6.5.

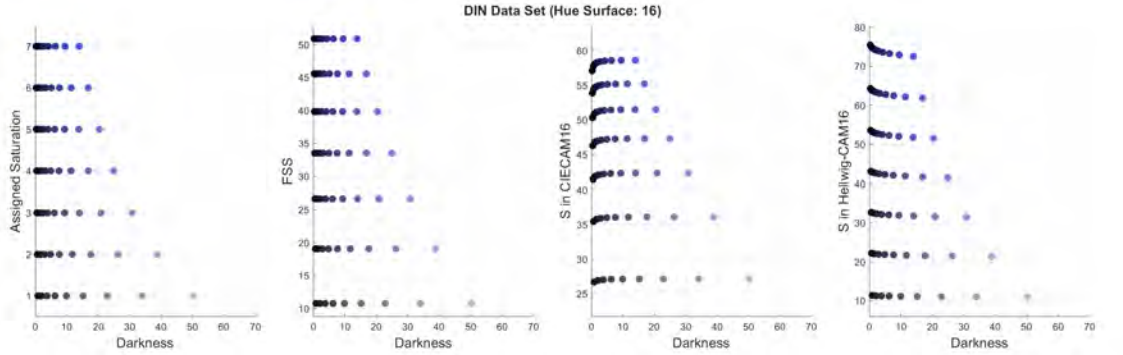

Figure 6.9: Predicted saturation for stimuli in the 16th page of the DIN data set. Plots are in the same order as Figure 6.5.

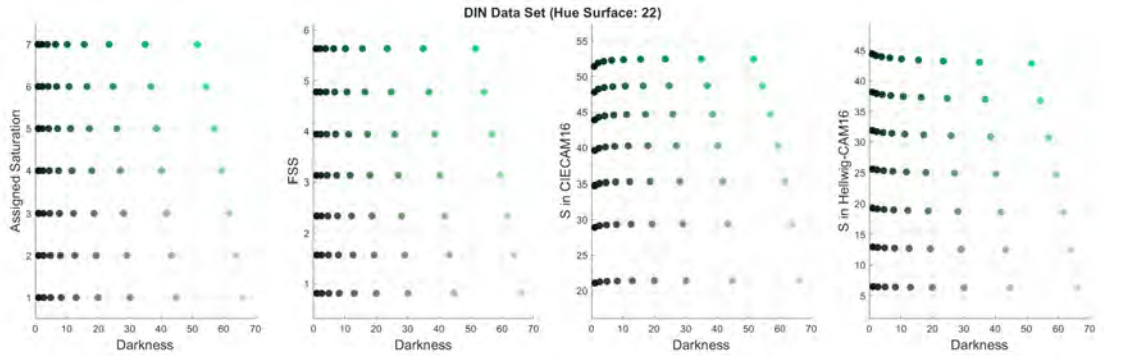

Figure 6.10: Predicted saturation for stimuli in the 22nd page of the DIN data set. Plots are in the same order as Figure 6.5.

The SDs of saturation prediction using the FSS, CIECAM16, and Hellwig-CAM16 models for constant saturation stimuli are reported in Table 6.1. The results show that the FSS has much smaller SDs compared to the CIECAM16 and Hellwig-CAM16. So, FSS has a better prediction of saturation for the DIN data set compared to the CIECAM16 and Hellwig-CAM16 models. The results show that there is a significant difference between FSS and other models, and it works significantly better than the CIECAM16 and Hellwig-CAM16.

Table 6.1: The average, SD, min, and max of saturation prediction for constant-saturation stimuli.

Model	Mean	SD	Min	Max
FSS	6.7e-15	7.6e-15	8.9e-16	3.6e-14
CIECAM16	0.14	0.02	0.10	0.16
Hellwig-CAM16	0.07	0.02	0.03	0.11

6.4 Conclusion and Discussion

This chapter introduced the *Fundamental Saturation Scale (FSS)*. Unlike existing saturation correlates that are derived from the CIE XYZ colorimetric system, the FSS is constructed directly from cone fundamentals, allowing saturation to be modeled more closely to the early stages of human visual processing.

The proposed approach defines saturation based on excitation purity computed in the *l,m* chromaticity diagram derived from the CIE 2006 cone fundamentals. To account for known hue-dependent variations in perceived saturation, a perceptual scaling factor based on Wright's classical experimental data was incorporated. Then, preliminary fundamental scales for colorfulness and chroma, derived directly from the FSS were introduced. These scales provide a coherent extension of the proposed saturation framework and establish a foundation for further refinement in future work.

The performance of the FSS was evaluated using the DIN data set and compared with CIECAM16 and Hellwig-CAM16. Results showed that the FSS provides nearly constant saturation predictions for stimuli that are perceptually defined to have constant saturation, independent of darkness. Quantitative analysis using standard deviation confirmed that the FSS significantly outperforms other models for constant-saturation stimuli. Overall, the results demonstrate that modeling saturation directly from cone fundamentals, combined with perceptual hue-dependent scaling, offers clear advantages over existing XYZ-based approaches. The Fundamental Saturation Scale serves as a key component of the fundamental color appearance model developed in this dissertation.

In this study, a weighting function that was extracted from Wright's data was used as a scaling factor to calculate the FSS. A new weighting function with a better performance than Wright's data might be a potential improvement in the future study. Also, the FCS and FMS can be optimized using scaling factors and be evaluated with relevant data sets.

Chapter 7

A Proposed System of Colorimetry

7.1 Introduction

The preceding chapters of this dissertation discussed development and evaluation of a set of independent, one-dimensional color appearance scales derived directly from cone fundamentals: the Fundamental Hue Scale (FHS), Fundamental Lightness Scale (FLS), Fundamental Brightness Scale (FBS), and Fundamental Saturation Scale (FSS). Each scale was developed based on well-established perceptual definitions, formulated using physiologically meaningful signals, and validated against psychophysical data sets. While these scales were introduced and analyzed individually in Chapters 4 through 6, they were designed from the outset as components of a unified framework.

This chapter is intended to bring together the independently developed appearance scales introduced in the previous chapters into a single unified framework, the Fundamental Color Appearance Model (FCAM). Although the individual scales for hue, lightness, brightness, and saturation have already been presented and validated separately, it is necessary to revisit them in this chapter so that their relationships, common computational starting point, and combined use within a complete color appearance system can be clearly established. The purpose of this chapter is therefore not to repeat the earlier developments, but to consolidate the scales into one coherent recommendation for practical application, including their joint use for color specification, appearance prediction, and color-difference evaluation. This integration is essential for demonstrating how the independent scales function collectively as a proposed system of colorimetry. Furthermore, this integrated chapter serves as the foundation for the final paper, where the proposed scales and their collective framework will be presented together as the complete Fundamental Color Appearance Model (FCAM).

In particular, this chapter (1) positions FCAM as an LMS-based color appearance model

grounded in cone fundamentals, (2) reviews the general features and advantages of FHS, FLS, FBS, and FSS as a set of one-dimensional perceptual scales, and (3) reiterates the key motivations for FCAM that were detailed in Chapters 1 through 3, now viewed from the perspective of a finished and validated system. This chapter emphasizes integration and system-level implications, so all proposed color scales are reviewed again.

By introducing FCAM explicitly as a color appearance model, this chapter establishes the conceptual transition from individual scale development to a new system of colorimetry that departs from traditional XYZ-based and three-dimensional paradigms, and adopts independent, physiologically grounded perceptual dimensions.

7.2 Conceptual Foundation of FCAM

FCAM is built upon two central notions that distinguish it from conventional color appearance models. First, perceptual color attributes such as hue, lightness, brightness, and saturation are treated as independent perceptual dimensions, each represented by a one-dimensional scale. Second, each scale is derived directly from cone fundamentals, rather than from tristimulus values.

Traditional color appearance models typically rely on a three-dimensional space derived from CIE XYZ, followed by a sequence of nonlinear transformations to predict multiple perceptual attributes. Although successful for many applications, this approach conflates stimulus representation with perceptual description and inherits limitations associated with the XYZ system, including weak physiological grounding and limited support for observer variability. FCAM addresses these limitations by anchoring all color appearance scales in LMS cone responses, and introducing one-dimensional independent color appearance scales.

In FCAM, chromatic adaptation is performed at the cone-response level using established LMS-based adaptation models such as vK20 [27] and WGM [28], after which each appearance attribute is computed independently. No assumption is made regarding an underlying Euclidean geometry or a unified color space in which all attributes coexist. Instead, FCAM is explicitly scale-based rather than space-based.

7.3 Structure of the Fundamental Color Appearance Model

The general computational structure of FCAM was introduced in Chapter 3 and is reviewed here to emphasize its role as an integrated system. The FCAM workflow can be described

in four stages:

7.3.1 Spectral Encoding and Cone Excitation

The input to FCAM is the cone fundamental responses (LMS). These LMS responses can be computed directly using the CIE 2006 fundamental CMFs, or derived from individualized observer functions such as the Asano model, or obtained from the XYZ tristimulus values through an appropriate transformation matrix.

Therefore, the spectral power distribution of a stimulus is converted to cone excitations. In this case, the CIE 2006 cone fundamentals, Asano categories, or Asano model are recommended. When the spectral power distribution of a stimulus is not available and only the CIE XYZ tristimulus values are available, they can be converted into the LMS cone responses using an appropriate matrix transformation (e.g., HPE matrix transformation [43]). This flexibility allows FCAM to account for both standard observers and individual differences in color vision.

7.3.2 Chromatic Adaptation

In developing the FCAM model, which is based on cone fundamental responses and designed to account for individual differences in color vision, it is important to include a chromatic adaptation step. Among the available chromatic adaptation models, vK20 [27] and Weighted Geometric Mean (WGM) [28] models are particularly suitable. Together, these models provide both theoretical robustness and empirical accuracy, making them strong candidates to serve as the chromatic adaptation stage within FCAM.

Several chromatic adaptation models have been introduced that are based on the von Kries model, to predict perceived colors across different media [1]. The von Kries hypothesis suggests that adaptation in the three cone types is independent and inversely proportional with the response to a neutral adapting stimulus [27].

The von Kries hypothesis is explicitly introduced in Eq. 7.1, where L,M,S are the initial cone responses, L_n, M_n, S_n are the cone responses to the adapting stimulus (it is usually a similarly-illuminated diffuse white) and L_a, M_a, S_a are the post-adaptation cone signals [27].

$$\begin{bmatrix} L_a \\ M_a \\ S_a \end{bmatrix} = \begin{bmatrix} \frac{1}{L_n} & 0 & 0 \\ 0 & \frac{1}{M_n} & 0 \\ 0 & 0 & \frac{1}{S_n} \end{bmatrix} \begin{bmatrix} L \\ M \\ S \end{bmatrix} \tag{7.1}$$

Various chromatic adaptation transformation based on the von Kries model have been

proposed. Even the chromatic adaptation transform, incorporated in CIECAM02 and CIECAM16, is a simple von Kries model with slight modifications of the spectral definitions of the LMS fundamentals [27]. Among different chromatic adaptation models, vK20 [27] and Weighted Geometric Mean (WGM) [28] models are suggested to be used in FCAM. These models are introduced in the following subsections.

7.3.2.1 The vK20 Model

Based on recent studies, adaptation is incomplete, and it depends on individuals and even on the previous adapting conditions. Based on these findings, Fairchild [27] introduced a modification to the von Kries model, named vK20, which incorporates three adapting chromaticities instead of one. These three chromaticities are the current adapting stimulus, the immediately preceding adapting stimulus, and a newly proposed reference point at approximately 15000K (sky blue).

The structure of vK20 is given in Eq. 7.2, where L, M, S refer to the initial cone responses, L_a, M_a, S_a refer to the post-adaptation cone signals, L_n, M_n, S_n refer to the cone responses for the adapting illuminant, L_r, M_r, S_r refer to the responses for the reference illuminant (taken to be $u' = 0.185$, $v' = 0.425$, approximately 15000K, sky blue), and L_p, M_p, S_p refer to the responses for the previous adapting illuminant. D_n, D_r, and D_p refer to the degrees of adaptation to each of the three adapting chromaticities and must sum to 1.0 [27].

$$\begin{bmatrix} L_a \\ M_a \\ S_a \end{bmatrix} = \begin{bmatrix} \frac{1}{D_n L_n + D_r L_r + D_p L_p} & 0 & 0 \\ 0 & \frac{1}{D_n M_n + D_r M_r + D_p M_p} & 0 \\ 0 & 0 & \frac{1}{D_n S_n + D_r S_r + D_p S_p} \end{bmatrix} \begin{bmatrix} L \\ M \\ S \end{bmatrix} \tag{7.2}$$

The vK20 model demonstrates improved accuracy in predicting incomplete and context-dependent adaptation, offering a more physiologically plausible framework for understanding human color inconstancy.

7.3.2.2 The WGM Model

Shen and Fairchild introduced a chromatic adaptation model named Weighted Geometric Mean (WGM) model [28]. Unlike traditional models such as CAT02 and CAT16, WGM uses a geometric mean computation that predicts incomplete adaptation along realistic illumination paths like the Planckian or daylight locus [28].

The complete formulation of the WGM model is given in Eq. 7.3, where the weighting term D can be included to represent varying degrees of sensory and cognitive adaptation

under different viewing conditions [28].

$$\begin{bmatrix} L_a \\ M_a \\ S_a \end{bmatrix} = \begin{bmatrix} L_n^D \cdot L_r^{1-D} & 0 & 0 \\ 0 & M_n^D \cdot M_r^{1-D} & 0 \\ 0 & 0 & S_n^D \cdot S_r^{1-D} \end{bmatrix} \begin{bmatrix} L \\ M \\ S \end{bmatrix} \tag{7.3}$$

Adapted cone responses are used to compute the four fundamental appearance scales: hue (FHS), lightness (FLS), brightness (FBS), and saturation (FSS). Each scale is defined by a dedicated mathematical formulation designed specifically for that perceptual attribute. These fundamental appearance scales are introduced at the following sections.

7.3.3 Fundamental Hue Scale (FHS)

Hue is one of the perceptual attributes used to describe color. According to the definition of hue, an area is described as similar to one of the perceptions such as the unique hues of red, yellow, green, and blue or their combination [1, 8].

Two types of hue scales can be used to describe hue: the Munsell-type scales and the NCS-type scales. The Munsell-type scales aim to create scales of equal color discrimination, or color differences, and they are based on five, equally spaced, principal hues, such as hue-angle of the CIELAB and CIECAM16. The NCS-type scales aim to specify colors according to their appearance, and they are based on four unique hues as cardinal axes, such as hue-quadrature of the CIECAM16 [17].

The FHS model with two scales was proposed for hue discrimination and hue appearance purposes in [16, 31]. The FHS includes two one-dimensional scales, and it is a fundamental and physiologically plausible model, also mathematically easy to implement and straightforward. By formulating hue directly from LMS-derived opponent mechanisms, FHS avoids reliance on XYZ-based systems and provides a more direct link to visual physiology. The resulting hue angles exhibit successful linearity and spacing when evaluated against several data sets.

As part of FCAM, FHS serves as the sole predictor of hue, independent of lightness, brightness, or saturation. This independence is particularly important for applications such as hue preservation in gamut mapping.

In the proposed model, the cone spectral sensitivity estimates of Stockman and Sharpe [44], available in [45], were used to calculate the LMS cone responses. Any observer model that predicts individual CMFs such as in [6, 7] can be used to calculate LMS cone responses as the input of the FHS model.

The first step of the model converts the LMS cone responses into two opponent axes

named yellow-blue (YB) and red-green (RG). This conversion is named FHS and presented in Eqs. 7.4 and 7.5. The matrix presentation of FHS is provided in Eq. 7.6.

$$YB = \frac{L+M}{2} - S \tag{7.4}$$

$$RG = 3 \times (L - M) \tag{7.5}$$

$$\begin{bmatrix} YB \\ RG \end{bmatrix} = \begin{bmatrix} 0.5 & 0.5 & -1.0 \\ 3.0 & -3.0 & 0.0 \end{bmatrix} \times \begin{bmatrix} L \\ M \\ S \end{bmatrix} \tag{7.6}$$

This step creates an opponent space, and it is the basis of two hue scales named FHS_h and FHS_H. The FHS opponent space is illustrated using five principal hues of the Munsell data set and four unique hues of the NCS data set in Figure 7.1.

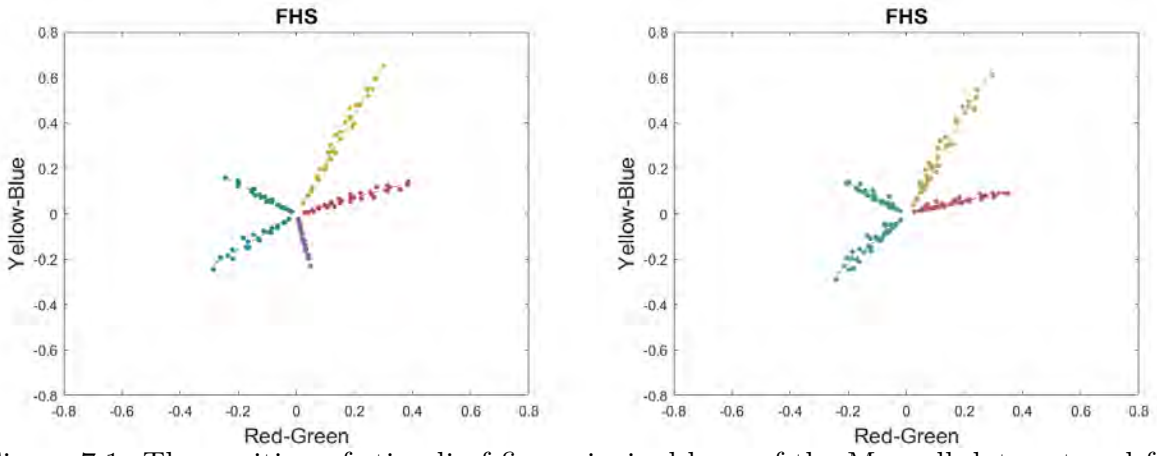

Figure 7.1: The position of stimuli of five principal hues of the Munsell data set and four unique hues of the NCS data set in *FHS*.

It can be seen in Figure 7.1 that the FHS is not equally spaced regarding the five principal hues. So, hue surfaces need to be rotated to have better spacing. Then the hue discrimination scale becomes the hue angle of stimuli in the rotated space, FHS_h.

Also, unique hues in Figure 7.1 are not orthogonal and they should be rotated to become orthogonal. Then hue appearance can be easily described using the hue-quadrature measure, FHS_H.

For these two purposes, two rotation matrices were designed and applied on the RG and YB axes of Eq. 7.6. The general rotation matrix is presented in Eq. 7.7, and θ was defined as a function of hue angle regarding the position of five principal hues or four unique hues.

$$\begin{bmatrix} YB' \\ RG' \end{bmatrix} = \begin{bmatrix} \cos(\theta) & \sin(\theta) \\ -\sin(\theta) & \cos(\theta) \end{bmatrix} \times \begin{bmatrix} YB \\ RG \end{bmatrix} \tag{7.7}$$

$$\theta_i = h'_i - h_i \tag{7.8}$$

$$\theta = \frac{(\theta_{i+1} - \theta_i)}{h_{i+1} - h_i} \times (h - h_i) + \theta_i \tag{7.9}$$

The h_i of five principal hues were determined by averaging the hue angle of all stimuli in each principal hue of the Munsell in the *FHS* space. The h_i is 18.33, 65.28, 148.00, 219.28 and 282.30 for red, yellow, green, blue, and purple, respectively. The h'_i is 18, 90, 162, 234 and 306 for red, yellow, green, blue and purple, respectively.

The h_i of four unique hues were determined by the average hue angle of all stimuli in each unique hue of the NCS in the *FHS* space. The h_i is 16.91, 64.82, 146.82 and 228.30 for red, yellow, green and blue, respectively. The h'_i is 0, 90, 180 and 270 for red, yellow, green and blue respectively.

Then the hue angle computed from the ratio of YB' to RG' in FHS_h in Eq. 7.10 becomes a Munsell type of hue scale. The hue quadrature computed from the ratio of YB' to RG' in FHS_H in Eq. 7.11 forms an NCS type of hue scale.

$$FHS_h = \arctan(\frac{YB'}{RG'}) \tag{7.10}$$

$$FHS_H = \frac{400}{360} \times \arctan(\frac{YB'}{RG'}) \tag{7.11}$$

The position of five principal hues of the Munsell data set in the FHS_h and four unique hues of the NCS data set in the FHS_H are shown in Figure 7.2. It can be seen that after rotation, five principal hues are equally spaced in FHS_h, and four unique hues are orthogonal in FHS_H.

Next step is evaluating the proposed hue scales in terms of linearity, spacing, and agreement with hue appearance. Hue linearity means stimuli with the same perceived hue result in constant model hue output. Hue spacing means each constant hue surface as input, on average, results in hue output that is equally spaced from the next hue surface [24]. Also, calculated hue quadrature should have a good agreement with hue appearance description.

The FHS was compared to other hue models using traditional data sets and the collected results from the conducted psychophysical experiments. The results of statistical analysis showed that the FHS is successful in terms of linearity. Although the FHS model is a simple

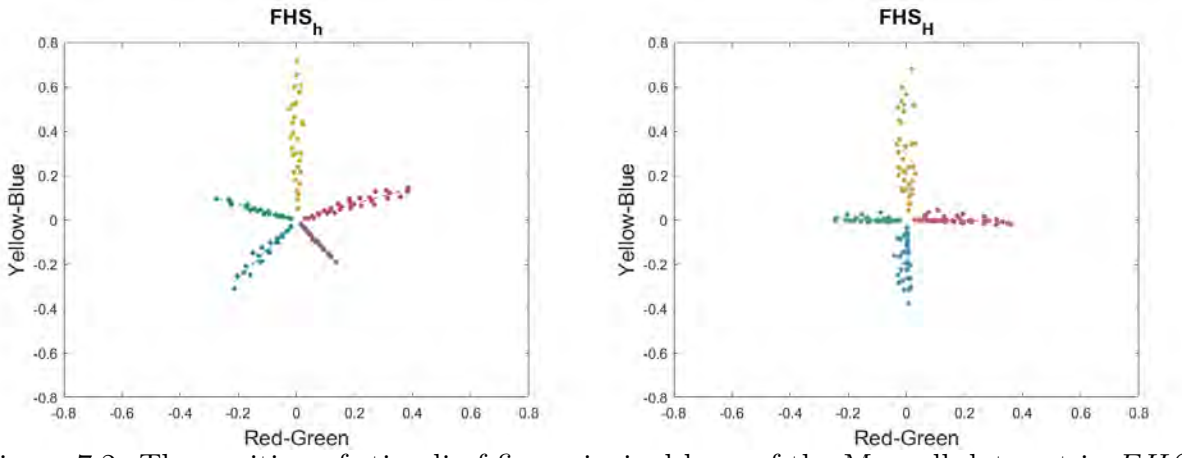

Figure 7.2: The position of stimuli of five principal hues of the Munsell data set in FHS_h and four unique hues of the NCS data set in FHS_H.

model, it achieves hue linearity at the level of complicated hue scales. The constant hue surfaces of a conducted visual experiment are plotted in Figure 7.3 in different hue scales to visualize the hue linearity of these hue scales.

In terms of spacing, the results showed that the FHS_h has a better or equal performance compared to other models. In terms of hue quadrature prediction, the FHS_H was equal to or worse than other hue scales.

It can be concluded that the formulated FHS hue scales are mathematically easy to implement, also physiologically and perceptually plausible. These scales are directly built from cone fundamentals to allow easy generalization to individual observers. FHS_h and FHS_H perform at least as well as more complicated and abstract colorimetric models in most situations.

7.3.4 Fundamental Lightness and Brightness Scales (FLS and FBS)

As a part of developing FCAM as a new colorimetric system, two one-dimensional scales of lightness and brightness were introduced in [82]. These scales are built directly based on the cone fundamentals, so they are called FLS for Fundamental Lightness Scale, and FBS for Fundamental Brightness Scale.

Brightness and lightness are important attributes of human visual perception. Brightness is defined as a perceptual attribute related to the amount of light that is emitting or reflecting from a surface or light source. Lightness is the brightness of an area judged relative to a white or highly transmitting area that is similarly illuminated. The main distinction is that brightness refers to the perception of absolute amounts of light, but lightness is a relative perception [1, 8].

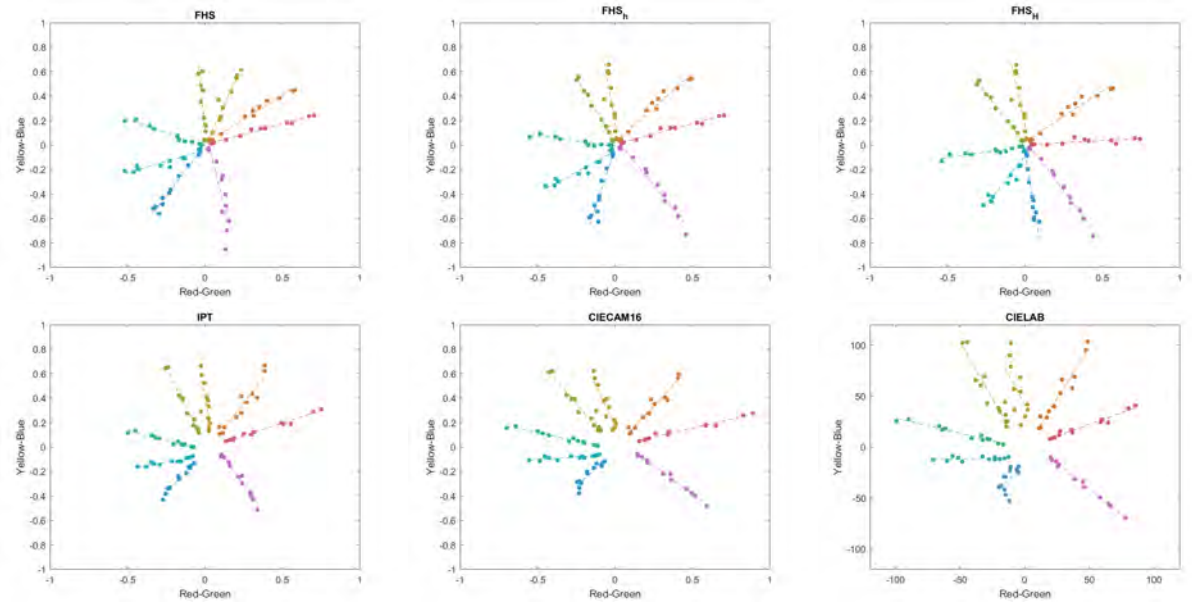

Figure 7.3: Results of constant hue surface experiment for linearity evaluation are presented in different hue scales.

Modeling lightness and brightness has some complexities, as these attributes are not a simple function of luminance [18, 19]. Two stimuli with equal luminance are perceived equally bright only under special circumstances, such as having identical spectral distributions or at least being judged to be equal in color [20].

The precise relationship between brightness/lightness and luminance has been studied using a variety of visual experiments. Based on these studies, perceived brightness increases with the logarithm or with some power (less than 1.0) of stimulus luminance [21].

Brightness and lightness as visual perception attributes have been modeled using luminance, which is a physical metric. Luminance is calculated by integrating spectral radiance multiplied by the luminous efficiency function [49, 50]. The perceived brightness and lightness are not a simple function of luminance, and they are affected by some color appearance phenomena. For example, the Helmholtz–Kohlrausch (H–K) effect conveys that stimuli with greater purity appear brighter than stimuli with less purity with hue dependency, although they have the same luminance [19, 51, 52].

Bartleson and Breneman studies showed that the perceived contrast of images increased when the image surround was changed from dark to dim to light. The dark surround of an image causes dark areas to appear lighter while having little effect on light areas, so the contrast of the image changes [1]. This phenomenon is known as the Bartleson–Breneman effect.

Another color appearance phenomenon is the Stevens effect that refers to an increase

in brightness (or lightness) contrast with increasing luminance. In this context, contrast is the rate of change in perceived brightness (or lightness) with respect to luminance, and luminance means the adapting luminance (or the luminance of white point) [1, 64].

To include the H–K effect, the Stevens effect, and the Bartleson–Breneman effect into the lightness model, the general form of the equation should be like Eq. 7.12.

$$FLS = (\frac{(A_{HK})^{(Q_{tbl} \times c)} + d}{1 + d}) \times 100 \tag{7.12}$$

$$A_{HK} = \frac{\begin{bmatrix} 2.0 & 1.0 & \frac{1}{20} \end{bmatrix} \times \begin{bmatrix} L \\ M \\ S \end{bmatrix}}{A_{G_0}} \tag{7.13}$$

$$Q_{tbl} = 0.6 \times [log10(Y_w + 1)]^{0.65} + 0.0572 \tag{7.14}$$

The A_{HK} is the achromatic response that is normalized to A_{G_0} to account for the H–K effect, and it can be calculated using Eq. 7.13. A_{G_0} is the achromatic response calculated from the G_0 luminance. The G_0 luminance, or zero gray content, defines the luminance of the 'equal chromatic brightness' and can be determined for the entire chromaticity diagram [53, 56–59]. The luminance of the stimulus in the G_0 state can be considered as an anchor for each chromaticity coordinate. So, the luminance of a specific chromaticity can be normalized to its G_0 luminance, instead of normalizing to a white luminance [5]. A function provided by Aghamohammadi et al. [61] was used to calculate the corresponding A_{G_0}.

Two constants, c and d, introduce the nonlinear relationship between achromatic response (or luminance) and perceived lightness. Also, c and d were optimized for different surround conditions to account for the Bartleson–Breneman effect. The optimization steps are detailed in [82]. The optimized constants are introduced in Table 7.1, and they can be optimized for a specific data set, or a specific application, or different viewing conditions. This feature makes the FLS model useful and flexible for different applications.

Table 7.1: The optimized constants for the FLS model introduced in Eq. 7.12.

	Dark	Dim	Average
c	$\frac{1}{2.8}$	$\frac{1}{2.5}$	$\frac{1}{2.25}$
d	0.004	0.003	0.002

Then, c in Eq. 7.12 is multiplied by terminal brightness to account for the Stevens effect. Terminal brightness is calculated using Eq. 7.14. Where Y_W is the absolute luminance of diffuse white in cd/m^2. Q_{tbl} is defined to be 1.0 at an adapting luminance of 100 cd/m^2 [64]. Figure 7.4 shows the FLS model with optimized constants for three surround conditions and different adaptive luminance that converges to one point.

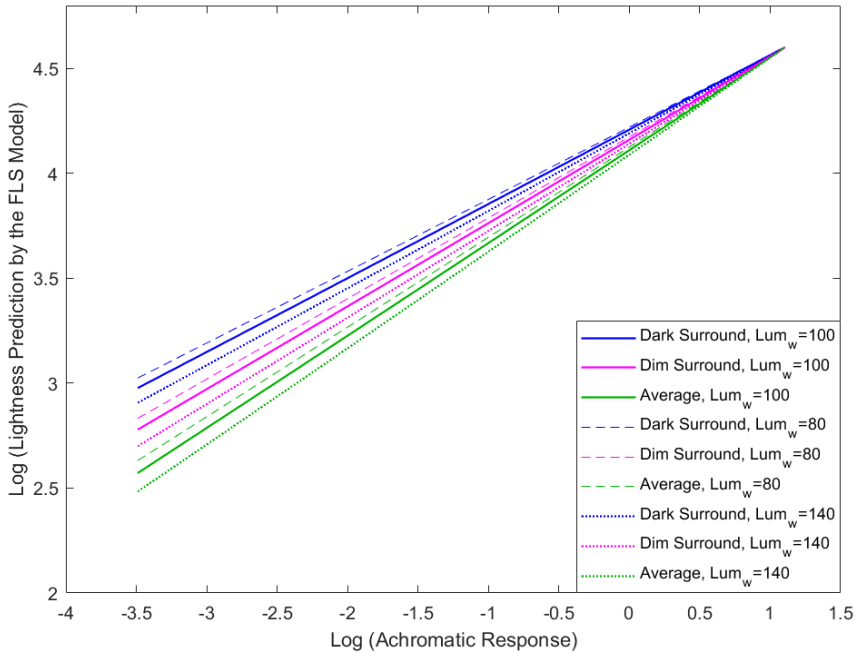

Figure 7.4: The FLS model converges to one point for three surround conditions at different adapting luminance.

The brightness scale is defined based on FLS (7.12) and it is named FBS, short for Fundamental Brightness Scale. The FBS is introduced in 7.15.

$$FBS = FLS \times Q_{tbl} \tag{7.15}$$

To evaluate the FLS performance, seven data sets were used, including the DIN data set, and six brightness matching data sets provided by Sanders and Wyszecki [65], Wyszecki [66], Fairchild and Pirrotta [67], Xie [68], High [13], and Hellwig [12].

The DIN data set was used as a ground truth to check the accuracy of the FLS in comparison with the Hellwig23 model, especially in terms of the H–K effect prediction. The lightness prediction by the Hellwig23 and FLS models for two pages of the DIN are presented in Figures 7.5 and 7.6. The stimuli with constant darkness are lined up in the FLS plot, but the Hellwig23 has overestimation and underestimation for constant darkness samples. The

standard deviations of lightness prediction using the FLS and Hellwig23 showed that the FLS has smaller standard deviations compared to the Hellwig23. So, the FLS has a better prediction of the H–K effect compared to the Hellwig23.

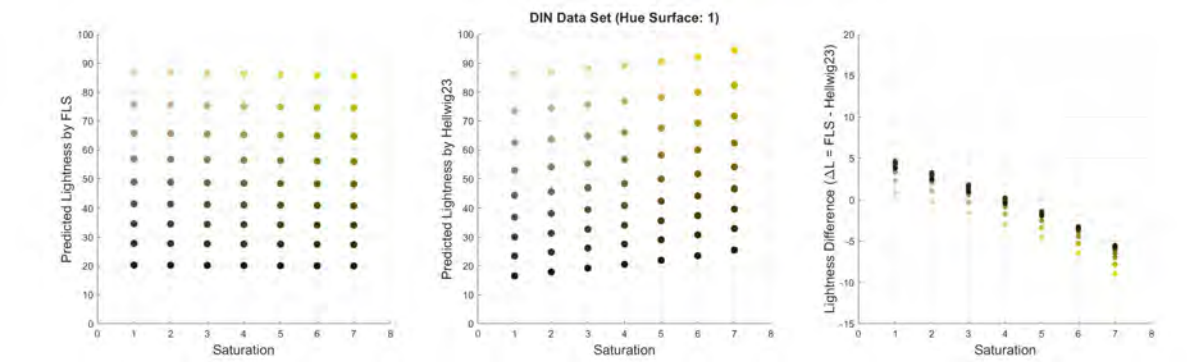

Figure 7.5: Left: The lightness prediction by the FLS. Middle: The lightness prediction by the Hellwig23. Right: The lightness difference between the FLS and Hellwig23. Stimuli of the 1st hue surface of the DIN data set.

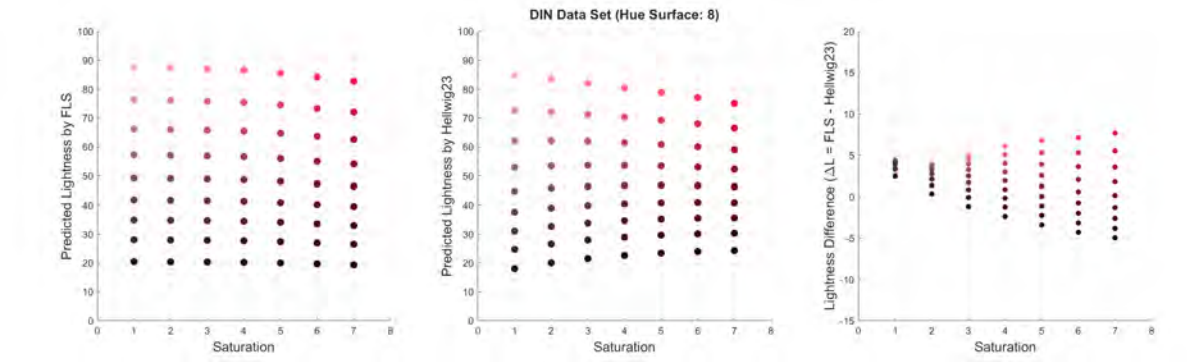

Figure 7.6: The same as Figure 7.5 for the 8th hue surface of the DIN data set.

Other data sets resulted from brightness matching experiments provided by researchers over several decades were used to evaluate the FLS model in comparison with other lightness models. The results showed that there is no significant difference between lightness models. It means that none of the models is better than the others for all data sets. Based on the results, some models work better for several data sets. The FLS is not significantly better than other models for these data sets, but it has good performance for all data sets, although it is a simple model compared to other models. This is a good feature that FLS works well for a variety of data sets and different luminance ranges and different viewing conditions. Also, the constants of FLS can be optimized for a specific data set or viewing condition. This makes FLS a flexible model for different applications. It should be mentioned that FBS was not evaluated separately, as FBS is a function of FLS and the luminance of the white point.

7.4 Fundamental Saturation Scale (FSS)

Saturation is a perceptual attribute in color appearance models, and it is defined as "*colorfulness of an area judged in proportion to its brightness*". Saturation can be defined as relative colorfulness and it is different from chroma, as it is the colorfulness of a stimulus relative to its own brightness. Chroma is defined as "*colorfulness of an area judged as a proportion of the brightness of a similarly illuminated area that appears white or highly transmitting*" [1].

Most existing saturation scales are ultimately rooted in the CIE XYZ colorimetric system, and they inherit limitations associated with the XYZ color matching functions (CMFs). A saturation scale derived directly from cone fundamentals is introduced here as a part of FCAM.

Saturation is a fundamental perceptual attribute, and it can be described as the degree to which a color differs from a neutral of the same lightness, ranging from achromatic to highly vivid appearances. In traditional colorimetry, one of the earliest correlates of saturation is excitation purity, defined as the ratio of the distances from the given white to the chromaticity and to the spectral locus or line of purples within a chromaticity diagram. Excitation purity quantifies the proportion of chromatic content relative to an achromatic reference [1, 8].

Excitation purity depends only on chromaticity coordinates and the selected white point, and it can be computed in any chromaticity diagram derived from a tristimulus space such as '*l,m*' chromaticity diagram [1, 8]. The '*l,m*' chromaticity diagram is constructed directly from cone fundamentals, and is tied to the earliest stages of human visual processing. Using LMS cone fundamentals, chromaticity coordinates can be defined using Eqs. 7.16, 7.17, and 7.18.

$$l = \frac{L}{L + M + S} \tag{7.16}$$

$$m = \frac{M}{L + M + S} \tag{7.17}$$

$$s = 1 - (l + m) \tag{7.18}$$

Classical excitation purity provides a geometrically well-defined measure of saturation, however it does not account for variations in perceived saturation as a function of hue. To address this limitation, the proposed FSS combines excitation purity computed in the *l,m* chromaticity diagram with a hue-dependent perceptual scaling factor derived from Wright's experimental observations [80].

The FSS is defined within the *l,m* chromaticity diagram constructed from the CIE 2006 cone fundamentals. This representation directly reflects the responses of the L-, M-, and S-cones and therefore corresponds to the earliest stage of human color vision. The chromaticity coordinates are defined based on Eqs. 7.16, 7.17, and 7.18.

The spectrum locus in the *l,m* chromaticity diagram was computed for monochromatic stimuli spanning the visible range from 390 nm to 760 nm in 5 nm intervals using the CIE 2006 cone fundamentals.

The Equal Energy (EE) illuminant was considered as white point, and its chromaticity coordinate, (l_n, m_n), was calculated using its cone excitations, L_{EE}, M_{EE}, and S_{EE}, in Eqs. 7.19 and 7.20. The (l_n, m_n) chromaticity coordinate is considered as the origin from which saturation is measured in the *l,m* chromaticity diagram.

$$l_n = \frac{L_{EE}}{L_{EE} + M_{EE} + S_{EE}}, \tag{7.19}$$

$$m_n = \frac{M_{EE}}{L_{EE} + M_{EE} + S_{EE}}. \tag{7.20}$$

To associate each chromaticity with a perceptual hue, a hue angle was computed for spectrum-locus points. The hue angle definition follows the conventional formulation used in CIELAB and is adapted here to the *l,m* chromaticity plane. For a chromaticity point (l, m), the hue angle h is defined relative to the white point using Eq. 7.21.

$$h = Arctan(\frac{l - l_n}{m - m_n}) \tag{7.21}$$

where *Arctan* denotes the inverse tangent function. Using this formulation, hue angles were computed for all spectrum-locus points between 390 nm and 760 nm, establishing a mapping between chromaticity coordinates and hue angle within the cone-based chromaticity representation.

Then excitation purity should be calculated. For a given stimulus chromaticity **S** and a reference white point **N**, the corresponding hue angle for that stimulus can be calculated. Then, the corresponding point **L** on the spectrum locus along the same hue direction can be found. Having these data, excitation purity p_e can be calculated using Eq. 7.22 [1, 8]. The *l,m* chromaticity diagram is presented in Figure 7.7 to show the position of stimulus, white point, and the corresponding point on the spectrum locus. By definition, excitation purity is zero at the white point and unity at the spectrum locus [1, 8].

$$p_e(l,m) = \frac{\sqrt{(l_s - l_n)^2 + (m_s - m_n)^2}}{\sqrt{(l_L - l_n)^2 + (m_L - m_n)^2}} \tag{7.22}$$

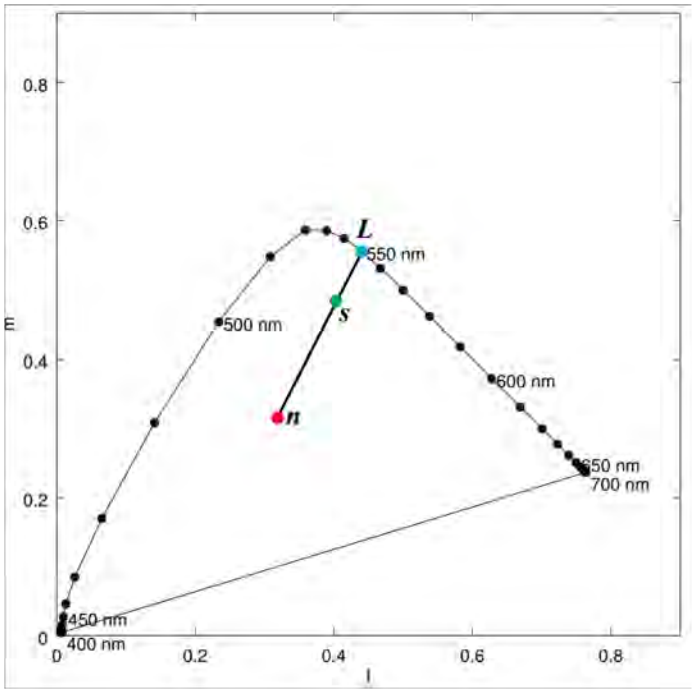

Figure 7.7: The *l,m* chromaticity diagram that is used to calculate the excitation purity.

Excitation purity cannot sufficiently represent the human perception of saturation. Psychophysical observations reported by Wright indicate that when the calculated excitation purity is identical, the perceived saturation is not constant across different hues. Colors of different hues may appear more or less saturated despite having equal excitation purity. To account for this effect, Wright introduced a hue-dependent scaling factor that modulates excitation purity to better align with human perception of saturation [80].

This hue-dependent scaling factor was extracted from Wright's experimental data that was published in [80] and organized as a lookup table (LUT). In order to extract this LUT, the mean sensitivity data are found in Figure 93 on Page 166 of Wright's book [80]. That plot was copied and enlarged and values were read off manually. Data were extrapolated down to 390 nm and up to 760 nm smoothly. Purple data were computed via linear interpolation. It should be noted that for arbitrary hue angles, the scaling factor is obtained by interpolation within the LUT.

The logarithmic Wright's data were then converted to linear sensitivity weightings and normalized to have a peak of 1.00. It is named k_h. This scaling factor was used to convert relative saturation (excitation purity) to an absolute saturation scale where the purples still

go up to 100 but the green wavelengths only peak at about 16. Better data should be developed in the future studies if more accurate saturation scales on an absolute basis are needed.

The Fundamental Saturation Scale is the excitation purity computed in the *l,m* chromaticity diagram multiplied by the hue-dependent scaling factor, k_h. For a given sample, FSS can be calculated using Eq. 7.23. It is multiplied by 100 to scale it in a range similar to CIECAM16 and Hellwig-CAM16.

$$FSS = k_h \times p_e \times 100 \tag{7.23}$$

A simple linear definition was used in this step to introduce the fundamental colorfulness and chroma scales. Saturation can be described as the colorfulness of a stimulus relative to its own brightness. So, colorfulness can be defined as saturation multiplied by its own brightness. Therefore, a simple linear function of saturation like Eq. 7.24 can be formulated to calculate the fundamental colorfulness scale. As colorfulness is denoted by M in some color appearance models, the fundamental colorfulness scale was named FMS.

$$FMS = FSS \times FBS \tag{7.24}$$

Saturation is defined as chroma divided by lightness. So, chroma can be defined as saturation multiplied by lightness [1]. Based on these definitions, the fundamental chroma scale, FCS, can be formulated by Eq. 6.18.

$$FCS = FSS \times FLS \tag{7.25}$$

These are preliminary models of colorfulness and chroma. They can be improved based on recent studies that have explored the effect of different parameters on perceived colorfulness and chroma.

The proposed saturation scale, FSS, was evaluated using the DIN data sets. Its performance was compared with that of the CIECAM16 and Hellwig-CAM16 [18] models, which are among the most recently developed and widely used color appearance models.

Two pages of the DIN data set are presented in Figures 7.8-7.9 to show the performance of different saturation scales. Stimuli with the same saturation level in a hue surface are assigned with the same number in the DIN data set. An ideal saturation scale must predict the same saturation level for all stimuli with the same assigned saturation level.

Different plots in Figures 7.8 and 7.9 show that the predicted saturation by FSS has an excellent alignment with assigned saturation. The FSS predicted an almost constant

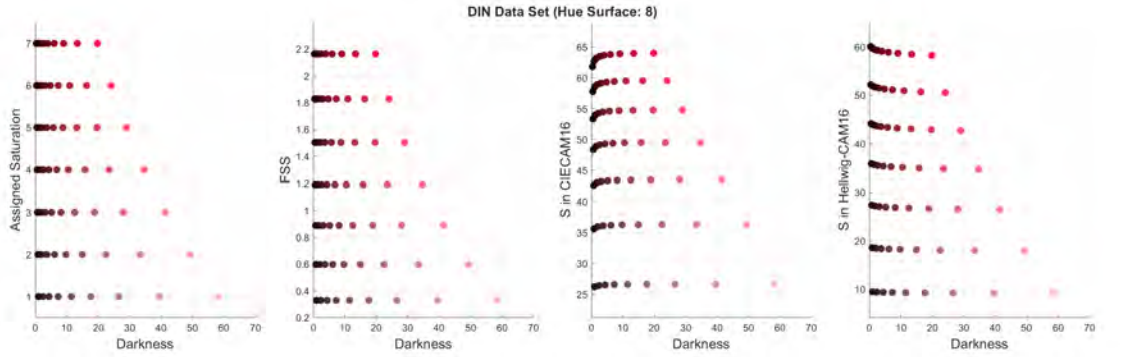

Figure 7.8: Predicted saturation for stimuli in the 8th page of the DIN data set. From left; First: The assigned saturation in the DIN system. Second: The predicted saturation by FSS. Third: The predicted saturation by CIECAM16. Fourth: The predicted saturation by Hellwig-CAM16 introduced in [18].

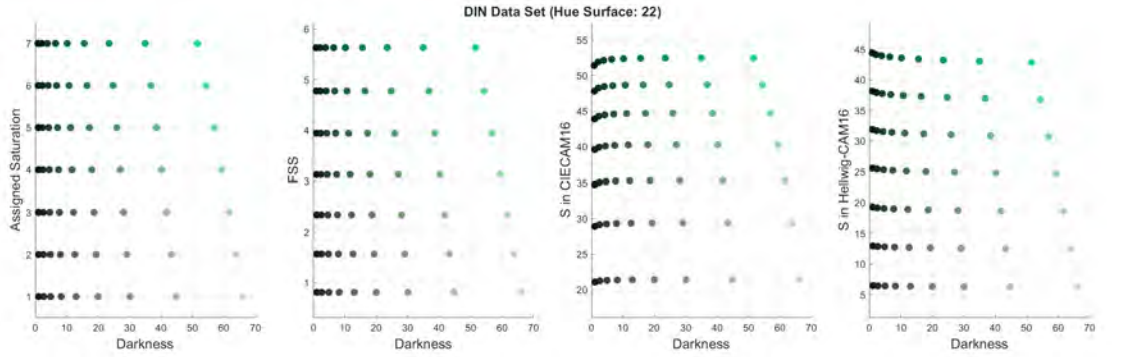

Figure 7.9: Predicted saturation for stimuli in the 22nd page of the DIN data set. Plots are in the same order as Figure 7.8.

saturation for all stimuli with the same assigned saturation. The CIECAM16 and Hellwig-CAM16 have over-estimation or under-estimation in their prediction for darker stimuli.

The SDs of saturation prediction using the FSS, CIECAM16, and Hellwig-CAM16 models for constant saturation stimuli are reported in Table 7.2. The results show that the FSS has much smaller SDs compared to the CIECAM16 and Hellwig-CAM16. So, FSS has a better prediction of saturation for the DIN data set compared to the CIECAM16 and Hellwig-CAM16 models.

Table 7.2: The average, SD, min, and max of saturation prediction for constant-saturation stimuli.

Model	Mean	SD	Min	Max
FSS	6.7e-15	7.6e-15	8.9e-16	3.6e-14
CIECAM16	0.14	0.02	0.10	0.16
Hellwig-CAM16	0.07	0.02	0.03	0.11

Overall, the results demonstrate that modeling saturation directly from cone fundamentals, combined with perceptual hue-dependent scaling, offers clear advantages over existing XYZ-based approaches. The Fundamental Saturation Scale serves as a key component of the fundamental color appearance model developed in this dissertation.

In this study, a weighting function that was extracted from Wright's data was used as a scaling factor to calculate the FSS. A new weighting function with a better performance than Wright's data might be a potential improvement in the future study. Also, the FCS and FMS can be optimized using scaling factors and be evaluated with relevant data sets.

7.5 Motivations for FCAM

All color appearance scales were introduced that form a new colorimetry system named FCAM. The motivations for developing FCAM were discussed in detail in Chapters 1 through 3 and can now be reconsidered in light of the completed model. The first motivation was the need for a color appearance model that is physiologically grounded. By building all scales directly from cone fundamentals, FCAM satisfies this requirement and aligns with current understanding of human visual processing.

The second motivation was the desire to move beyond rigid three-dimensional color spaces toward independent perceptual scales. The successful development and validation of FHS, FLS, FBS, and FSS demonstrate that perceptual attributes can be modeled more flexibly when treated independently. This approach reduces conceptual ambiguity.

The third motivation was the need for observer adaptability in modern imaging applications. Because FCAM is formulated in terms of cone fundamentals, it can naturally incorporate observer-specific CMFs, enabling personalized color appearance prediction.

7.5.1 Color Appearance Difference

Color appearance differences between stimuli can be evaluated independently for each scale, allowing perceptual judgments to be expressed in terms of attribute-specific differences rather than a single aggregated metric. This modular structure is a specific characteristic of FCAM. Each scale can be used independently, depending on the application. Moreover, extensions or refinements to one scale do not require restructuring the entire model.

Although the proposed scales are developed independently, they may be combined to define an overall color difference or tolerance metric when required by a specific application. In such cases, the combination of the individual scale differences should not be assumed to follow a single universal metric, as the relative importance of hue, lightness, brightness, and saturation differences is inherently application dependent. For example, imaging, display calibration, textile tolerancing, and psychophysical evaluation may each require different weightings of the independent attributes. Furthermore, the relative contribution of each scale may vary depending on the magnitude of the color difference and the location of the reference color within the appearance domain, since perceptual sensitivity is not necessarily constant across all regions of the scales. Consequently, an overall difference metric may be formulated as a weighted combination of the independent scale differences, where the weighting functions are selected according to the intended application, tolerance requirements, and local perceptual behavior around the reference stimulus. This framework allows FCAM to retain its conceptual independence while still supporting practical color-difference and tolerancing tasks.

7.6 FCAM as a New System of Colorimetry

Viewed as a whole, FCAM is a new system of colorimetry that is fundamentally different from conventional XYZ-based frameworks. In traditional colorimetric systems, the primary goal is to specify color stimuli in a way that supports color matching and reproduction. Color appearance models built on these systems extend this goal by predicting perceptual correlates through a sequence of transformations applied to XYZ tristimulus values. FCAM, by contrast, begins at the level of cone excitations and treats appearance attributes as primary quantities rather than secondary correlates. Also, individual variations in lens density,

macular pigment, and photopigment sensitivities can be incorporated directly through personalized CMFs without altering the structure of the model. This capability positions FCAM as a system of colorimetry, well suited to emerging technologies that demand personalized or adaptive color rendering, such as wide-gamut and HDR displays, virtual and augmented reality systems, and advanced imaging pipelines. The graphical abstract of FCAM is presented in Figure 7.10.

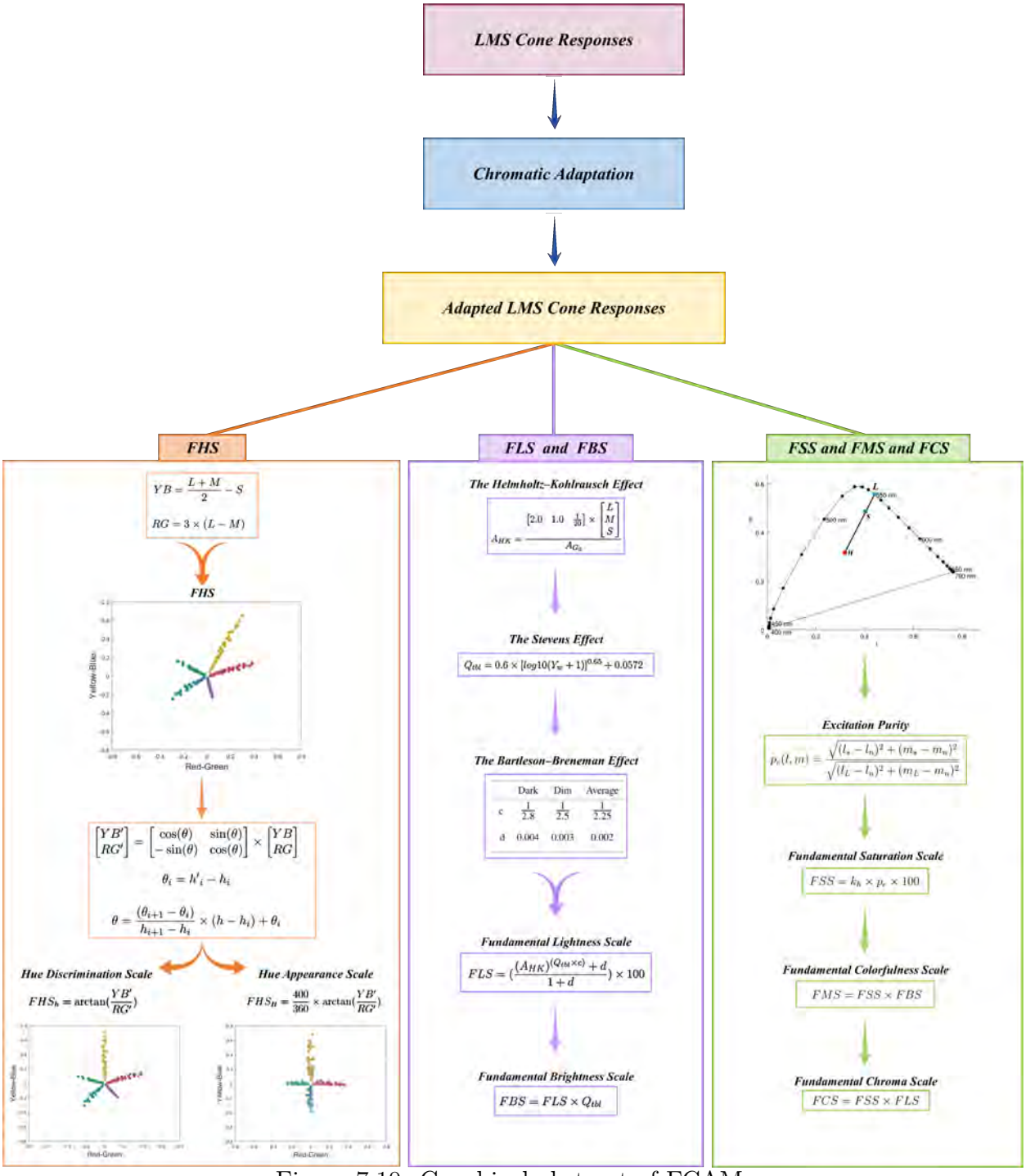

Figure 7.10: Graphical abstract of FCAM.

7.7 Computational Examples

Several computational examples are provided in Table 7.3. Also, an instruction for each FCAM color appearance scale is provided here. Each instruction is independent, simple to follow, and includes a numerical example (No. 1 sample) from the Table 7.3.

1. Hue Discrimination Predictor (FHS_h)

Steps:

1. Obtain cone responses L, M, and S.
2. Compute opponent signals RG and YB.
3. Calculate the required rotation θ based on five principal hues.
4. Apply the rotation matrix on the opponent signals to obtain adjusted opponent responses RG' and YB'.
5. Calculate hue angle in the adjusted opponent space to obtain hue discrimination scale, named FHS_h.

Example (No. 1): $RG' = 0.198$, $YB' = 0.069$, $\theta = 0.091$

$$\Rightarrow \mathrm{FHS_h} = 19.211$$

2. Hue Appearance Predictor (FHS_H)

Steps:

1. Obtain cone responses L, M, and S.
2. Compute opponent signals RG and YB.
3. Calculate the required rotation θ based on four unique hues.
4. Apply the rotation matrix on the opponent signals to obtain adjusted opponent responses RG' and YB'.
5. Calculate hue quadrature in the adjusted opponent space to obtain hue appearance scale, named FHS_H.

Example (No. 1): $RG' = 0.209$, $YB' = 0.015$, $\theta' = -14.969$

$$\Rightarrow \mathrm{FHS_H} = 4.612$$

3. Lightness (FLS)

Steps:

1. Determine surround parameters, luminance adaptation level, and terminal brightness.
2. Determine constants c and d for this surround condition.
3. Calculate the corresponding G_0 luminance for this sample.
4. Calculate the normalized achromatic response, named A_{HK} using G_0 luminance.
5. Compute FLS using these parameters.

Example (No. 1): $A_{G_0} = 1.752$, $A_{HK} = 340$ $c = 0.357$, $d = 0.004$, $Q_{tbl} = 1$

$$\Rightarrow \mathrm{FLS} = 68.140$$

4. Brightness (FBS)

Steps:

1. Determine terminal brightness.
2. Use calculated FLS in previous step.
3. Compute FBS.
4. It should be noted when Q_{tbl} is approximately 1, FBS is not exactly equal to FLS due to rounding Q_{tbl} to 1.

Example (No. 1): $FLS = 68.140$, $Q_{tbl} = 1$

$$\Rightarrow \mathrm{FBS} = 68.142$$

5. Saturation (FSS)

Steps:

1. Compute chromaticity coordinates l and m.
2. Determine the hue-dependent factor k_h.
3. Determine the wavelength of this sample.
4. Calculate excitation purity and hue angle.
5. Compute FSS using these parameters.

Example (No. 1): $l = 0.448$, $m = 0.313$, $k_h = 0.064$, $wvl = 604.258$, $p_e = 0.282$,

$$\Rightarrow \text{FSS} = 1.801$$

6. Colorfulness (FMS)

Steps:

1. Obtain FSS and FBS from previous steps.
2. Compute FMS.

Example (No. 1): Using FSS = 1.801 and FBS = 68.142

$$\Rightarrow \text{FMS} = 122.694$$

7. Chroma (FCS)

Steps:

1. Obtain FSS and FLS from previous steps.
2. Compute FCS.

Example (No. 1): Using FSS = 1.801 and FLS = 68.140

$$\Rightarrow \text{FCS} = 122.691$$

Table 7.3: FCAM Computational Examples.

		No. 1	No. 2	No. 3	No. 4	No. 5	No. 6
	Sample Specification	Munsell H=5R C=8 V=5	Munsell H=5G C=8 V=6	NCS H=B C=40 B=10	NCS H=Y C=50 B=20	DIN T=12 S=7 D=12.146	DIN T=20 S=4 D=26.769
	L	0.219	0.269	0.402	0.430	0.147	0.219
	M	0.153	0.320	0.465	0.384	0.112	0.266
	S	0.117	0.198	0.630	0.106	0.428	0.275
Hue	RG	0.198	-0.153	-0.189	0.139	0.104	-0.142
	YB	0.069	0.096	-0.196	0.301	-0.299	-0.033
	FHS	19.119	147.752	226.032	65.227	289.225	193.064
	θ_h	0.091	14.032	15.682	24.692	21.967	14.455
	RG'_h	0.198	-0.172	-0.129	0.000	0.208	-0.130
	YB'_h	0.069	0.056	-0.240	0.332	-0.238	-0.067
	θ_H	-14.969	33.277	41.463	25.220	17.672	38.015
	RG'_H	0.209	-0.181	-0.012	-0.003	0.190	-0.092
	YB'_H	0.015	-0.003	-0.273	0.332	-0.253	-0.114
	FHS_h	19.211	161.784	241.714	89.918	311.192	207.519
	FHS_H	4.612	201.144	297.216	100.496	340.996	256.755
Lightness and Brightness	*Surround*	Dark	Dark	Dark	Dark	Dark	Dark
	c	0.357	0.357	0.357	0.357	0.357	0.357
	d	0.004	0.004	0.004	0.004	0.004	0.004
	Y_w	100	100	100	100	100	100
	Q_tbl	1	1	1	1	1	1
	A_{G_0}	1.752	2.516	2.060	2.560	0.979	2.503
	A_{HK}	0.340	0.345	0.632	0.488	0.436	0.287
	FLS	68.140	68.507	84.934	77.490	74.466	64.134
	FBS	68.142	68.508	84.936	77.492	74.468	64.136
Saturation	l	0.448	0.342	0.269	0.468	0.214	0.288
	m	0.313	0.407	0.311	0.417	0.163	0.350
	Wavelength	604.258	502.024	476.852	566.604	0.476	482
	p_e	0.282	0.392	0.364	0.656	0.577	0.432
	hue angle	-0.179	1.455	-2.806	0.559	-2.184	2.790
	k_h	0.064	0.073	0.131	0.018	0.547	0.110
	FSS	1.801	2.871	4.786	1.202	31.605	4.753
	FMS	122.694	196.680	406.466	93.133	2353.541	304.821
	FCS	122.691	196.676	406.456	93.131	2353.487	304.814

7.8 Summary

This chapter formally introduced the Fundamental Color Appearance Model (FCAM) as an integrated LMS-based color appearance model. The general features of the Fundamental Hue, Lightness, Brightness, and Saturation Scales were summarized and positioned within a unified framework. By revisiting the motivations established earlier in the dissertation, this chapter demonstrated how FCAM addresses long-standing conceptual and practical limitations of traditional color appearance models. Several computational examples were provided to facilitate implementing the proposed scales. The following chapter concludes the dissertation by summarizing key findings and outlining directions for future research.

Chapter 8

Conclusions and Future Directions

This dissertation presented the development, formulation, and evaluation of the Fundamental Color Appearance Model (FCAM), a new color appearance framework grounded directly in cone fundamentals. The primary objective of this research was to develop a new colorimetry system with one-dimensional independent scales that are directly built based on cone fundamentals.

To achieve this objective, FCAM was developed as a system of independent, one dimensional perceptual scales, each corresponding to a fundamental attribute of color appearance: hue, lightness, brightness, and saturation. Rather than embedding these attributes within a single three-dimensional color space, FCAM treats them as distinct perceptual quantities derived from LMS cone responses following chromatic adaptation.

8.1 Major Contributions

The major contributions of this dissertation can be summarized as follows:

- **Fundamental Hue Scale:** The *FHS* model was developed which includes two scales, the hue discrimination scale named FHS_h and the hue appearance scale named FHS_H. The *FHS* model was evaluated for linearity, spacing, and hue quadrature.
  - A paper was published to introduce the *FHS* model [16].
  - A paper was published to introduce the improved model and to evaluate the *FHS* performance [31].
- **Fundamental Brightness and Lightness Scale:** Separate predictors for lightness and brightness were formulated. The resulting scales successfully model key phe-

nomena such as the Helmholtz–Kohlrausch effect, the Stevens effect, and the Bartleson–Breneman effect. The effect of size on perceived brightness and lightness was also explored in a study.

  - A paper was published to introduce the FLS and FBS scales [82].
  - A paper was published to introduce the effect of size on perceived brightness/lightness [78].

- **Fundamental Saturation Scale:** Saturation was defined in terms of excitation purity within an LMS-based chromaticity framework, incorporating hue-dependent scaling derived from classical psychophysical observations. FSS showed improved consistency with constant-saturation data. Fundamental chroma and colorfulness scales were defined based on FSS.

- **FCAM as a new colorimetry system:** This work introduced FCAM as a scale-based color appearance model. It includes the above-mentioned color attributes along with a chromatic adaptation model. Color appearance differences can be defined using one scale at a time. FCAM offers an alternative system to traditional color appearance models.

  - A paper was submitted to introduce Fundamental Color Appearance Model (FCAM) as a new colorimetry system.

Each fundamental scale in FCAM was evaluated using multiple experimental data sets, including Munsell, NCS, DIN, published psychophysical experiments, and new conducted experiments. The results demonstrate that FCAM achieves performance comparable to, and in several cases exceeding, current color appearance models, despite its simpler structure.

8.2 Implications for Color Science and Colorimetry

The development of FCAM has several important implications for color science. First, it demonstrates that color appearance modeling does not require a unified perceptual space to be effective. Independent, attribute-specific scales can provide accurate predictions while improving interpretability and flexibility.

Second, FCAM is based on cone-fundamentals, so it facilitates observer-specific colorimetry and provides a straight forward way for incorporating individual differences and chromatic adaptation models in mathematical modeling.

Although the model was validated using multiple data sets, further experimental work would strengthen its generalization across a broader range of viewing conditions and stimulus classes.

8.3 Practical Applications

FCAM is well suited to a range of practical applications in imaging and display technology. Its modular structure and reliance on cone fundamentals make it particularly applicable to wide-gamut and high-dynamic-range imaging. Potential applications include color appearance prediction for advanced display systems, gamut mapping, color difference evaluation in quality control, and observer-dependent AR/VR devices. Because each scale can be applied independently, FCAM can be tailored to the perceptual priorities of specific tasks without unnecessary computational complexity.

8.4 Future Work

A promising direction is the systematic incorporation of observer variability through personalized cone fundamentals. FCAM provides a natural foundation for such extensions, which are expected to become increasingly important as display technologies continue to diversify.

Finally, broader evaluation of FCAM in applied imaging systems and industrial workflows would help establish its practical value and inform potential standardization efforts.

Bibliography

[1] M. D. Fairchild, *Color appearance models*, John Wiley & Sons, 2013.

[2] M. D. Fairchild, "On the questionable utility of color space for understanding perception," *Color Research & Application.* **48**(3), pp. 1–7, 2023.

[3] CIE, "A roadmap toward basing CIE colorimetry on cone fundamentals," tech. rep., International Commission on Illumination, CIE 254:2024.

[4] S. Song, M. R. Luo, T. Huang, A. Rider, and A. Stockman, "Individual color matching functions and application in cross-media color reproduction," *Society for Imaging Science and Technology, 32nd Color and Imaging Conference* , pp. 70–75, 2024.

[5] M. D. Fairchild and R. L. Heckaman, "Deriving appearance scales," *Color and Imaging Conference.* **20**(1), pp. 281–286, 2012.

[6] Y. Asano, M. D. Fairchild, and L. Blondé, "Individual colorimetric observer model," *PLoS ONE.* **11**(2), pp. 1–19, 2016.

[7] A. Stockman and A. T. Rider, "Formulae for generating standard and individual human cone spectral sensitivities," *Color Research & Application.* **48**(-), pp. 818–840, 2023.

[8] R. S. Berns, *Principles of Color Technology*, John Wiley & Sons, 2019.

[9] D. J. C. Briggs, "The elements of colour i: colour perceptions, colour stimuli, and colour measurement," *Journal of the International Colour Association* **33**, pp. 79–96, 2023.

[10] R. W. G. Hunt, *A model of colour vision for practical applications, Ch. 31 in The Reproduction of Colour*, Fountain Press, 1995.

[11] C. Li, Z. Li, Z. Wang, Y. Xu, M. R. Luo, G. Cui, M. Melgosa, M. H. Brill, and M. Pointer, "Comprehensive color solutions: CAM16, CAT16, and CAM16-UCS," *Color Research & Application.* **42**, pp. 703–718, 2017.

[12] L. Hellwig, D. Stolitzka, and M. D. Fairchild, "The brightness of chromatic stimuli," *Color Research & Application.* **49**(1), pp. 113–123, 2024.

[13] G. High, P. Green, and P. Nussbaum, "The Helmholtz-Kohlrausch effect on display-based light colours and simulated substrate colours," *Color Research & Application.* **48**, pp. 167–177, 2023.

[14] M. Kim, J. H. Jo, Y. K. Park, and S. W. Lee, "Amendment of CIECAM02 with a technical extension to compensate Helmholtz-Kohlrausch effect for chromatic characterization of display devices," *Displays* **56**, pp. 1–10, 2019.

[15] A. Stockman, "Cone fundamentals and CIE standards," *Current Opinion in Behavioral Sciences* **30**, pp. 87–93, 2019.

[16] S. Abasi and M. D. Fairchild, "Fundamental scales of hue appearance and discrimination," *Color Research & Application.* **48**(6), pp. 673–688, 2023.

[17] M. D. Fairchild, "Unique hues and principal hues," *Color Research & Application.* **43**, pp. 804–809, 2018.

[18] L. Hellwig and M. D. Fairchild, "Brightness, lightness, colorfulness, and chroma in CIECAM02 and CAM16," *Color Research & Application.* **47**, pp. 1083–1095, 2022.

[19] L. Hellwig, D. Stolitzka, and M. D. Fairchild, "Extending CIECAM02 and CAM16 for the Helmholtz–Kohlrausch effect," *Color Research & Application.* **47**(5), pp. 1096–1104, 2022.

[20] P. K. Kaiser, "Luminance and brightness," *Applied Optics (Letters to the Editor).* **10**(12), pp. 2768–2770, 1971.

[21] D. Jameson and L. M. Hurvich, "Complexities of perceived brightness," *Science.* **133**(3447), pp. 174–179, 1961.

[22] N. Moroney, "Background and the perception of lightness," *9th Congress of the International Colour Association.* **4421**, pp. 571–574, 2002.

[23] A. L. Gilchrist, "When does perceived lightness depend on perceived spatial arrangement?," *Perception and Psychophysics.* **28**(6), pp. 527–538, 1980.

[24] A. Chapiro, T. Kunkel, R. Atkins, and S. Daly, "Influence of screen size and field of view on perceived brightness," *ACM Transactions on Applied Perception.* **15**(3), pp. 18:1–18:13, 2018.

[25] A. Choudhury, R. Wanat, J. Pytlarz, and S. Daly, "Image quality evaluation for high dynamic range and wide color gamut applications using visual spatial processing of color differences," *Color Research & Application.* **46**, pp. 46–64, 2021.

[26] G. W. Wyszecki and W. S. Stiles, *Color Science: Concepts and Methods, Quantitative Data and Formulae*, John Wiley & Sons, 2000.

[27] M. D. Fairchild, "Von kries 2020: Evolution of degree of chromatic adaptation," *Society for Imaging Science and Technology* **28th Color and Imaging Conference Final Program and Proceedings**, pp. 252–257, 2020.

[28] C. Shen and M. D. Fairchild, "Weighted Geometric Mean (WGM) method: A new chromatic adaptation model," *PLoS ONE.* **18**(8), pp. 1–15, 2023.

[29] H. Xie and M. D. Fairchild, "Representing color as multiple independent scales: brightness versus saturation," *Journal of the Optical Society of America.* **40**(3), pp. 452–461, 2023.

[30] A. Hård, L. Sivik, and G. Tonnquist, "NCS, natural color system – from concept to research and applications. part I," *Color Research & Application.* **21**(3), pp. 180–205, 1996.

[31] S. Abasi and M. D. Fairchild, "Derivation and evaluation of fundamental hue scales," *Color Research & Application.* **50**, pp. 522–541, 2025.

[32] F. Ebner and M. D. Fairchild, "Finding constant hue surfaces in color space," *Journal of Electronic Imaging.* **3300**, pp. 107–117, 2010.

[33] M. Safdar, G. Cui, Y. J. Kim, and M. R. Luo, "Perceptually uniform color space for image signals including high dynamic range and wide gamut," *Optics express.* **25**(13), pp. 15131–15151, 2017.

[34] P. C. Hung and R. S. Berns, "Determination of constant hue loci for a CRT gamut and their predictions using color appearance spaces," *Color Research & Application.* **20**(5), pp. 285–295, 1995.

[35] K. Xiao, S. Wuerger, C. Fu, and D. Karatzas, "Unique hue data for colour appearance models. part i: Loci of unique hues and hue uniformity," *Color Research & Application.* **36**(5), pp. 316–323, 2011.

[36] H. Wang, M. Wie, and X. Qu, "Constant hue loci in different color spaces for stimuli in rec. 2020 color gamut and hdr conditions," *Optics Express.* **30**(25), pp. 44896–44907, 2022.

[37] R. W. Pridmore, "A new transformation of cone responses to opponent color responses," *Attention, Perception, & Psychophysics.* **83**, pp. 1797–1803, 2021.

[38] E. Hering, *Outlines of a Theory of the Light Sense*, Harvard University Press, Cambridge, MA, 1964. Translated by L. M. Hurvich and Dorothea Jameson.

[39] J. S. Werner and B. R. Wooten, "Opponent chromatic response functions for an average observer," *Perception & Psychophysics* **25**(5), pp. 371–374, 1979.

[40] L. M. Hurvich and D. Jameson, "An opponent-process theory of color vision," *Psychological Review* **64**(6), pp. 384–404, 1957.

[41] G. Svaetichin and E. F. MacNichol, "Retinal mechanisms for chromatic and achromatic vision," *Annals of the New York Academy of Sciences* **74**(2), pp. 385–404, 1959.

[42] A. Stockman, D. I. A. MacLeod, and N. E. Johnson, "Spectral sensitivities of the human cones," *Journal of the Optical Society of America A* **10**(12), pp. 2491–2521, 1993.

[43] F. Ebner and M. D. Fairchild, "Development and testing of a color space (ipt) with improved hue uniformity," *Color Imaging Conference: Color Science, Systems, and Applications* , pp. 72–77, 1998.

[44] A. Stockman and L. T. Sharpe, "Spectral sensitivities of the middle- and long-wavelength sensitive cones derived from measurements in observers of known genotype," *Vis Res* **40**, pp. 1711–1737, 2000.

[45] www.cvrl.org

[46] G. Wyszecki and W. S. Stiles, *Color Science: Concepts and Methods, Quantitative Data and Formulae*, John Wiley & Sons, 2000.

[47] M. Liu, C. Gao, X. Zhang, M. Melgosa, K. Xiao, D. Vázquez, and C. Li, "Transformations from cone responses to opponent color spaces," *Color Research & Application.* **47**, pp. 243–251, 2021.

[48] D. R. Wyble and M. D. Fairchild, "Prediction of Munsell appearance scales using various color appearance models," *Color Research & Application.* **25**(2), pp. 132–144, 2000.

[49] P. Lennie, J. Pokorny, and V. C. Smith, "Luminance," *Journal of the Optical Society of America A.* **10**(6), pp. 1283–1293, 1993.

[50] J. Koenderink, A. van Doorn, and K. Gegenfurtner, "Color weight photometry," *Vision Research.* **151**, pp. 88–98, 2018.

[51] D. J. C. Briggs, "The elements of colour II: the attributes of perceived colour," *Journal of the International Colour Association.* **33**, pp. 97–118, 2023.

[52] R. L. Donofrio, "The Helmholtz–Kohlrausch effect," *Journal of the SID.* **19**(10), pp. 658–664, 2011.

[53] H. Xie and M. D. Fairchild, "Deriving and dissecting an equally bright reference boundary," *Optics Express.* **31**(10), pp. 15637–15652, 2023.

[54] R. M. Evans, "Fluorescence and gray content of surface colors," *Journal of the Optical Society of America.* **49**(11), pp. 1049–1059, 1959.

[55] R. M. Evans and B. K. Swenholt, "Chromatic strength of colors: Dominant wavelength and purity," *Journal of the Optical Society of America.* **57**(11), pp. 1319–1324, 1967.

[56] M. Ayama and M. Ikeda, "Brightness-to-luminance ratio of colored light in the entire chromaticity diagram," *Color Research & Application.* **23**(5), pp. 274–287, 1998.

[57] Y. Nayatani, H. Sobagaki, and K. Hashimoto, "Relation between Helmholtz-Kohlrausch effect, purity discrimination, and G_0 function," *Journal of Light & Visual Environment.* **17**(2), pp. 16–24, 1993.

[58] Y. Nayatani and H. Sakai, "A relationship between zero-grayness luminance by Evans and perceived brightness of spectrum colors," *Color Research & Application.* **33**(1), pp. 19–26, 2008.

[59] R. L. Heckaman and M. D. Fairchild, "G_0 and the gamut of real objects," *in Proceedings of AIC Color.* **9**, 2009.

[60] Y. Y. Li and H. C. Lee, "Color brightness model and its imaging applications," *Journal of the Optical Society of America A.* **36**(3), pp. 377–386, 2019.

[61] S. Aghamohammadi, M. D. Fairchild, and S. Farnand, "Computation of a G_0-referenced lightness metric based on CIE L*," *Under Review* **1**(1), pp. 1–10, 2025.

[62] C. J. Bartleson and E. J. Breneman, "Brightness perception in complex fields," *Journal of the Optical Society of America.* **57**(7), pp. 953–957, 1967.

[63] M. D. Fairchild, "Refinement of the RLAB color space," *Color Research & Application.* **21**(5), pp. 338–346, 1996.

[64] J. C. Stevens and S. S. Stevens, "Brightness function: Effects of adaptation," *Journal of the Optical Society of America A.* **53**(3), pp. 375–385, 1963.

[65] C. L. Sanders and G. Wyszecki, "Correlate for brightness in terms of CIE color matching data," *Proc. 15th Session. CIE* , pp. 221–230, 1963.

[66] G. Wyszecki, "Correlate for lightness in terms of CIE chromaticity coordinates and luminous reflectance," *Journal of the Optical Society of America* **57**, pp. 254–257, 1967.

[67] M. D. Fairchild and E. Pirrotta, "Predicting the lightness of chromatic object colors using CIELAB," *Color Research & Application.* **16**(6), pp. 385–393, 1991.

[68] H. Xie and M. D. Fairchild, "G_0 revisited as equally bright reference boundary," *29th Color and Imaging Conference, Society for Imaging Science and Technology* **48**, pp. 247–252, 2021.

[69] M. Richter, "The official German standard color chart," *Journal of the Optical Society of America* **45**(3), pp. 223–226, 1954.

[70] M. Richter and K. Witt, "The story of the DIN color system," *Color Research & Application.* **11**(2), pp. 138–145, 1986.

[71] Standard, "DIN colour chart: System based on the 10 degree standard colorimetric observer," *DIN Deutsches Institut fur Normung, Berlin, DE* , 1981.

[72] K. D. Xiao, M. R. Luo, and C. J. Li, "Colour size effect modeling," *Color Research & Application.* **37**(1), pp. 4–12, 2012.

[73] K. Xiao, M. R. Luo, C. J. Li, G. Cui, and D. Park, "Investigation of colour size effect for colour appearance assessment," *Color Research & Application.* **36**(3), pp. 201–209, 2011.

[74] G. Kutas and P. Bodrogi, "Color appearance of large homogenous visual field," *Color Research & Application.* **33**(1), pp. 45–54, 2008.

[75] M. Withouck, K. A. G. Smet, and P. Hanselaer, "Brightness prediction of different sized unrelated self-luminous stimuli," *Optics Express.* **23**(10), pp. 13455–13466, 2015.

[76] C. Gao, C. Li, K. Xiao, M. R. Luo, and M. R. Pointer, "An extension to the CAM16 colour appearance model to predict the size effect," *Color Research & Application.* **46**, pp. 740–748, 2021.

[77] C. Gao, M. R. Luo, M. R. Pointer, and C. Li, "Evaluation of color difference prediction with CIECAM16 using CIE 2- and 10-degree observers," *Journal of Imaging Science and Technology.* **67**(2), pp. 020405.1–020405.6, 2023.

[78] S. Abasi, L. Hellwig, D. Stolitzka, and M. D. Fairchild, "Changes in displayed brightness/lightness with stimulus size," *Journal of Imaging Science and Technology.* **69**(2), pp. 1–11, 2025.

[79] G. A. Gescheider, *Psychophysics: The fundamentals*, Lawrence Erlbaum Associates Publishers, 1997.

[80] W. D. Wright, *Researches on Normal and Defective Colour Vision*, C.V. Mosby, St. Louis, 1947.

[81] Y. Park and M. J. Murdoch, "Perceived colorfulness of high-brightness color stimuli," *Color Research & Application.* **50**, pp. 630–641, 2025.

[82] S. Abasi and M. D. Fairchild, "Fundamental lightness and brightness scales," *Optics Express* **33**(21), pp. 44405–44421, 2025.